PhD Thesis

SURFACE MODIFICATIONS OF LONG-PERIOD FIBER GRATINGS FOR BIOSENSING APPLICATIONS

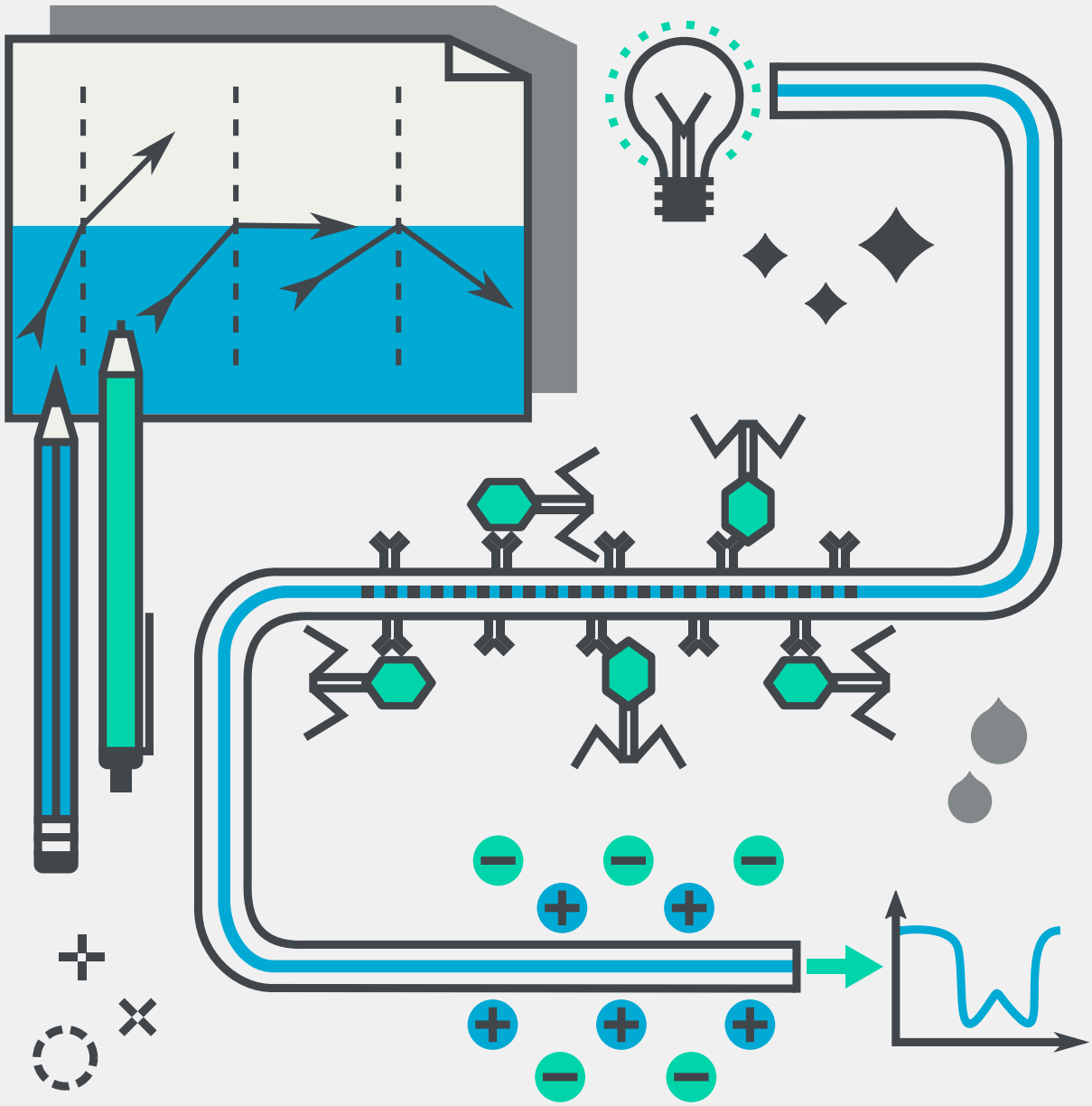

Marta Janczuk-Richter

Surface modifications of long-period fiber gratings for biosensing applications

Marta Janczuk-Richter

Supervisors:
dr hab. inż. Joanna Niedziółka-Jönsson, prof. IChF PAN
dr hab. inż. Mateusz Śmietana, prof. PW

The dissertation was prepared within
the International Doctoral Studies at the
Institute of Physical Chemistry of the Polish Academy of Sciences
Kasprzaka 44/52, 01-224 Warsaw

September 2019

Acknowledgements

Most af all, I would like to thank my supervisors:

- dr hab. inż. Joanna Niedziółka-Jönsson for all the experience and knowledge I got being a part of her group, for giving me scientific freedom and opportunities. I greatly appreciate her guidance and dedicated time;
- dr hab. inż. Mateusz Śmietana for giving me opportunity to be a part of his team, for great collaboration and all shared knowledge in the field that was new to me.

It has been a pleasure working with you.

I am very grateful to my co-workers who were involved in the work described herein: Magdalena Dominik, dr inż. Ewa Roźniecka, dr hab. inż. Marcin Koba, Predrag Mikulic, prof. Wojtek J. Bock, prof. Marcin Łoś, prof. Sebastian Maćkowski, Monika Piestrzyńska, dr Katarzyna Szot-Karpińska, dr hab. Martin Jönsson-Niedziółka, Dariusz Burnat, and other co-authors.

Warm thanks go to the members of Surface Nanoengineering Group and other IPC PAS workers for their help and fruitful discussions. I especially thank dr Jan Paczesny and my office roommates.

I would also like to thank my parents for their constant support and for making me decent and curious person.

Last but not least, I want to thank my Husband for his love, good advice and constructive criticism. Thanks for believing in me.

This work was supported by:

The City of Gdynia
within the project 3/DOT/2016

The National Centre for Research and Development
within the LIDER Grant LIDER/15/24/L-2/10/NCBiR/2011
and within the Techmatstrateg Grant 347324/12/NCBR/2017

The National Science Centre
within the SONATA BIS Grant 2014/14/E/ST7/00104

List of publications

Publications related to the topic of the dissertation:

1. **Janczuk-Richter, M.**; Dominik, M.; Roźniecka, E.; Koba, M.; Mikulic, P.; Bock, W.J.; Łoś, M.; Śmietana, M.; Niedziółka-Jönsson, J. Long-period fiber grating sensor for detection of viruses. *Sensors and Actuators B: Chemical* **2017**, *250*, 32–38
   MJR contribution: MJR designed the experiments, etched the LPFGs, modified the surface, performed experiments with the help of MD, analyzed the data, prepared graphical content, drafted the manuscript, wrote response to reviews

2. **Janczuk-Richter, M.**; Piestrzyńska, M.; Burnat, D.; Sezemsky, P.; Stranak, V.; Bock, W.J.; Bogdanowicz, R.; Niedziółka-Jönsson, J.; Śmietana, M. Optical investigations of electrochemical processes using a long-period fiber grating functionalized by indium tin oxide. *Sensors and Actuators B: Chemical* **2019**, *279*, 223–229
   MJR contribution: MJR designed the experiments, performed optical and electrochemical measurements with the help of MP, analyzed the data, prepared graphical content, drafted the manuscript, wrote response to reviews

3. Piestrzyńska, M.; Dominik, M.; Kosiel, K.; **Janczuk-Richter, M.**; Szot-Karpińska, K.; Brzozowska, E.; Shao, L.; Niedziółka-Jönsson, J.; Bock, W.J.; Śmietana, M. Ultrasensitive tantalum oxide nano-coated long-period gratings for detection of various biological targets. *Biosensors and Bioelectronics*, **2019**, *133*, 8–15
   MJR contribution: MJR designed biosensing experiments, performed biosensing experiments with the help of KSK, analyzed the data and prepared graphical content concerning biosensing experiments, wrote part of the manuscript, wrote response to reviews

4. **Janczuk-Richter, M.***; Dominik, M.; Koba, M.; Mikulic, P.; Bock, W.J.; Maćkowski, S.; Jönsson-Niedziółka, M.; Niedziółka-Jönsson, J.; Śmietana, M. Water-induced fused silica glass surface alterations monitored using long-period fiber gratings. *Journal of Lightwave Technology* **2019**, DOI: 10.1109/JLT.2019.2909947

MJR contribution: MJR designed the experiments, etched the LPFGs, designed flow cell, performed the experiments, analyzed the data, prepared graphical content, drafted the manuscript, wrote response to reviews

Other publications:

1. Paczesny, J.; Binkiewicz, I.; **Janczuk, M.**; Wybrańska, K.; Richter, Ł.; Hołyst, R. Optical investigations of electrochemical processes using a long-period fiber grating functionalized by indium tin oxide. *Journal of Physical Chemistry C* **2015**, *119*, 27007–27017

2. **Janczuk, M.**; Niedziółka-Jönsson, J.; Szot-Karpińska, K. Bacteriophages in electrochemistry: A review. *Journal of Electroanalytical Chemistry* **2016**, *779*, 207–219

3. Dominik, M.; Leśniewski, A.; **Janczuk, M.**; Hołdyński, M.; Niedziółka-Jönsson, J.; Wachnicki, Ł.; Godlewski, M.; Śmietana, M. Titanium oxide thin films obtained with physical and chemical vapour deposition methods for optical biosensing purposes. *Biosensors and Bioelectronics* **2017**, *93*, 102–109

4. **Janczuk, M.**;† Richter, Ł.;† Hoser, G.; Kawiak, J.; Łoś, M.; Niedziółka-Jönsson, J.; Paczesny, J.; Hołyst, R. Bacteriophage-Based Bioconjugates as a Flow Cytometry Probe for Fast Bacteria Detection. *Bioconjugate Chemistry* **2017**, *28*, 419–425
† Authors contributed equally

5. Richter, Ł.;† **Janczuk-Richter, M.**;† Niedziółka-Jönsson, J.; Paczesny, J.; Hołyst, R. Recent advances in bacteriophage-based methods for bacteria detection. *Drug Discovery Today* **2018**, *23*, 448–455
† Authors contributed equally

6. Grzelak, J.; Sulowska, K.; Leśniewski, A.; Roźniecka, E.; **Janczuk-Richter, M.**; Richter, Ł.; Łoś, M.; Jönsson-Niedziółka, M.; Maćkowski, S.; Niedziółka-Jönsson, J. Capturing fluorescing viruses with silver nanowires. *Sensors and Actuators B: Chemical* **2018**, *273*, 689–695

7. Janczuk-Richter, M.;* Marinović, I.; Niedziółka-Jönsson, J.; Szot-Karpińska, K.* Recent applications of bacteriophage-based electrodes: A mini-review. *Electrochemistry Communications* **2019**, *99*, 11–15

8. Wróblewski, G.; **Janczuk-Richter, M.**; Wolkowicz, T.; Jakubowska, M.; Niedziółka-Jönsson, J. Printed carbon based interface for protein immobilization. *Journal of Materials Science: Materials in Electronics* **2019**, *30*, 12465–12474

9. Matuła, K.; Richter, Ł.; **Janczuk-Richter, M.**; Nogala, W.; Grzeszkowiak, M.; Peplińska, B.; Jurga, S.; Wyroba, E.; Suski, S. et al. Phenotypic plasticity of *Escherichia coli* upon exposure to physical stress induced by ZnO nanorods *Scientific reports* **2019**, *9*, 8575

Abstract

The biosensor market is developing fast in recent years mainly due to the growing demand for point-of-care devices and fast detection solutions that may be applied in healthcare, biodefence, environmental monitoring, and food industry. Significant improvements have been made in optical label-free biosensors that provide fast, simple, and accurate analysis. Another advantages, such as small size, low cost, and flexibility, can be obtained by using optical fiber sensors. The main goal of my thesis was to develop simple and reliable surface modification methods and implement them for preparation of long-period fiber grating (LPFG) biosensors for virus detection.

The first part of my thesis describes characterization of the LPFGs used in further work. The LPFGs were tuned to their highest refractive index (RI) sensitivity by chemical etching. The obtained RI sensitivity ($\sim$2000 nm/RIU) indicated great potential for label-free biosensing. Additionally, I analyzed the effect of surface drying on the optical response of the LPFG. The results showed that drying between measurements performed in liquid significantly influences the transmission spectrum of the LPFG due to changes in the cladding surface. This indicates that any drying should be avoided because it may cause getting misleading conclusions. Therefore, I designed a flow cell in which the surface drying was limited. It was used in my studies for other measurements with LPFG-based sensors.

Biosensor preparation requires robust methods for bioreceptor immobilization. In my work I tested and described vapor phase silanization methods to introduce proper functional groups that may be used for covalent bonding of protein receptors. Until now, such methods were used for flat glass surfaces, but my work demonstrated that they are also suitable for cylindrical optical fibers. The best procedures were further used for modification of LPFGs with antibodies and other receptors.

The next part is focused on the utilization of sensitive LPFGs and developed surface modification methods for preparation of highly demanded biosensors for virus detection. By application of antibody-modified LPFG biosensors in label-free approach it was possible to detect 5×10^3 PFU/mL of T7 bacteriophage and 1 ng/mL of norovirus virus-like particles in 40-min assay. Moreover, the method of surface regeneration, which may decrease production costs and enable conducting different measurements on the same LPFG sensor, was presented.

In the last experimental part, I used LPFG sensors coated with thin metal oxide overlays. A tantalum oxide thin film was used for sensitivity enhancement of LPFG-based device in both RI sensing and in biosensing. Compared to the bare LPFGs used in this work, the improvement of RI sensitivity was almost sixfold and translated also into better label-free biosensing capabilities. Additionally, thin metal oxide films make it possible to expand application range of LPFG sensors. I demonstrated that indium tin oxide (ITO)-coated LPFG can be used for simultaneous electrochemical and optical measurements in specially prepared combined setup. The ITO overlay served as both working electrode in the electrochemical system and as a coating that enhances the sensitivity of an LPFG to changes of the external RI. The optical response of the sensor was strongly dependent on the voltage applied to the ITO-LPFG working electrode and on the composition of the electrolyte.

All described achievements were finally summarized and put into perspective of future research to understand their input in the biosensing field.

Streszczenie

W ostatnich latach rynek bioczujników rozwija się szybko w związku z rosnącym zapotrzebowaniem na urządzenia typu point-of-care (tzw. przyłóżkowe testy laboratoryjne) oraz szybkie metody detekcji, które mogłyby zostać wykorzystane w opiece zdrowotnej, ochronie środowiska czy przemyśle spożywczym. Dlatego dużym zainteresowaniem cieszą się czujniki optyczne zapewniające szybką, prostą i precyzyjną analizę badanych próbek bez konieczności znakowania wykrywanej substancji bądź receptora. Dodatkowo, wykorzystanie światłowodów pozwala na otrzymanie urządzeń o małych rozmiarach oraz niskich kosztach produkcji, a także na zwiększenie bezpieczeństwa dzięki możliwości oddzielenia miejsca detekcji od miejsca analizy otrzymanego sygnału w przypadku próbek niebezpiecznych. Głównym celem mojej pracy było opracowanie prostych i uniwersalnych metod modyfikacji powierzchni długookresowych siatek światłowodowych (LPFG) oraz ich zastosowanie jako bioczujników do oznaczania m.in. wirusów i cząstek wirusopodobnych.

W pierwszej części pracy scharakteryzowałam LPFG użyte w badaniach. W celu uzyskania wysokiej czułości na współczynnik załamania (RI) otoczenia zastosowałam metodę chemicznego trawienia powierzchni płaszcza światłowodu. Uzyskana czułość (∼2000 nm/RIU) umożliwiała również zastosowanie LPFG do bezznacznikowej detekcji biomolekuł. Dodatkowo, zbadałam wpływ wysychania powierzchni czujnika na odpowiedź optyczną. Otrzymane wyniki pokazały, że wysuszenie powierzchni pomiędzy pomiarami prowadzonymi w roztworze znacząco wpływa na widmo transmisyjne użytych czujników LPFG. Obserwowane różnice wynikają ze zmian w morfologii powierzchni płaszcza światłowodu pod wpływem suszenia. Aby wyeliminować to niekorzystne zjawisko, a tym samym uniknąć otrzymania nieprawidłowych wyników, zaprojektowałam celkę przepływową umożliwiającą wymianę badanych roztworów przy stałym zanurzeniu czujnika w roztworze podczas modyfikacji powierzchni i oznaczania badanych analitów.

Przygotowanie bioczujnika wymaga opracowania niezawodnej metody unieruchamiania bioreceptorów na jego powierzchni. W mojej pracy testowałam i opisałam metody silanizacji z fazy gazowej, dzięki którym możliwe było wprowadzenie na powierzchnię grup funkcyjnych umożliwiających kowalencyjne przyłączenie receptorów białkowych. Metody te były do tej pory stosowane do modyfikacji płaskich powierzchni szklanych, a moje badania wykazały, że z powo-

dzeniem mogą być stosowane także do cylindrycznych światłowodów. Najlepsze z testowanych metod wykorzystano do modyfikacji czujników LPFG.

W kolejnej części pracy opisałam wykorzystanie wysokoczułych LPFG oraz opracowanych przeze mnie metod modyfikacji do przygotowania bioczujników do wykrywania wirusów. Czujniki LPFG modyfikowane specyficznymi przeciwciałami umożliwiły oznaczenie niskich stężeń bakteriofagów T7 (5×10^3 cząstek/ml) oraz cząstek wirusopodobnych norowirusa (1 ng/ml) w czasie analizy nieprzekraczającym 40 minut. Co więcej, opracowałam metodę regeneracji powierzchni, dzięki której możliwe będzie obniżenie kosztów produkcji oraz prowadzenie różnych pomiarów z wykorzystaniem tego samego czujnika LPFG.

W ostatniej części eksperymentalnej zaprezentowałam wykorzystanie czujników LPFG pokrytych cienkimi warstwami tlenków metali. Warstwy tlenku tantalu zostały wykorzystane do zwiększenia czułości czujników LPFG na zmiany RI. Uzyskano sześciokrotny wzrost czułości na zmiany RI w stosunku do czujników bez osadzonej warstwy, co przełożyło się również na wzrost czułości opracowanych z ich udziałem bioczujników. Drugim badanym pokryciem był tlenek cyny indu (ITO). Czujnik LPFG pokryty cienką warstwą ITO wykorzystałam do prowadzenia równoczesnych pomiarów optycznych i elektrochemicznych w specjalnie przygotowanym układzie. Warstwa ITO służyła zarówno jako elektroda pracująca w układzie elektrochemicznym, jak i pokrycie zwiększające czułość na zmiany RI. Zaobserwowałam, że odpowiedź optyczna czujnika była zależna od potencjału przyłożonego do ITO oraz od składu wykorzystanego elektrolitu.

W ostatnim rozdziale przedstawiłam podsumowanie wszystkich opisanych osiągnięć, a także możliwe ścieżki rozwoju opracowanych technologii w przyszłości.

List of abbreviations

ALD	atomic layer deposition
APTES	(3-aminopropyl)triethoxysilane
AuNP	gold nanoparticle
BSA	bovine serum albumin
CDC	Centers for Disease Control and Prevention
CE	counter electrode
CFU	colony forming unit
CRP	C-reactive protein
CV	cyclic voltammetry
DTP	dispersion turning point
EC-SPR	electrochemical surface plasmon resonance
EDC	1-ethyl-3-(-3-dimethylaminopropyl) carbodiimide hydrochloride
EDS	energy-dispersive X-ray spectroscopy
EDTA	ethylenediaminetetraacetic acid
EFBG	etched fiber Bragg grating
ELISA	enzyme-linked immunosorbent assay
FBG	fiber Bragg grating
FTO	fluorine-doped tin oxide
GFP	green fluorescent protein
HA	influenza hemagglutinin
IgG	immunoglobulin G
ITO	indium tin oxide
LB	lysogeny broth
LMR	lossy-mode resonance
LOD	limit of detection
LPFG	long-period fiber grating
LSPR	localized surface plasmon resonance
MT	mode transition

MZI	Mach-Zehnder interferometer
NHS	N-hydroxysuccinimide
PBS	phosphate buffered saline
PC	photonic crystal
PCR	polymerase chain reaction
PDMS	polydimethylsiloxane
PFU	plaque forming unit
RE	reference electrode
RHDV	rabbit hemorrhagic disease virus
RI	refractive index
RIU	refractive index unit
SPR	surface plasmin resonance
TESPSA	3-(triethoxysilyl)propylsuccinic anhydride
TFBG	tilted fiber Bragg grating
VLP	virus-like particle
WE	working electrode
XPS	X-ray photoelectron spectroscopy
YI	Young's interferometer

Contents

Chapter 1

General introduction

1.1 The importance of biosensors

The growing demand for biosensors in healthcare, biodefense, environmental monitoring, and food industry is driving the development of the biosensors market. According to the report "Biosensors Market by Application (POC, Home Diagnostics, Research Labs, Biodefense, Environmental Monitoring, Food & Beverages Industry), Technology, Product (Wearable and Non-Wearable), and Geography - Global Forecast to 2022" the biosensor market is expected to exceed USD 27 billion by 2022 (from USD 16 billions in 2016). Such an increase is mainly caused by the recent significant developments of chemo- and biosensors, bioelectronics, nanotechnology, and microfabrication. Moreover, the growing prevalence of infectious and lifestyle diseases, and increasing geriatric population causes an increased demand for biosensing devices on the market. The most important areas of biosensors implementation are related to glucose monitoring, cardiac complications, and point-of-care diagnostics, however non-medical market is also gaining much attention.

According to International Union of Pure and Applied Chemistry definition, "biosensor" is a device capable of providing specific and quantitative or semi-quantitative analytical information using a biological recognition element (sensing element, bioreceptor) that is in contact with transduction element (transducer) [1]. Biosensor must be designed to detect analytically significant molecules, such as pathogens, biomarkers, or toxic compounds to provide reliable, fast, and accurate information about target analyte. The biological recognition element is a biologically derived or biomimetic material immobilized on

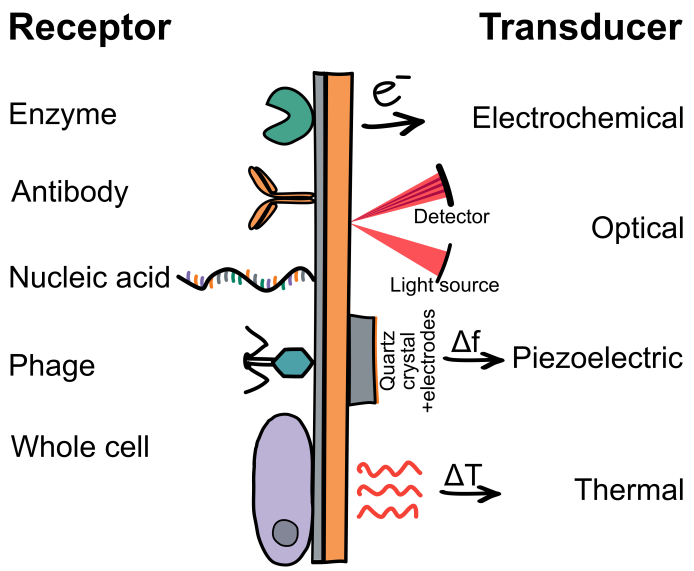

Figure 1.1: The most popular types of receptors and transducers used in biosensors.

the transducer that can specifically recognize and/or bind to the target analyte and therefore is crucial to ensure high selectivity of the sensor. Among the most popular bioreceptors are antibodies, enzymes, and nucleic acids, but recently a lot of work has been devoted to the application of viruses (e.g. bacteriophages), whole cells, and short peptides as sensing elements (Figure 1.1) [2]. Transducer translates signals generated during detection event between target analyte and the sensing layer to a signal understandable for hardware and software (usually an electrical signal). Depending on different types of transducers, typical biosensors can be divided into electrochemical, optical, piezoelectric, and thermal (Figure 1.1). The detection techniques used in biosensors can be also divided into label-based and label-free techniques. Label-based techniques rely on the properties of labels (e.g. fluorescent, chemiluminescent, or radioactive tags) attached to either target molecule or recognition molecules in order to detect particular analyte. In contrast, label-free methods can be used to detect molecules that are unlabeled and unmodified, and therefore such assays are usually easier and cheaper to perform [3]. In recent years a great progress has been made in the field of label-free techniques with particular advancements in optical sensors and biosensors [4, 5].

Due to many possible targets detected with the use of biosensors, their application range is very broad from the most popular glucose monitoring in blood

to very specialized detection of cardiac biomarkers or highly toxic organophosphates [6–8]. Currently, a lot of attention is put on the development of point-of-care biosensors for the detection of diseases of the greatest importance for resource-limited countries, e.g. virus infections, as well as for home monitoring of chronic diseases [9]. In case of food industry, biosensors find applications in safety and quality control of products and starting materials. Detection of chemical and biological contaminants, such as methanol or *Escherichia coli* O157:H7, and analysis of food composition are one of the most common applications [10]. Due to the increasing threat of bioterrorist or biological warfare attack, another important field for biosensor development is related to security and biodefence. Analytes of the highest priority that can be easily transmitted and result in high mortality includes anthrax, smallpox, botulinum toxin, and others [11]. Additionally, biosensors are becoming more and more popular as daily-basis tool in research facilities, e.g. to facilitate drug discovery. According to Scopus database, search term "biosensor" resulted in almost 50,000 articles considering only full paper contributions (accessed 26.06.2019). Although a lot of research has been devoted to the development of this field, number of commercially available biosensors is still limited. Therefore, there is a constant need to expand the number of application of available technologies and to test new devices in order to find solutions that will be suitable for transfer from academia to industry. In the coming years, the market for optical biosensors is expected to grow at the highest rate among all biosensing devices and deserves particular attention.

1.2 Label-free optical biosensors

Recently, the popularity of label-free sensing techniques has been growing due to their advantages over label-based methods and technological advances enabling fast and accurate analysis of various samples. In case of optical devices the detection mechanism is mostly based on the measurements of local refractive index (RI) changes induced by interactions between target molecules and bioreceptors on the transducer surface [12]. The binding event modifies the interaction with optical wave in a detectable way. Among all techniques enabling the label-free biosensing, those based on surface plasmon resonance (SPR) phenomenon are the most common due to their presence on the market (e.g. Biacore [13]). SPR ocuurs at the interface between a metal (typically gold

or silver) and dielectric that interacts with a photon of incident light (Figure 1.2A). There is a particular incident angle at which the light couples with the electrons in the metal surface layer. The electrons oscillate due to excitation and propagate parallel to the metal/dielectric surface. They are now called plasmon. The plasmon oscillations generates an electric field (evanescent field) at the boundary between metal surface and dielectric medium (sample solution). Therefore, the SPR angle, at which the resonance occurs, depends on the RI of the media near the surface. Experimentally, the SPR is observed as a minimum of the reflected light for varying angle of incidence [14]. First biosensing application of SPR was shown in 1983 by Liedberg et al. for studying the interactions between human antibody (immunoglobulin G - IgG) and anti-human IgG antibody [15]. Since then the number of possible SPR biosensing applications greatly increased and this technique became one of the most important tool to study the interactions between bioreceptors and target molecules [16]. In the past few years, SPR biosensors have been used for detection of proteins, viruses, and bacteria [17–19]. The main disadvantages of a typical SPR system is a big size of the device and short depth of evanescence wave penetration that hinders detection of big biomolecules, such as whole cells. To overcome the first problem, it is possible to change the prism coupling [20] into waveguide coupling [21] or fiber optic coupling [22]. Penetration depth may be extended by using metal layer sandwiched between two dielectric layers with similar RI. Thanks to that, long range surface plasmon mode is formed enabling detection of bacterial or eukaryotic cells [23]. Another variant of SPR is localized SPR (LSPR) that occurs for metal nanostructures. In LSPR interactions between the incident photons and the conduction band of a noble metal nanostructure cause a collective oscillation of valence electrons and subsequent absorption with a maximum at the plasmon resonant frequency. The induced plasmons oscillate locally on the nanostructure surface and resulting decay length of electromagnetic field is shorter than in case of SPR. Therefore, this technique is less sensitive for bulk RI changes, but can be advantageous in case of small molecule detection [24, 25]. Many label-free LSPR biosensors were described that utilizes different nanostructures, such as nanospheres [26], nanorods [27], or nanocubes [28]. For example, Faridli et al. [29] developed a LSPR-based immunoassay to determine prolactin (small protein hormone, 23 kDa) in human serum. In this assay, gold nanospheres covered with antibodies were used for determination of prolactin concentration in human control serum. Detection

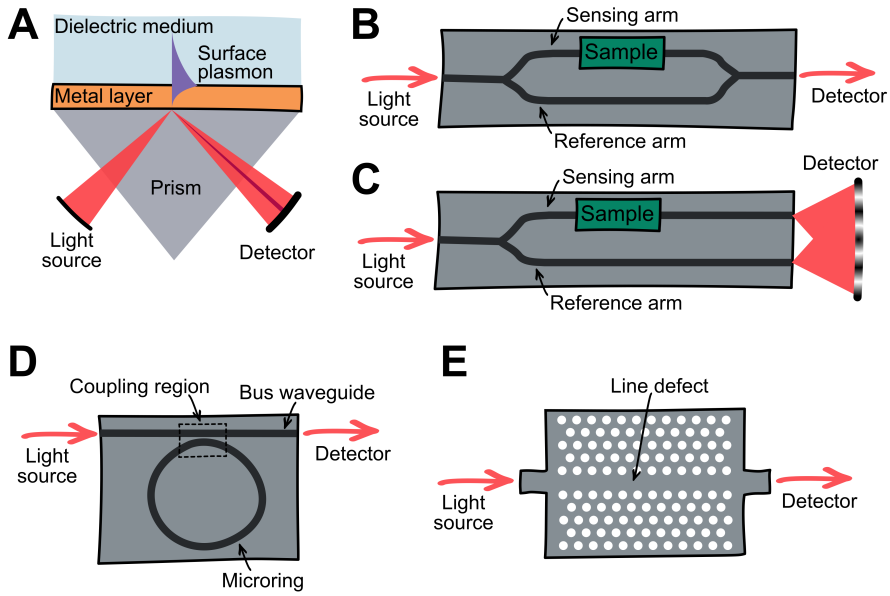

Figure 1.2: Various label-free sensing techniques: surface plasmon resonance (A), Mach-Zehnder interferometer (B), Young's interferometer (C), optical microring resonator (D), and photonic crystal sensor (E).

was based on the measurements of LSPR wavelength shift.

Label-free sensing strategy can be also implemented by using interferometer-based biosensors. The most popular solutions are based on Mach-Zehnder interferometer (MZI) or Young's interferometer (YI). The coherent, single mode, single polarized light enters the waveguide and is split equally into two arms. Sensing arm has a window on top enabling evanescent field to interact with the test sample while reference arm is covered with the thick cladding layer to protect it from the sample. In MZI the arms recombine at the output and resulting interference is measured by photodetector (Figure 1.2B). In case of YI the optical output of the arms combines and forms interference fringes on a detector screen (Figure 1.2C). A change in the RI near the surface of the sensing arm results in change in the light intensity at the photodetector array [30]. First label-free interferometric biosensors were demonstrated by Heideman et al. for human chorionic gonadotropin [31] and by Ingenhoff et al. for detection of biotinylated IgG monolayer formation [32], both of them based on MZI. Development of waveguide technology and microfluidics allowed to increase the number of possible configurations and biosensing applications of interferomet-

ric devices. The devices have been used not only for protein detection [33], but also for detection of viruses (e.g. herpes simplex virus type 1 [34]), studying DNA-DNA interactions [35], and detection of small organic molecules [36]. The main advantages of interferometric biosensors include mechanical stability, reliability, and possibility for miniaturization and mass production. On the other hand they are highly sensitive to mechanical vibrations and temperature changes and therefore have to be stabilized and isolated from the environment.

Another solution for label-free sensing technology is based on rapidly growing field of optical microring resonators. An optical ring resonator is a set of waveguides in which at least one is a closed loop and it is coupled to input and output (bus) waveguides to get a transfer of optical energy (Figure 1.2D). This structure supports a number of circulating wavelengths that satisfy the resonance conditions. Resonance wavelength depends on the resonator radius and effective RI experienced by the optical resonant mode. Wavelength that satisfy the resonance conditions are coupled to the ring. The resonant light circulates along the ring resonator and the constructive interference after each round increase the optical power in the resonator. The transfer of optical power is done by coupling between the evanescent modes in the ring and bus waveguides, therefore the distance between the waveguides should be in the range of hundreds of nanometers. As the resonance wavelength depends on the RI, binding of target analytes to the ring surface can be detected as a change in output signal [37]. Different configurations of optical ring resonators may be implemented and used as biosensors, e.g. (i) ring, disk, or toroid-shaped resonators fabricated on silicon wafers [38], (ii) microspheres made of liquid, fused silica, or polymers, [39] (iii) capillary-based ring resonators [40]. Thanks to the small size of single resonator it is possible to prepare high density sensor integration that enable multiplexing [41]. An additional advantages are low sample volumes that may be used for biodetection and long effective length of possible detection of light-analyte interactions.

Recently, photonic crystal (PC) sensors are gaining importance in terms of their use as a biosensors. PC consists of a spatially periodic arrangement of dielectric materials. Characteristic feature of this material is the presence of photonic bandgap. The wavelengths which are within the bandgap are not allowed to propagate in the PC. By introducing the defect into the ordered periodic structure, the defect mode is formed (Figure 1.2E). The light that is in resonance with the defect mode can propagate in the structure. It manifests

as a sharp peak within the bandgap on the transmission or reflection spectrum whose position depends on the surrounding environment of the structural defect [42]. Different configurations of PCs were used for biodetection of proteins and viruses [43–45]. Small sensing volumes, high sensitivity and possible multiplexing [46] make the PC sensors attractive in bioanalysis. However, very high precision is required to fabricate sensitive and reproducible PC devices and further investigation is still needed to integrate compatible microfuidics.

Presented list of possible optical label-free biosensors is not comprehensive, but in order to introduce the reader to the topic, the most popular optical label-free techniques were described. In the next paragraph, more detailed characterization of optical fiber grating sensors, that are also a great label-free biosensing solution and are the main concern of this thesis, will be given.

1.3 Optical fiber refractometers

An important part of optical label-free biosensors market is related to optical fiber sensors. Constantly developed optical fiber technology and increase in the number of different optical sensing mechanisms attract scientific community and are beneficial for development of biosensors. Main advantages of optical fiber-based sensors are low cost, small size, flexibility, possibility of real-time and remote sensing, and immunity to electromagnetic interferences.

An optical fiber is a cylindrical filament made by drawing fused silica or plastic. It consists of a core surrounded by a cladding with different RIs (Figure 1.3A). The RI is higher for the core (n_{core}) than for the cladding (n_{clad}). Fiber acts as a waveguide and light is kept in the core by the principle of total internal reflection. According to Snell's law the total internal reflection occurs when light is incident from the core to the cladding at incident angle (θ_i) greater that the critical angle (θ_c). Critical angle can be calculated by:

$$\theta_c = arcsin\left(\frac{n_{clad}}{n_{core}}\right) \tag{1.1}$$

Thanks to that, signal in optical fiber can be transmitted over long distance with little attenuation. The geometrical optics can be applied only to the fibers with large fiber core diameter (multi-mode fibers). Single-mode fibers with small core (8 – 10 μm) cannot be modeled with geometrical optics. Instead, to analyze light propagation in those fibers it is necessary to apply Maxwell equations (reduced to electromagnetic wave equation). The possible solutions

of the equation are called modes and they define how the wave is distributed in space. For single-mode fibers only one solution is possible. The light travels parallel to the length of the fiber but the electromagnetic oscillations occur perpendicular to the fiber length. This mode is often called transverse mode. The behavior of light propagation in large-core fibers can also be modeled with electromagnetic wave equation. In such a case more than one mode is supported. Each mode is characterized by effective refractive index (n_{eff}). Effective RI is a number quantifying the phase delay per unit length in a waveguide, relative to the phase delay in vacuum and it is dependent on the phase constant (β) and the vacuum wavenumber (k):

$$\beta = n_{eff}k = n_{eff}\frac{2\pi}{\lambda} \tag{1.2}$$

The modes in optical fibers with small difference between core and cladding RI can be simplified to linearly polarized (LP) [47]. The electromagnetic field is not completely confined in the core. Instead, it penetrates a short distance of the cladding (lower RI medium) and propagates parallel to the interface with exponential decay with the distance from the surface. This is called evanescent field. The physical principle of this phenomenon results from the solution of Maxwell equations. In such a case the tangential components of electric and magnetic fields have to be continuous across the surface and the field cannot abruptly go to zero at the border between media. Therefore, the small portion of light penetrates the lower RI medium [48]. In case of sensing and biosensing purposes, the most important parameter is the penetration depth of the evanescent wave (d_p). This parameter is the distance from the interface at which the electric field amplitude is decreased to 1/e (about 37%) of its original value at the interface. It depends on the wavelength of light, the refractive indices of core and cladding, and the angle of incidence. Typically, the penetration depth varies from 50 to 1000 nm.

The optical fibers that were used in this studies had a core diameter of 8.2 μm and a cladding diameter of 125 μm. Therefore, the penetration depth is much smaller than the cladding thickness and no interaction between optical signal and the external medium occurs. Although it is beneficial in case of transmission of signal in communication, it can not be directly used to create a biosensor. Therefore, some modifications of optical fiber have to be made in order to provide interaction of light with external environment. One possibility is to enable energy transfer from fundamental core mode to other modes, either

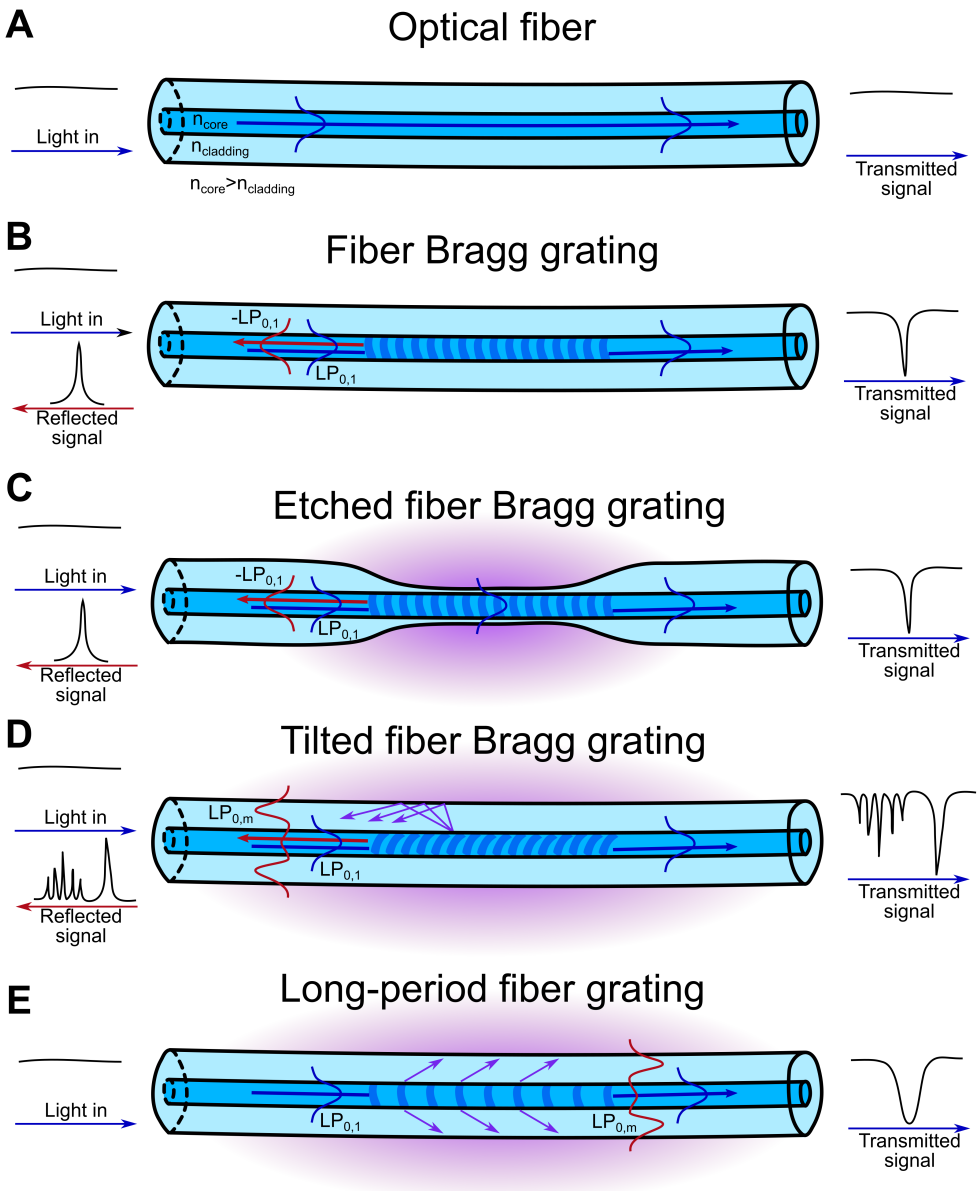

Figure 1.3: Operation principle of optical fiber and optical fiber gratings.

the core mode or the cladding modes, by formation of fiber gratings. Fiber grating is a diffraction structure with periodical modulation of the RI of the core of a single-mode fiber, which satisfies the phase matching conditions between modes [49]. Typically, grating is induced by exposing the fiber to an interference pattern of UV light or to a femtosecond radiation. If the coupling of core and cladding modes occurs, the evanescent field appears at the interface between cladding and external medium. In such a case, the penetration depth depends not only on the wavelength and cladding refractive index, but also on the order of cladding mode as well as of the external refractive index. What is even more important in case of biosensing applications of optical fibers, power transfer between modes leads to the modulation of the transmitted light and the changes of external refractive index (and other factors) manifests as changes in the transmitted spectrum. Biological sensing based on the specific binding between receptors immobilized on the sensor surface and the target molecules causes a change in the effective thickness and density of the biological layer on the surface. As a consequence the optical signal is also altered. Conversely, if the grating satisfies phase matching conditions of fundamental core mode and its respective counter-propagating mode, the light is well confined within the core and those structures are not sensitive to external RI. Depending on the grating period, fiber gratings are broadly classified into fiber Bragg gratings and long-period fiber gratings.

1.4 Fiber Bragg gratings

Fiber Bragg grating (FBG) has a grating period Λ in the order of hundreds of nm. This device satisfies the phase matching between fundamental core mode and its respective counter-propagating mode. When light reaches the grating, the majority of its power is transmitted while the narrow part is strongly reflected. The resonance wavelength λ_{res} at which coupling occurs is described by Bragg condition:

$$\lambda_{res} = 2n_{eff}^{core}\Lambda \tag{1.3}$$

where n_{eff}^{core} is effective RI of the mode propagating in the core of the fiber and Λ is grating period. Figure 1.3B illustrated the principle of operation of a FBG.

FBG sensors are of great interest through the last few decades due to their wide industrial and environmental applications. Standard FBGs are sensitive to temperature, strain, and pressure, and therefore are often used for mea-

surements of physical parameters [49, 50]. Due to the fact that the light is well confined within the core, the FBGs are not sensitive to the external RI and therefore, they can not be used as refractometers nor biosensors. In order to make this kind of structures sensitive to external RI it is necessary to remove or partially remove the cladding by chemical etching [51], tapering [52], or side-polishing [53], or to write FBGs in the microfibers [54]. The operation principle of etched FBG (EFBG) is shown in Figure 1.3C. Due to the thin cladding, the evanescent wave can interact with external medium. The RI sensitivity of EFBG is dependent on the fiber diameter in the grating region and the thinner the cladding, the higher the RI sensitivity of EFBG. However, etching or polishing of the optical fiber makes it more susceptible to damage, especially to breakage. In the first demonstration of EFBG as a refractometer, the etching was done in 40% hydrofluoric acid (HF) and the fiber diameter reached 11 μm (1 μm of the cladding remained) [51]. The sensor was measured in different sucrose solutions (RI between 1.333-1.345) and obtained sensitivity was 1 nm/RI unit (RIU) that gives the resolution of about 5×10^{-4} RIU. Better results were obtained when etching also affected the core [55]. When the fiber diameter was reduced to 3.4 μm, the maximum sensitivity of 1394 nm/RIU was obtained (resolution of about 7×10^{-6} RIU), but the vulnerability of the fiber was also increased. Thanks to the sensitivity to external RI, EFBG was also used as a label-free biosensor for detection of medically relevant C-reactive protein (CRP) by monitoring the shift in Bragg wavelength [56]. Gratings were coated with an anti-CRP antibody-graphene oxide complex and obtained limit of detection (LOD) was 10 μg/L. Because of high fragility and problems with handling, EFBGs are not widely used in biodetection [57].

Another possibility to use FBG as refractometer was demonstrated by Laffont in 2001 [58]. The authors proposed the use of tilted FBG (TFBG) where the index modulation pattern is tilted by the angle θ with respect to the fiber axis. In TFGB fundamental core mode is coupled to cladding modes and to counter-propagating core mode as shown in Figure 1.3D. In the transmission spectrum there is a series of attenuation bands corresponding to the coupling with different cladding modes, and the main band as in standard FBG. The Bragg condition for TFBG is modified to take into account resonance wavelengths of different cladding modes $\lambda_{res,m}$ [59]:

$$\lambda_{res,m} = \left(n_{eff}^{core} - n_{eff}^{clad,m} \right) \frac{\Lambda}{cos\theta} \tag{1.4}$$

where n_{eff}^{core} is effective RI of the core mode and $n_{eff}^{clad,m}$ is effective RI of the m-th cladding mode. Thanks to the coupling to cladding modes the light reaches the cladding-surrounding interface and therefore $n_{eff}^{clad,m}$ depends on external RI and the resonance wavelengths are modulated with the changes in external RI. Only the main band corresponding to the coupling with the core mode is insensitive to RI changes. Refractometers based on TFBG typically have a sensitivity of 10 nm/RIU and resolution of about 10^{-4} RIU [58, 60]. The main disadvantage of TFBG-based refractometers is connected with a number of cladding modes that are coupled in a large wavelength bandwidth. This causes problems with signal readout and analysis. Despite this, several biosensing applications with TFBGs were demonstrated. For example Maguis et al. [61] used TFBG as a sensor for detection of anti-bovine serum albumin (BSA) antibody. Biotinylated BSA was immobilized on the TFBG modified with electrostatic self-assembled film by adsorption or by using avidin-biotin interactions. Detection of anti-BSA antibody was done in buffer solution and obtained LOD was 86 μg/L.

1.5 Long-period fiber gratings

Another optical fiber-based refractometer is long-period fiber grating (LPFG). LPFG is also a diffraction structure with modulated RI of the core, but grating period is 2-3 orders of magnitude higher than in case of FBG and typically ranges from 100 to 700 μm (which makes them easier to fabricate than FBGs). This perturbation leads to phase matching between fundamental core mode and forward propagating cladding modes (Figure 1.3E). It results in several attenuation bands in the transmitted spectrum, each band corresponds to the coupling into different cladding mode. Obtained bands have spectral width that varies from few up to tens of nm so typically they are wider than in case of FBGs [62]. A typical transmission spectrum of LPFG is shown in Figure 1.4. The resonance wavelength for particular coupled cladding mode $\lambda_{res,m}$ satisfies the following phase matching condition:

$$\lambda_{res,m} = \left(n_{eff}^{core} - n_{eff}^{clad,m}\right)\Lambda \tag{1.5}$$

Similarly as in case of TFBG, $n_{eff}^{clad,m}$ depends on the external refractive index and therefore a change in external RI causes a shift in the resonance wavelength of LPFG. The highest sensitivity is obtained for external RIs close to that of the cladding, while for external RIs higher than that of the cladding or significantly

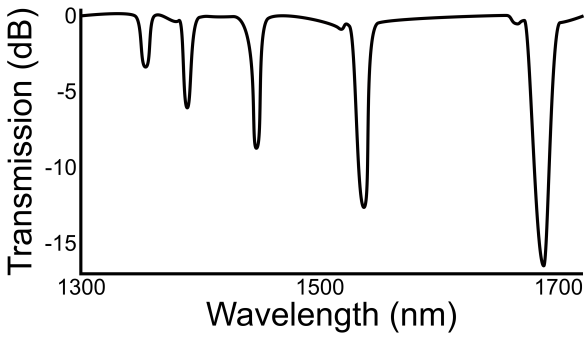

Figure 1.4: A typical tranmsission spectrum of LPFG.

lower, the sensitivity is considerably reduced [63]. The first application of LPFGs was reported in 1996 by Vengsarkar et al. [62] for band-rejection filters. The same year Bhatia et al. [64] demonstrated the application of LPFGs for RI sensing. In this work the wavelength shift of 62 nm for RI change between 1.40 and 1.45 was shown for LPFG with a grating period of 320 μm. Since then many refractometric sensors were demonstrated for the measurements of RI [63], but also concentration of sodium chloride, calcium chloride [65], ethylene glycol [65, 66], ethanol, glucose and sucrose [67] in water. Shu et al. [63] shown the RI sensing for LPFGs with different grating periods. The best sensitivity reported in this work was obtained for the period 202 μm and was equal to 1481 nm/RIU in the range 1-1.36 RIU. Detection of xylene in heptane was demonstrated by Allsop et al. [68] with the minimum detectable change in volumetric concentration of 0.04%. All of these sensors were based on the measurement of RI of the volume around the LPFG and the whole evanescent field related to the coupled cladding mode was modulated by analyte. However, this approach is not selective as all species present in the sample contribute into the generated signal. Thus, such simple approach is not effective in case of biosensing. However, when the sensing layer is deposited on the LPFG, the biochemical interaction, that modulates local RI, takes place on its surface with target molecules only. In this case only the portion of evanescent field is modified, depending on the thickness of the sensing layer and the size of the analyte. Therefore, we can distinguish two types of refractomeric optical sensors: (i) with volume RI sensing when the whole evanescent field is modified, and (ii) with surface RI sensing when the biolayer thickness d_{bl} (receptor + analyte) is smaller than the penetration depth d_p (Figure 1.5). In this case the

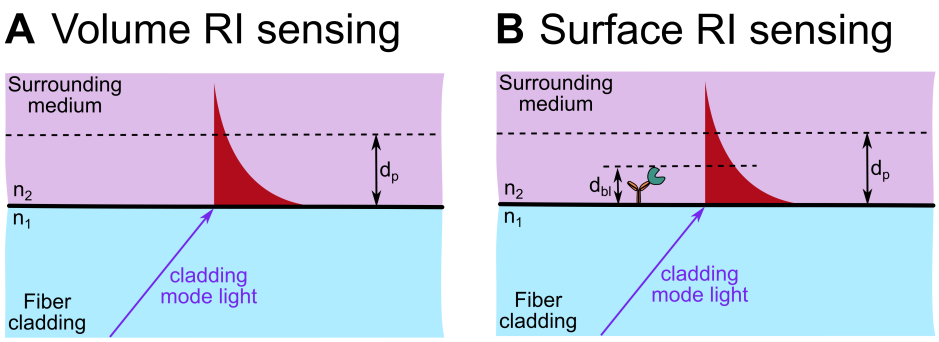

Figure 1.5: Schematic representation of the volume (A) and surface (B) RI sensing. In the volume RI sensing the whole evanescent field is modulated in the presence of the analyte in the bulk. In the surface RI sensing, when biolayer thickness d_{bl} is smaller than penetration depth d_p, only a portion of the field is modified by the presence of the analyte. n_1 and n_2 are fiber cladding RI and external medium RI, respectively.

washing step in the buffer solution is necessary to measure only the RI change caused by the local surface phenomenon due to specific binding on the surface.

First biosensing application of LPFG that uses the second sensing mechanism was described by DeLisa et al. [69] Goat anti-human IgG was immobilized on the LPFG surface and the detection of human IgG was investigated in concentration range 2-50 μg/mL. Study of antigen-antibody interaction on LPFG was also shown by other authors [70–75]. Another biosensing applications of LPFGs were real-time monitoring of DNA hybridization [76–78] and bacteria detection [79–83]. Due to the relatively long penetration depth of LPFG (typically 200-500 nm) they are especially suitable for detection of big biological targets, such as bacteria ($> 1\ \mu$m). In the first report concerning bacteria detection with LPFG the authors used bacteriophages (viruses that infect bacteria) as recognition elements [79]. The resonance wavelength shift for the sample containing 10^8 colony forming units (CFU)/mL of *Escherichia coli* equals 1.3 nm. The sensitivity was further improved by using more sensitive LPFG and the resonance wavelength ranged from 2 nm to 4 nm for *E. coli* concentrations varying between 10^3 CFU/mL and 10^9 CFU/mL [80]. Specific bacteria detection was also done with the utilization of bacteriophage adhesins (proteins on the phage surface enabling recognition and binding to host bacteria) [81] and antibodies [82, 83] as bioreceptors. Surprisingly, although viruses were used as sensing elements, no LPFG-based sensor for virus detection was reported

to date. Recently, LPFGs were also used for detection of hemoglobin [84] and triacylglycerides [85]. Biosensing applications of optical fiber gratings were reviewed in [57, 86, 87].

1.6 Aim of the research

Increasing demand for new biosensors on the market is driving the development of new technological solutions. Great interest concerns the use of optical sensors and biosensors due to the possible label-free approach with smaller number of steps and shorter time required for target detection. Optical fiber sensors offer additional advantages, such as low cost, small size, flexibility, possibility of real-time and remote measurements. In my work, long-period fiber gratings (LPFGs) were chosen as transducers due to their great sensitivity to changes occurring on the surfaces induced, e.g., by antigen-antibody interactions.

One of the most important steps in biosensor fabrication is immobilization of bioreceptors. Therefore, the aim of my research was the development of surface modification method that would be suitable for optical fiber sensors. The method should be reliable and relatively simple and enable modification of multiple sensors at the same time. Moreover, receptors immobilized with proposed method had to be evenly distributed over the whole sensor surface.

The second reserch objective was to implement the developed modification method for preparation of sensitive and label-free LPFG-based biosensors. For the first time, LPFGs were used as biosensing platforms for detection of viruses. Such sensors may be useful in biotechnology industry as well as in healthcare.

Additional aim was related to improvement of LPFG-based devices by the use of thin metal oxide overlays. High-RI films can increase sensor sensitivity and give the possibility of new applications, e.g., in electrochemistry.

Chapter 2 discusses the main parameters that had impact on the optical response of LPFG-based sensors. In particular, the sensitivity to external RI and the influence of surface drying on the spectral response are demonstrated and explained. **Chapter 3** shows the methods used for chemical modification of LPFG surface and techniques for protein immobilization on an example of green fluorescent protein. In **chapter 4**, LPFGs-based biosensors are presented. First, preliminary work with avidin detection by biotin-modified LPFG sensor is demonstrated. Then, biosensors for detection of bacteriophages and human viruses are shown. **Chapter 5** demonstrates the utilization of thin metal oxide

layers for sensitivity enhancement of LPFG-based devices and also for preparation of multi-domain sensing device working in optical and electrochemical domains. In **chapter 6**, the summary of this thesis is presented and future perspectives concerning practical applications of developed LPFG sensors and biosensors are discussed.

1.7 References

(1) Thévenot, D. R.; Toth, K.; Durst, R. A.; Wilson, G. S. Electrochemical biosensors: recommended definitions and classification. *Biosensors & bioelectronics* **2001**, *16*, 121–31.

(2) Kahn, K.; Plaxco, K. W., *Recognition Receptors in Biosensors*; Zourob, M., Ed.; Springer New York: New York, NY, 2010, pp 3–45.

(3) Fan, H.; Tong, Y. Potential Duel-Use of Bacteriophage Related Technologies in Bioterrorism and Biodefense. *Journal of Bioterrorism & Biodefense* **2012**, *03*, 1–4.

(4) Sang, S.; Wang, Y.; Feng, Q.; Wei, Y.; Ji, J.; Zhang, W. Progress of new label-free techniques for biosensors: a review. *Critical Reviews in Biotechnology* **2016**, *36*, 465–481.

(5) Khansili, N.; Rattu, G.; Krishna, P. M. Label-free optical biosensors for food and biological sensor applications. *Sensors and Actuators B: Chemical* **2018**, *265*, 35–49.

(6) Witkowska Nery, E.; Kundys, M.; Jeleń, P. S.; Jönsson-Niedziółka, M. Electrochemical Glucose Sensing: Is There Still Room for Improvement? *Analytical Chemistry* **2016**, *88*, 11271–11282.

(7) Kumar, P.; Kim, K.-H.; Deep, A. Recent advancements in sensing techniques based on functional materials for organophosphate pesticides. *Biosensors and Bioelectronics* **2015**, *70*, 469–481.

(8) Qureshi, A.; Gurbuz, Y.; Niazi, J. H. Biosensors for cardiac biomarkers detection: A review. *Sensors and Actuators B: Chemical* **2012**, *171-172*, 62–76.

(9) Gubala, V.; Harris, L. F.; Ricco, A. J.; Tan, M. X.; Williams, D. E. Point of Care Diagnostics: Status and Future. *Analytical Chemistry* **2012**, *84*, 487–515.

(10) Bahadır, E. B.; Sezgintürk, M. K. Applications of commercial biosensors in clinical, food, environmental, and biothreat/biowarfare analyses. *Analytical Biochemistry* **2015**, *478*, 107–120.

(11) Nikoleli, G.-P.; Karapetis, S., *Biosensors for Security and Bioterrorism Applications*; Nikolelis, D. P., Nikoleli, G.-P., Eds.; Advanced Sciences and Technologies for Security Applications March; Springer International Publishing: Cham, 2016.

(12) Fan, X.; White, I. M.; Shopova, S. I.; Zhu, H.; Suter, J. D.; Sun, Y. Sensitive optical biosensors for unlabeled targets: A review. *Analytica Chimica Acta* **2008**, *620*, 8–26.

(13) Webpage, Biacore Life Sciences, https://www.biacore.com/lifesciences/index.html.

(14) Raether, H. In *Surface Plasmons on Smooth and Rough Surfaces and on Gratings*; Springer Berlin Heidelberg: Berlin, Heidelberg, 1988, pp 4–39.

(15) Liedberg, B.; Nylander, C.; Lunström, I. Surface plasmon resonance for gas detection and biosensing. *Sensors and Actuators* **1983**, *4*, 299–304.

(16) Nguyen, H. H.; Park, J.; Kang, S.; Kim, M.; Nguyen, H. H.; Park, J.; Kang, S.; Kim, M. Surface Plasmon Resonance: A Versatile Technique for Biosensor Applications. *Sensors* **2015**, *15*, 10481–10510.

(17) Vashist, S. K.; Schneider, E. M.; Luong, J. H. T. Surface plasmon resonance-based immunoassay for human C-reactive protein. *The Analyst* **2015**, *140*, 4445–4452.

(18) Baac, H.; Hajós, J. P.; Lee, J.; Kim, D.; Kim, S. J.; Shuler, M. L. Antibody-based surface plasmon resonance detection of intact viral pathogen. *Biotechnology and Bioengineering* **2006**, *94*, 815–819.

(19) Tawil, N.; Sacher, E.; Mandeville, R.; Meunier, M. Surface plasmon resonance detection of E. coli and methicillin-resistant S. aureus using bacteriophages. *Biosensors and Bioelectronics* **2012**, *37*, 24–29.

(20) Matsubara, K.; Kawata, S.; Minami, S. Optical chemical sensor based on surface plasmon measurement. *Applied Optics* **1988**, *27*, 1160.

(21) Lavers, C.; Wilkinson, J. A waveguide-coupled surface-plasmon sensor for an aqueous environment. *Sensors and Actuators B: Chemical* **1994**, *22*, 75–81.

(22) Sharma, A. K.; Jha, R.; Gupta, B. D. Fiber-Optic Sensors Based on Surface Plasmon Resonance: A Comprehensive Review. *IEEE Sensors Journal* **2007**, *7*, 1118–1129.

(23) Jing, J.-Y.; Wang, Q.; Zhao, W.-M.; Wang, B.-T. Long-range surface plasmon resonance and its sensing applications: A review. *Optics and Lasers in Engineering* **2019**, *112*, 103–118.

(24) Petryayeva, E.; Krull, U. J. Localized surface plasmon resonance: Nanostructures, bioassays and biosensing—A review. *Analytica Chimica Acta* **2011**, *706*, 8–24.

(25) Kaminska, I.; Maurer, T.; Nicolas, R.; Renault, M.; Lerond, T.; Salas-Montiel, R.; Herro, Z.; Kazan, M.; Niedziolka-Jönsson, J.; Plain, J.; Adam, P.-M.; Boukherroub, R.; Szunerits, S. Near-Field and Far-Field Sensitivities of LSPR Sensors. *The Journal of Physical Chemistry C* **2015**, *119*, 9470–9476.

(26) Fujiwara, H., *Spectroscopic ellipsometry: principles and applications*; John Wiley & Sons: 2007, p 369.

(27) Marinakos, S. M.; Chen, S.; Chilkoti, A. Plasmonic Detection of a Model Analyte in Serum by a Gold Nanorod Sensor. *Analytical Chemistry* **2007**, *79*, 5278–5283.

(28) Galush, W. J.; Shelby, S. A.; Mulvihill, M. J.; Tao, A.; Yang, P.; Groves, J. T. A Nanocube Plasmonic Sensor for Molecular Binding on Membrane Surfaces. *Nano Letters* **2009**, *9*, 2077–2082.

(29) Faridli, Z.; Mahani, M.; Torkzadeh-Mahani, M.; Fasihi, J. Development of a localized surface plasmon resonance-based gold nanobiosensor for the determination of prolactin hormone in human serum. *Analytical Biochemistry* **2016**, *495*, 32–36.

(30) Kozma, P.; Kehl, F.; Ehrentreich-Förster, E.; Stamm, C.; Bier, F. F. Integrated planar optical waveguide interferometer biosensors: A comparative review. *Biosensors and Bioelectronics* **2014**, *58*, 287–307.

(31) Heideman, R.; Kooyman, R.; Greve, J. Performance of a highly sensitive optical waveguide Mach-Zehnder interferometer immunosensor. *Sensors and Actuators B: Chemical* **1993**, *10*, 209–217.

(32) Ingenhoff, J.; Drapp, B.; Gauglitz, G. Biosensors using integrated optical devices. *Fresenius' Journal of Analytical Chemistry* **1993**, *346*, 580–583.

(33) Lin, S.; Lee, C.-K.; Lin, Y.-H.; Lee, S.-Y.; Sheu, B.-C.; Tsai, J.-C.; Hsu, S.-M. Homopolyvalent antibody–antigen interaction kinetic studies with use of a dual-polarization interferometric biosensor. *Biosensors and Bioelectronics* **2006**, *22*, 715–721.

(34) Ymeti, A. et al. Fast, Ultrasensitive Virus Detection Using a Young Interferometer Sensor. *Nano Letters* **2007**, *7*, 394–397.

(35) Murib, M. S.; Martens, D.; Bienstman, P. Label-free real-time optical monitoring of DNA hybridization using SiN Mach–Zehnder interferometer-based integrated biosensing platform. *Journal of Biomedical Optics* **2018**, *23*, 1.

(36) Özalp, V. C. Dual-polarization interferometry for quantification of small molecules using aptamers. *Analytical and Bioanalytical Chemistry* **2012**, *402*, 799–804.

(37) Sun, Y.; Fan, X. Optical ring resonators for biochemical and chemical sensing. *Analytical and Bioanalytical Chemistry* **2011**, *399*, 205–211.

(38) Ramachandran, A.; Wang, S.; Clarke, J.; Ja, S.; Goad, D.; Wald, L.; Flood, E.; Knobbe, E.; Hryniewicz, J.; Chu, S.; Gill, D.; Chen, W.; King, O.; Little, B. A universal biosensing platform based on optical micro-ring resonators. *Biosensors and Bioelectronics* **2008**, *23*, 939–944.

(39) Vollmer, F.; Arnold, S.; Braun, D.; Teraoka, I.; Libchaber, A. Multiplexed DNA quantification by spectroscopic shift of two microsphere cavities. *Biophysical journal* **2003**, *85*, 1974–9.

(40) Zhu, H.; White, I. M.; Suter, J. D.; Zourob, M.; Fan, X. Opto-fluidic micro-ring resonator for sensitive label-free viral detection. *The Analyst* **2008**, *133*, 356.

(41) Qavi, A. J.; Kindt, J. T.; Gleeson, M. A.; Bailey, R. C. Anti-DNA:RNA Antibodies and Silicon Photonic Microring Resonators: Increased Sensitivity for Multiplexed microRNA Detection. *Analytical Chemistry* **2011**, *83*, 5949–5956.

(42) Pitruzzello, G.; Krauss, T. F. Photonic crystal resonances for sensing and imaging. *Journal of Optics* **2018**, *20*, 073004.

(43) Lee, M. R.; Fauchet, P. M. Two-dimensional silicon photonic crystal based biosensing platform for protein detection. *Optics Express* **2007**, *15*, 4530.

(44) Chakravarty, S.; Lai, W.-C.; Zou, Y.; Drabkin, H. A.; Gemmill, R. M.; Simon, G. R.; Chin, S. H.; Chen, R. T. Multiplexed specific label-free detection of NCI-H358 lung cancer cell line lysates with silicon based photonic crystal microcavity biosensors. *Biosensors and Bioelectronics* **2013**, *43*, 50–55.

(45) Pal, S.; Yadav, A. R.; Lifson, M. A.; Baker, J. E.; Fauchet, P. M.; Miller, B. L. Selective virus detection in complex sample matrices with photonic crystal optical cavities. *Biosensors and Bioelectronics* **2013**, *44*, 229–234.

(46) Scullion, M.; Fischer, M.; Krauss, T.; Scullion, M. G.; Fischer, M.; Krauss, T. F. Fibre Coupled Photonic Crystal Cavity Arrays on Transparent Substrates for Spatially Resolved Sensing. *Photonics* **2014**, *1*, 412–420.

(47) Woliński, T. Polarization in Optical Fibers. *Acta Physica Polonica A* **1999**, *95*, 749–760.

(48) Hecht, E., *Optics, 4th ed.* Addison Wesley: 2002.

(49) Kersey, A.; Davis, M.; Patrick, H.; LeBlanc, M.; Koo, K.; Askins, C.; Putnam, M.; Friebele, E. Fiber grating sensors. *Journal of Lightwave Technology* **1997**, *15*, 1442–1463.

(50) Mihailov, S. J.; Mihailov; J., S. Fiber Bragg Grating Sensors for Harsh Environments. *Sensors* **2012**, *12*, 1898–1918.

(51) Asseh, A.; Sandgren, S.; Ahlfeldt, H.; Sahlgren, B.; Stubbe, R.; Edwall, G. Fiber Optical Bragg Grating Refractometer. *Fiber and Integrated Optics* **1998**, *17*, 51–62.

(52) Li, T.; Dong, X.; Chan, C. C.; Zhao, C.-L.; Zu, P. Humidity Sensor Based on a Multimode-Fiber Taper Coated With Polyvinyl Alcohol Interacting With a Fiber Bragg Grating. *IEEE Sensors Journal* **2012**, *12*, 2205–2208.

(53) Schroeder, K.; Ecke, W.; Mueller, R.; Willsch, R.; Andreev, A. A fibre Bragg grating refractometer. *Measurement Science and Technology* **2001**, *12*, 757.

(54) Fang, X.; Liao, C. R.; Wang, D. N. Femtosecond laser fabricated fiber Bragg grating in microfiber for refractive index sensing. *Optics Letters* **2010**, *35*, 1007.

(55) Chryssis, A.; Lee, S.; Lee, S.; Saini, S.; Dagenais, M. High sensitivity evanescent field fiber Bragg grating sensor. *IEEE Photonics Technology Letters* **2005**, *17*, 1253–1255.

(56) Sridevi, S.; Vasu, K.; Asokan, S.; Sood, A. Sensitive detection of C-reactive protein using optical fiber Bragg gratings. *Biosensors and Bioelectronics* **2015**, *65*, 251–256.

(57) Chiavaioli, F.; Baldini, F.; Tombelli, S.; Trono, C.; Giannetti, A. Biosensing with optical fiber gratings. *Nanophotonics* **2017**, *6*, 663–679.

(58) Laffont, G.; Ferdinand, P. Tilted short-period fibre-Bragg-grating-induced coupling to cladding modes for accurate refractometry. *Measurement Science and Technology* **2001**, *12*, 765–770.

(59) Albert, J.; Shao, L.-Y.; Caucheteur, C. Tilted fiber Bragg grating sensors. *Laser & Photonics Reviews* **2013**, *7*, 83–108.

(60) Chan, C.-F.; Chen, C.; Jafari, A.; Laronche, A.; Thomson, D. J.; Albert, J. Optical fiber refractometer using narrowband cladding-mode resonance shifts. *Applied Optics* **2007**, *46*, 1142.

(61) Maguis, S.; Laffont, G.; Ferdinand, P.; Carbonnier, B.; Kham, K.; Mekhalif, T.; Millot, M.-C. Biofunctionalized tilted Fiber Bragg Gratings for label-free immunosensing. *Optics Express* **2008**, *16*, 19049.

(62) Vengsarkar, A.; Lemaire, P.; Judkins, J.; Bhatia, V.; Erdogan, T.; Sipe, J. Long-period fiber gratings as band-rejection filters. *Journal of Lightwave Technology* **1996**, *14*, 58–65.

(63) Xuewen Shu; Lin Zhang; Bennion, I. Sensitivity characteristics of long-period fiber gratings. *Journal of Lightwave Technology* **2002**, *20*, 255–266.

(64) Bhatia, V.; Vengsarkar, A. M. Optical fiber long-period grating sensors. *Optics letters* **1996**, *21*, 692–694.

(65) Falciai, R.; Mignani, A. G.; Vannini, A. Long period gratings as solution concentration sensors. *Sensors Actuators B* **2001**, *74*, 74–77.

(66) Patrick, H.; Kersey, A.; Bucholtz, F. Analysis of the response of long period fiber gratings to external index of refraction. *Journal of Lightwave Technology* **1998**, *16*, 1606–1612.

(67) Korposh, S.; Lee, S.-W.; James, S. W.; Tatam, R. P. Refractive index sensitivity of fibre-optic long period gratings coated with SiO ₂ nanoparticle mesoporous thin films. *Measurement Science and Technology* **2011**, *22*, 075208.

(68) Allsop, T.; Zhang, L.; Bennion, I. Detection of organic aromatic compounds in paraffin by a long-period fiber grating optical sensor with optimized sensitivity. *Optics Communications* **2001**, *191*, 181–190.

(69) DeLisa, M. P.; Zhang, Z.; Shiloach, M.; Pilevar, S.; Davis, C. C.; Sirkis, J. S.; Bentley, W. E. Evanescent wave long-period fiber bragg grating as an immobilized antibody biosensor. *Analytical Chemistry* **2000**, *72*, 2895–2900.

(70) Yang, J.; Sandhu, P.; Liang, W.; Xu, C. Q.; Li, Y. Label-free fiber optic biosensors with enhanced sensitivity. *IEEE Journal on Selected Topics in Quantum Electronics* **2007**, *13*, 1691–1696.

(71) Wang, D. Y.; Wang, Y.; Han, M.; Gong, J.; Wang, A. Fully distributed fiber-optic biological sensing. *IEEE Photonics Technology Letters* **2010**, *22*, 1553–1555.

(72) Pilla, P.; Sandomenico, A.; Malachovská, V.; Borriello, A.; Giordano, M.; Cutolo, A.; Ruvo, M.; Cusano, A. A protein-based biointerfacing route toward label-free immunoassays with long period gratings in transition mode. *Biosensors and Bioelectronics* **2012**, *31*, 486–491.

(73) Chiavaioli, F.; Biswas, P.; Trono, C.; Jana, S.; Bandyopadhyay, S.; Basumallick, N.; Giannetti, A.; Tombelli, S.; Bera, S.; Mallick, A.; Baldini, F. Sol-Gel-Based Titania-Silica Thin Film Overlay for Long Period Fiber Grating-Based Biosensors. *Analytical Chemistry* **2015**, *87*, 12024–12031.

(74) Quero, G. et al. Long period fi ber grating nano-optrode for cancer biomarker detection. *Biosensors and Bioelectronic* **2016**, *80*, 590–600.

(75) Liu, L.; Marques, L.; Correia, R.; Morgan, S. P.; Lee, S.-W.; Tighe, P.; Fairclough, L.; Korposh, S. Highly sensitive label-free antibody detection using a long period fibre grating sensor. *Sensors and Actuators B: Chemical* **2018**, *271*, 24–32.

(76) Chen, X.; Zhang, L.; Zhou, K.; Davies, E.; Sugden, K.; Bennion, I.; Hughes, M.; Hine, A. Real-time detection of DNA interactions with long-period fiber-grating-based biosensor. *Optics letters* **2007**, *32*, 2541–2543.

(77) Jang, H. S.; Park, K. N.; Kim, J. P.; Sim, S. J.; Kwon, O. J.; Han, G.; Lee, K. S. Sensitive DNA biosensor based on a long-period grating formed on the side-polished fiber surface. *Optics Express* **2009**, *17*, 3855–3860.

(78) Czarnecka, K. H.; Dominik, M.; Janczuk-Richter, M.; Niedziółka-Jönsson, J.; Bock, W. J.; Śmietana, M. In *Proceedings of SPIE - The International Society for Optical Engineering*, ed. by Chung, Y.; Jin, W.; Lee, B.; Canning, J.; Nakamura, K.; Yuan, L., International Society for Optics and Photonics: 2017; Vol. 10323, p 1032313.

(79) Smietana, M.; Bock, W. J.; Mikulic, P.; Ng, A.; Chinnappan, R.; Zourob, M. Detection of bacteria using bacteriophages as recognition elements immobilized on long-period fiber gratings. *Optics express* **2011**, *19*, 7971–7978.

(80) Tripathi, S. M.; Bock, W. J.; Mikulic, P.; Chinnappan, R.; Ng, A.; Tolba, M.; Zourob, M. Long period grating based biosensor for the detection of Escherichia coli bacteria. *Biosensors and Bioelectronics* **2012**, *35*, 308–312.

(81) Brzozowska, E.; Koba, M.; Śmietana, M.; Górska, S.; Janik, M.; Gamian, A.; Bock, W. J. Label-free Gram-negative bacteria detection using bacteriophage-adhesin-coated long-period gratings. *Biomedical Optics Express* **2016**, *7*, 829.

(82) Bandara, A. B.; Zuo, Z.; Ramachandran, S.; Ritter, A.; Heflin, J. R.; Inzana, T. J. Detection of methicillin-resistant staphylococci by biosensor assay consisting of nanoscale films on optical fiber long-period gratings. *Biosensors and Bioelectronics* **2015**, *70*, 433–440.

(83) Yang, F.; Chang, T.-L.; Liu, T.; Wu, D.; Du, H.; Liang, J.; Tian, F. Label-free detection of Staphylococcus aureus bacteria using long-period fiber gratings with functional polyelectrolyte coatings. *Biosensors and Bioelectronics* **2019**, *133*, 147–153.

(84) Liu, C.; Xu, B.; Zhou, L.; Sun, Z.; Mao, H.; Zhao, J.; Zhang, L.; Chen, X. Graphene oxide functionalized long period fiber grating for highly sensitive hemoglobin detection. *Sensors and Actuators B: Chemical* **2018**, *261*, 91–96.

(85) Baliyan, A.; Sital, S.; Tiwari, U.; Gupta, R.; Sharma, E. K. Long period fiber grating based sensor for the detection of triacylglycerides. *Biosensors and Bioelectronics* **2016**, *79*, 693–700.

(86) Baldini, F.; Brenci, M.; Chiavaioli, F.; Giannetti, A.; Trono, C. Optical fibre gratings as tools for chemical and biochemical sensing. *Analytical and Bioanalytical Chemistry* **2012**, *402*, 109–116.

(87) Chiavaioli, F.; Gouveia, C.; Jorge, P.; Baldini, F. Towards a Uniform Metrological Assessment of Grating-Based Optical Fiber Sensors: From Refractometers to Biosensors. *Biosensors* **2017**, *7*, 23.

Chapter 2

Influence of external factors on LPFG response[1]

2.1 Introduction

As shown in chapter 1, LPFGs are sensitive to external RI and may be used for biodetection. For standard LPFGs the sensitivity is the highest for external RIs close to that of the fiber cladding, while for external RIs close to that of water the sensitivity is considerably reduced [1]. The RI sensitivity of LPFG structures, which refers to their label-free biosensing capabilities, may be highly improved by optimizing the working point of the device up to dispersion turning point (DTP) of the higher order cladding modes. To predict the conditions of DTP occurrence it is possible to calculate the core and cladding modes dispersions as a function of e.g. grating period or cladding diameter. Dispersion curves for higher order cladding modes indicate the presence of turning point in which the slope of the curve changes sign from positive to negative. Around this point the RI sensitivity is the highest [1]. LPFGs working at DTP can be fabricated using the same methods as for traditional LPFGs (i.e. exposure to UV laser [2], CO_2 laser [3], femtosecond laser [4], or by electrical arc discharge [5]), but with very high production precision. LPFGs can be also tuned to DTP after fabrication by tapering [6], chemical etching [7], plasma etching

[1]Parts of this chapter have been published as:
Janczuk-Richter, M.; Dominik, M.; Koba, M.; Mikulic, P.; Bock, W.J.; Maćkowski, S.; Jönsson-Niedziółka, M.; Niedziółka-Jönsson, J.; Śmietana, M. *Journal of Lightwave Technology* **2019**, DOI: 10.1109/JLT.2019.2909947, ©2019 IEEE

[8], deposition of high-refractive-index thin film [9], or combination of those methods [10].

In case of the etching procedure, reduction of fiber cladding diameter decreases effective RI of cladding mode $n_{eff}^{clad,m}$ and induces resonance wavelength shift towards DTP [8, 11]. The response of the transmission spectrum of a LPFG to etching is illustrated in Figure 2.1. As can be seen, the resonances first get closer, then merge into single band at the DTP that finally disappears. Then, new resonance (corresponding to the coupling to the next cladding mode) appears and the cycle repeats. This behavior can be explained by calculating phase matching curves using couple mode theory (equation 1.5) and weakly guided approximation [12]. These curves show the coupling from the core to the cladding modes and there is a turning point in each curve. Around this point, a single mode is coupled at two wavelengths simultaneously [1, 9]. RI sensitivity is the highest just before the DTP is reached. Therefore, the spectral distance between the resonances should be minimized, but at the same time it should enable precise definition of resonance wavelengths (orange curve in Figure 2.1) [8]. For example, by using wet etching in hydrofluoric acid it was possible to increase refractive index sensitivity of LPFG with 165 μm period from 1350 to 1847 nm/RIU [7] in the RI range 1.335–1.360 RIU. With increasing external RI the resonances were moving away from each other. Utilization of combination of plasma etching and deposition of diamond-like carbon nanocoating enable obtaing a RI sensitivity of 12 000 nm/RIU in narrow RI range (1.3344–1.3355 RIU) [10].

Unfortunately (in case of refractometric applications), LPFGs are at the same time sensitive to other factors, such as temperature or strain (tension). Moreover, with the increase in RI sensitivity also sensitivities for other parameters increase. Although it makes LPFG suitable as physical parameters sensors, at the same time it may be problematic in case of biosensing applications. Shu et al. [1] demonstrated that the temperature sensitivity can reach 3.2 nm/°C for LPFG operating near DTP, while much lower sensitivity of 0.3 nm/°C was obtained for LPFG with the single resonance band away from DTP. The response of dual resonance LPFG was non-linear with a decrease in sensitivity with moving away from DTP. Similar results were shown for Al_2O_3-coated LPFGs [13]. By careful selection of deposition parameters LPFGs were tuned to DTP and it was demonstrated that both RI and temperature sensitivities were greatly increased in comparison with LPFG working away from DTP. The

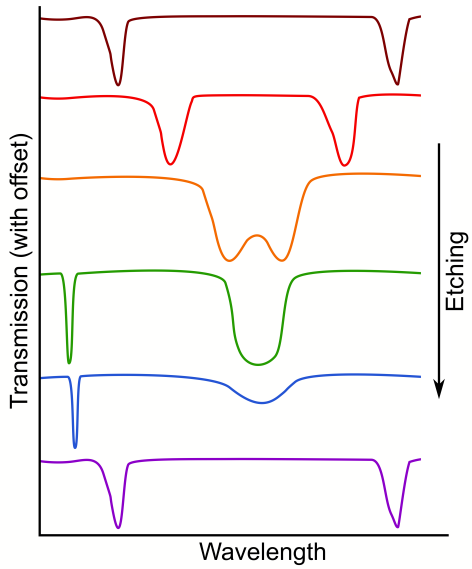

Figure 2.1: The response of the transmission spectrum of LPFG to etching for higher order cladding modes. During reduction of the fiber cladding diameter the resonances get closer, then merge into single band at the DTP, and finally disappear.

temperature sensitivity was $>$ 2nm/°C traced for only one resonance of the pair and RI sensitivity exceeded 8000 nm/RIU. Strain sensors based on LPFGs were also demonstrated. For a 133-μm period LPFG the strain sensitivity of 33.6 nm/mϵ was obtained and the individual peaks move closer together with increasing strain [1]. Grubsky et al. [14] demonstrated strain sensor with the resolution of 1 $\mu\epsilon$. In this case the wavelength remained fixed, but the decrease in power with the increase of strain was observed.

To sum up, many factors has to be taken into consideration while applying LPFG for biosensing. While measuring selected parameter it is necessary to keep all the other factors constant to obtain reliable results. I will address this problem during characterization of LPFGs optimized to DTP by chemical etching in HF, which will be presented in this chapter. In addition to RI sensitivity, I will also study the influence of surface drying and subsequent immersing in water on the optical response of the sensor. The problem has to be taken into account especially for long-term measurements, as in the case of biosensing. During biosensor functionalization and detection of the target the sensor surface is often exposed to subsequent drying and immersing steps that can influence the obtained results. The issue is important, yet still poorly

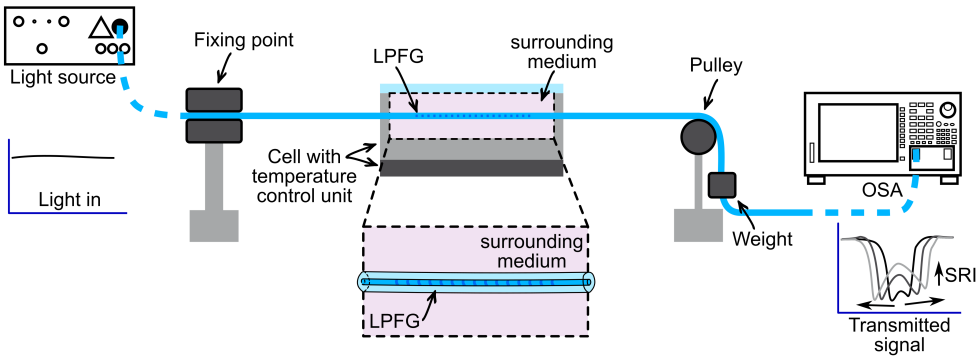

Figure 2.2: Schematic setup for the characterization of LPFG to external RI (not in scale). OSA - optical spectrum analyzer.

addressed. Thus, in this chapter I will investigate the behavior of LPFG during drying-immersing cycles, especially in the context of biosensor preparation.

2.2 Results and discussion

2.2.1 Refractive index sensitivity

The LPFGs used in the studies had grating period of 226.8 μm and were 5 cm long. The gratings were chemically etched to obtain sensing structures operating at the vicinity of the DTP, where the RI sensitivity for the certain cladding mode coupling is the highest. The process was carried out until dual resonance regime was observed in water and the resonances were in close proximity. To characterize the LPFG structures, measurements of the RI sensitivity were performed in water/glycerol solutions in various ratios. The measuring setup consisted of supercontinuum white-light laser source, optical spectrum analyzer, measuring closed (flow) cell with temperature control system, and positioning elements (Figure 2.2). Details are described in section 2.4. Results from RI sensitivity measurements were shown in Figure 2.3. As shown, with increasing RI of surrounding medium the resonances shifted in opposite directions. For the left (blue-shifting) resonance, the RI sensitivity reached almost 2,000 nm/RIU in the RI range 1.333–1.345 RIU (high sensitivity close to the DTP), then it decreased to about 1,150 nm/RIU for 1.35–1.40 RIU, and then increased again to about 1,900 nm/RIU for 1.41–1.44 RIU. The second increase in sensitivity is attributed to conditions, where external RI gets closer to that of the

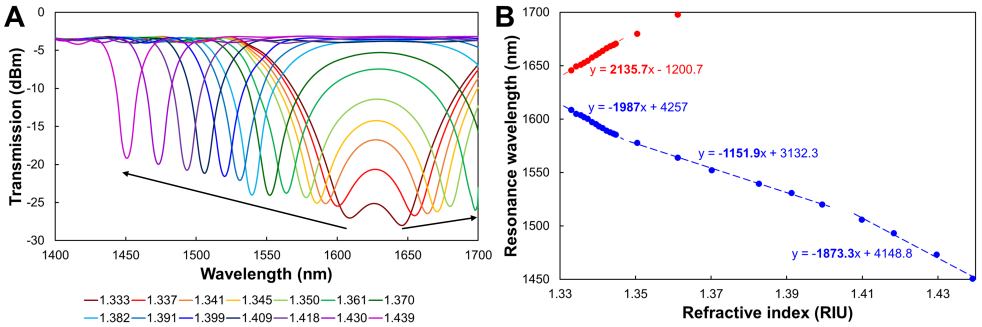

Figure 2.3: Response of the LPFG sensor to external RI. (A) Transmission spectra for selected external RIs. (B) Resonance wavelength dependence on RI for the left (blue-shifting) and right (red-shifting) resonances.

fiber cladding. For the right (red-shifting) resonance, the sensitivity exceeded 2,000 nm/RIU in the RI range close to water. For RI greater than 1.36 RIU it was impossible to determine the resonance wavelength due to spectral range limitations of the setup. All LPFGs used for further studies had similar RI sensitivity of about 2,000 nm/RIU for RIs close to that of water. RI sensitivities obtained for other optical fiber platforms are usually lower. For example the RI sensitivity of non-etched LPFG was 570 nm/RIU [15]. Better results were only obtained with application of high refractive index overlays, for example sensitivity over 20 000 nm/RIU was reached for Al_2O_3-coated LPFG in RI range close to that of water [13]. To compare the LPFG sensor performance to other optical techniques, a minimum detectable index resolution was calculated. Assuming a detectable spectral resolution of 0.01 nm (the resolution of Yokogawa AQ6370B spectrum analyzer), our sensor achieves a minimum possible detectable index resolution of about 10^{-6} RIU. This result is comparable to those for optical fiber coupled SPR biosensors and waveguide-based SPR biosensors which typically achieve detectable index change of around 10^{-5} to 10^{-6} RIU [16, 17]. Similar results were also presented for grating coupled optical waveguide interferometer [18]. It must be noted that some optical sensors are capable of detecting even smaller RI changes [19], but their fabrication is often much more complicated.

2.2.2 Soaking-drying experiments

During preliminary experiments with LPFG I observed that the optical signal changed after the sensor was dried and then immersed in the same liquid. Because the temperature, strain, and RI of external medium were constant during measurements, the changes might have been caused by some alterations of the cladding surface. In many studies concerning optical biosensing the authors are using flow cells to change the solutions during experiments and therefore they are avoiding surface drying. However, there are still many studies in which sensor surface is subjected to cycles of drying and immersing in liquids, for example during washing. Therefore, the problem was carefully studied in this thesis.

Immersing-drying cycles

First, I did the measurements with consecutive cycles of immersing of LPFG sensor in water and drying in air. All measurements were done in the open cell (shown in Figure 2.4A) and the spectra were recorded in water. In this configuration the sensor can be lifted and dried between measurements in different (or the same) liquid media. 5 or 10 measurements were done in each cycle followed by 60 s drying in air at atmospheric pressure. The resonance wavelength did not change during measurements in first water portion (Figure 2.5B, step 1). After drying and immersing again a significant change in the transmission spectrum was observed, but further measurements were repeatable until the next drying. Separation between the resonance peaks increased and the shift was the largest during the first water exchange cycle (> 5 nm). The more cycles were done, the smaller was the shift (Figure 2.5). This effect is caused by the decrease in RI sensitivity with the distance from DTP, but can be also attributed to the fact that the surface structure undergoes the biggest alterations during first drying steps and subsequent dryings have smaller effect. Observed changes, i.e., increasing separation between the peaks, indicate the increase of the effective refractive index of the investigated cladding mode. Since the temperature, strain, and external medium was the same during all the measurements (25.0 ± 0.1 °C, distilled water), the changes correspond to the surface conditions, i.e., increase in RI at certain depth inside and/or on the cladding. During drying and immersing in water the surface is exposed to stresses that may cause surface alterations and result in surface fracturing, shrinkage of pores (that may be formed during etching) and change in their size

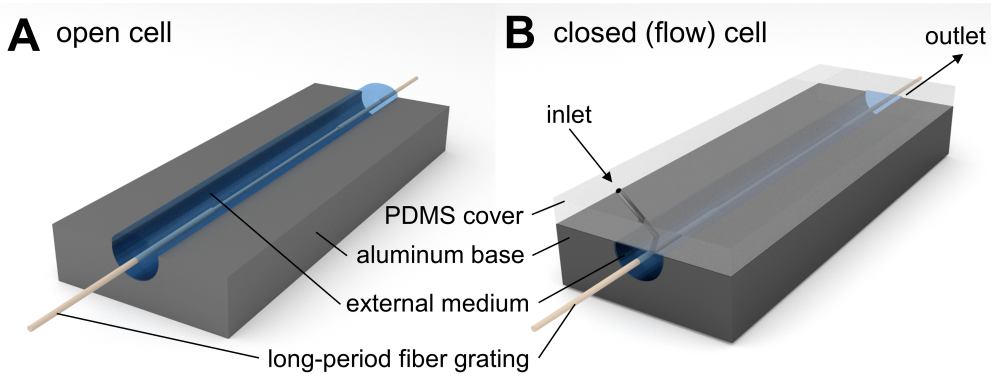

Figure 2.4: Schematic representation of the cells used for LPFG measurements: open (A) and closed (flow) (B). Aluminum base was supported with temperature control system.

and distribution [20]. Fused silica is widely considered to be water-soaking resistant, i.e., it does not allow for penetration of molecular water into its volume [21]. However, any fracture present on the surface, resulting, e.g. from drying, makes water penetration into the glass possible. This causes the glass just below the surface to swell, i.e., its specific volume increases, what is followed by induction of additional stress and tension on the surface and may cause crack growth [22–24]. All of these effects influence the state of the surface and result in the distortion of the RI distribution on the fiber surface and increase of the average local RI and in consequence have an impact on the optical response of the sensors [25, 26].

To confirm these findings, the cladding surface was investigated with scanning electron microscope in order to check the influence of immersing-drying cycles on the surface morphology. Additionally, I investigated the influence of HF etching, because it was previously shown that such etching of optical fiber can cause morphological changes of the cladding, such as roughening [27]. Fiber surface before etching, after etching, and after 10 cycles of immersing in water and drying in air was compared (Figure 2.6). According to SEM pictures, after etching fiber diameter was reduced from 123 μm (Figure 2.6A) to 117 μm (Figure 2.6B), but the surface remains the same as before etching, i.e. rugged but clear and free from significant surface damages or defects at nanoscale. As shown in Figure 2.6C, after etching and 10 cycles of immersing-drying, the fiber diameter remained unchanged, but various additional defects can be seen that were absent before. First, some macroscopic damages are present on the sur-

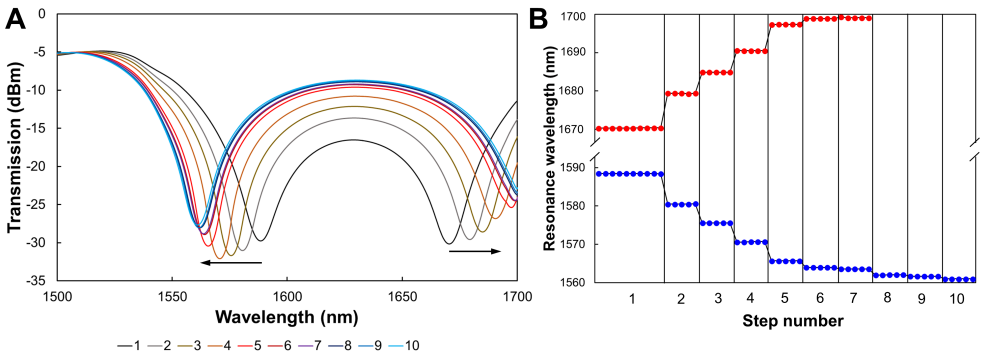

Figure 2.5: Response of the LPFG to subsequent immersing-drying steps. (A) Transmission spectra recorded in water before (1) and after (2-10) consecutive dryings of the fiber. (B) Corresponding resonance wavelength during measurements in water for left (blue-shifting) and right (red-shifting) resonances. Vertical lines show drying steps. For steps 8-10 for right resonance it was impossible to determine resonance wavelength due to spectral range limitations of the setup.

face (Figure 2.6C, middle panel). Second, in higher magnification (100,000×, Figure 2.6D) a lot of pores (marked with white arrows) and nanosized particles (marked with black arrows) can be observed on the surface. None of these features were present on the fiber analyzed before or just after the etching.

Energy-dispersive X-ray spectroscopy (EDS) was done to compare chemical composition of the surface for the fiber before and after immersing-drying experiment. As shown in Figure 2.7 signals from O and Si that originate from silica material were almost identical. Additionally, similar in intensities peaks from C and Al were also present for both the cases indicating the presence of typical carbon contamination and signal from aluminum SEM table, respectively. These results suggest that no external material was introduced from water, but observed defects are made in the cladding material. The possible effects of the drying and immersing in water on the cladding surface structure are schematically summarized in Figure 2.8.

Influence of organic solvent treatment on immersing-drying effect

After observing the changes in optical response caused by drying of the optical fiber, I checked if surface cleaning in the organic solvents may have an influence on those changes by e.g. facilitating evaporation of water from the surface or smoothing/removing the observed defects. First, reference measurements

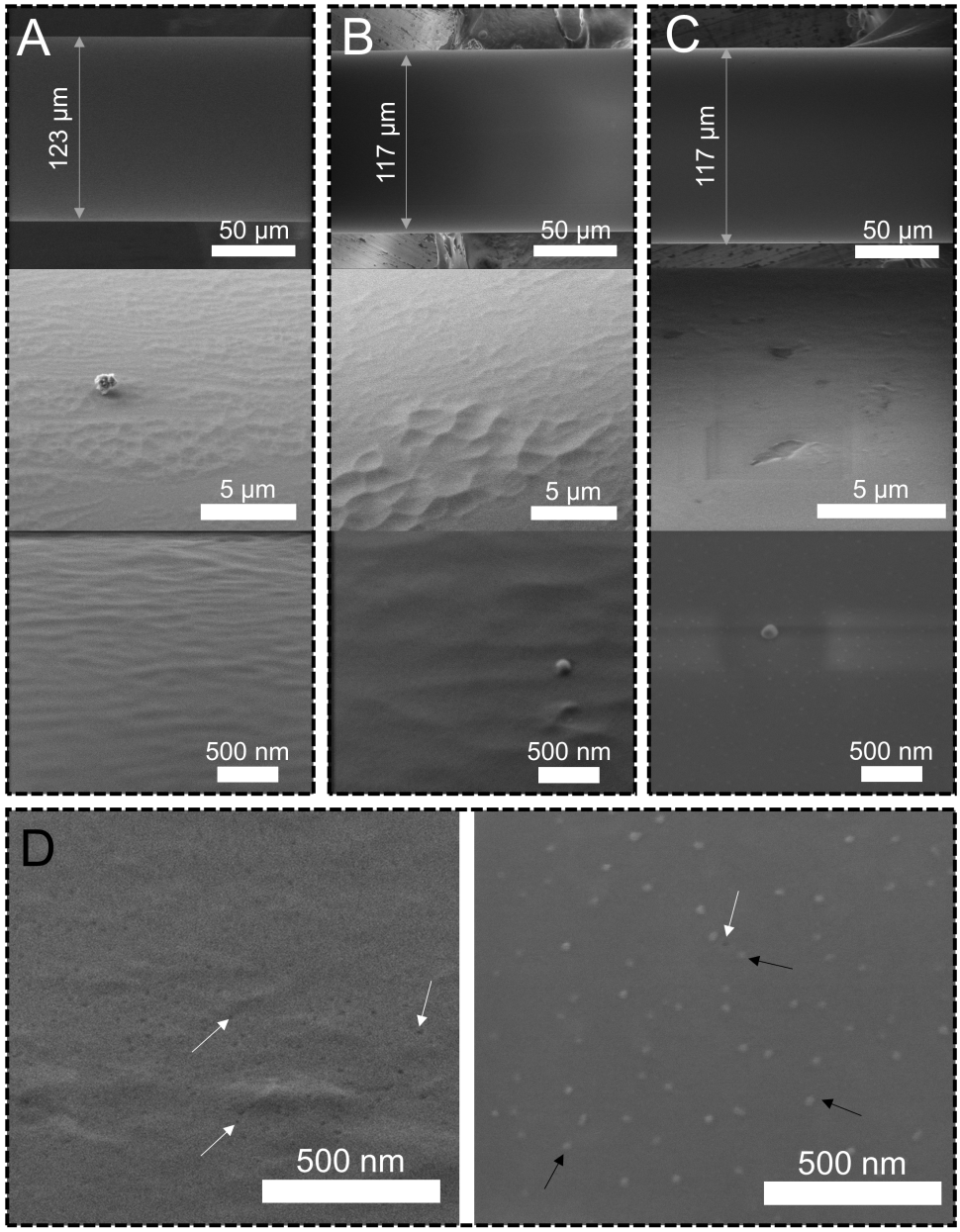

Figure 2.6: SEM images showing cladding surface (A) before etching in HF (B) after etching in HF, and (C) after 10 cycles of immersing-drying experiment. In (D) cladding surface in higher magnification after immersing-drying experiment is shown. Some pores and nanosized particles are marked with white and black arrows, respectively.

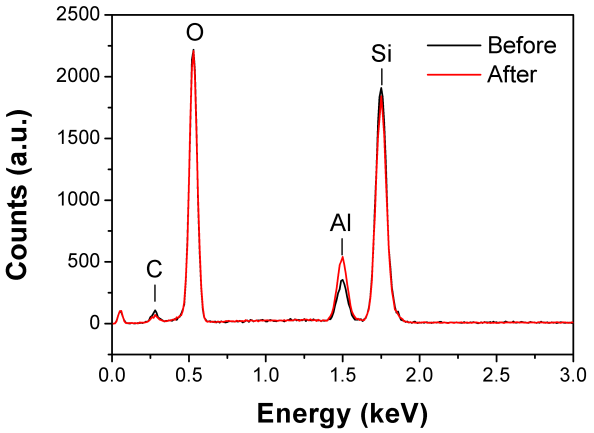

Figure 2.7: EDS spectra of the optical fiber before and after 10 cycles of immersing in water and drying in air.

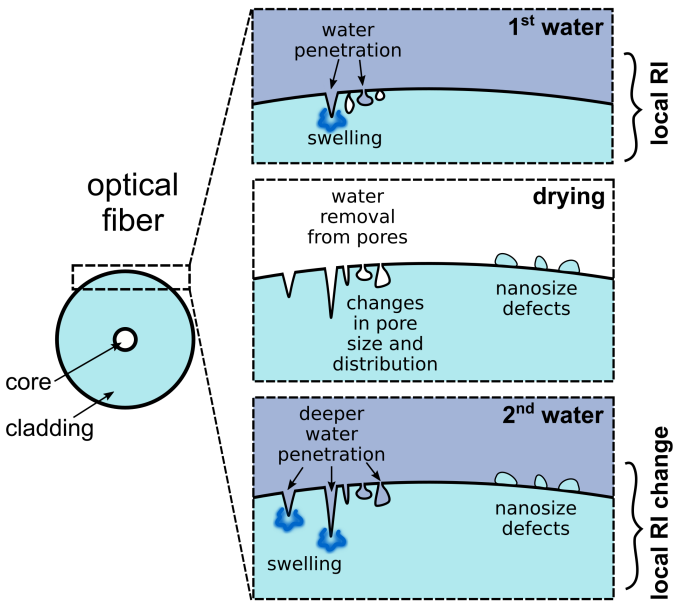

Figure 2.8: Schematic representation of the effects induced by drying of the optical fiber surface. During the first immersion in water, the pores are filled with water. Stress induced during drying of the surface causes alteration in the pore size and distribution, creation of new cracks and nanosized deformations. In next immersion in water the surface is altered, cracks are deeper, and swelling occurs at the crack tips. All these have an impact on the local RI.

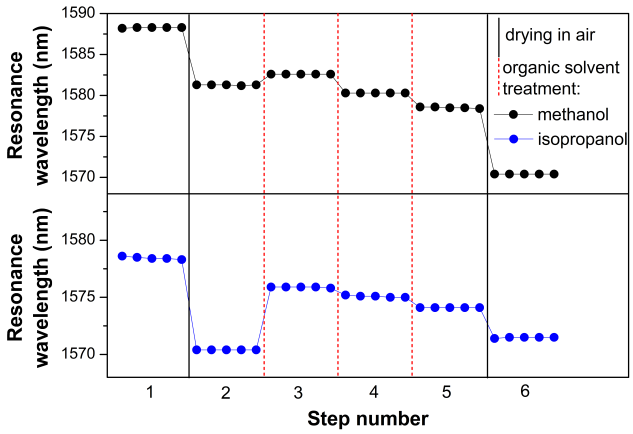

Figure 2.9: LPFG response during drying tests with the use of organic solvents: methanol (black) and isopropanol (blue). Shift of the left resonance wavelength during measurements in water was shown. Drying steps are marked with black lines and drying steps after immersion in organic solvent are marked with red dashed lines.

in distilled water were done and then the surface was dried as in previous experiment before next immersion in water. As previously, air drying of the fiber resulted in a significant blue shift of the left resonance (Figure 2.9, steps 1 and 2). Then, before next drying, the sensor was immersed in methanol or isopropanol for 60 s. After that the fiber was left to dry in air and then measured in water again. This treatment was repeated 3 times for each solvent. After first organic solvent treatment, the resonance wavelength shifted in opposite direction than in previously shown drying steps (step 3). This shift indicated decrease of the local RI and may correspond to the "cleaning effect" for both methanol and isopropanol, which helps to remove possible nanodefects and organic contamination and eliminate water from the surface and deep pores [28]. The effect of isopropanol treatment is higher as it dissolves broader range of organic and inorganic impurities. Interestingly, after next organic solvent treatments for both solvents the effect is inverted (blue shifts of the resonance wavelength, much smaller than with typical drying procedure), because the increase in local RI induced by drying dominates the smaller cleaning effect (steps 4 and 5).

Measurements in a Flow Cell (No Sample Drying)

According to the obtained results, unwanted changes in resonance wavelength induced by surface drying can be avoided if the fiber is kept in the flow system where the drying effect is not present. To check that, the measurements were done in specially designed flow cell. It consists of aluminum grooves with temperature control system closed with a polydimethylsiloxane (PDMS) cover. The inlet was made in the PDMS cover from one side and the liquid could flow out from the other side of the cell. In this system exchanges of liquids were done with a syringe without drying of the fiber surface (Figure 2.4B; more details in section 2.4). The measurements were performed in distilled water ($n_D = 1.333$ RIU) and in phosphate buffered saline (PBS, $n_D = 1.334$ RIU) in following order: 5 min in PBS, 5 min in PBS (new portion), 5 min in water, 5 min in water (new portion), and so on.

The use of flow cell resulted in obtaining stable and repeatable results. Almost no changes in resonance wavelengths were observed for the new portions of the same liquid, while significant differences were present between the measurements made in water and in PBS due to different RIs of these liquids (Figure 2.10). Some disturbances in resonance wavelengths were only observed during liquid injections (marked on Figure 2.10B with orange and grey for PBS and water flow, respectively) and the signal stabilized quickly after the flow was stopped.

By keeping the sensor wet throughout the measurements it was possible to avoid surface changes caused by the stresses introduced during drying and also no nanosized objects were deposited on the cladding surface due to elimination of the drying step and evaporation of water. Therefore, the results obtained in the closed cell are much more reliable and repeatable and this type of the system should be used for all measurements with optical fiber sensors made in liquids.

2.3 Conclusions

The influence of many parameters, such as temperature or strain, on the optical response of LPFG was already described in the literature. Therefore, in my work I was focused on the RI sensitivity (a main characteristic parameter of optical fiber refractometers) of LPFGs optimized to the DTP. I also did the analysis of the influence of sequential drying in air and immersing in water of

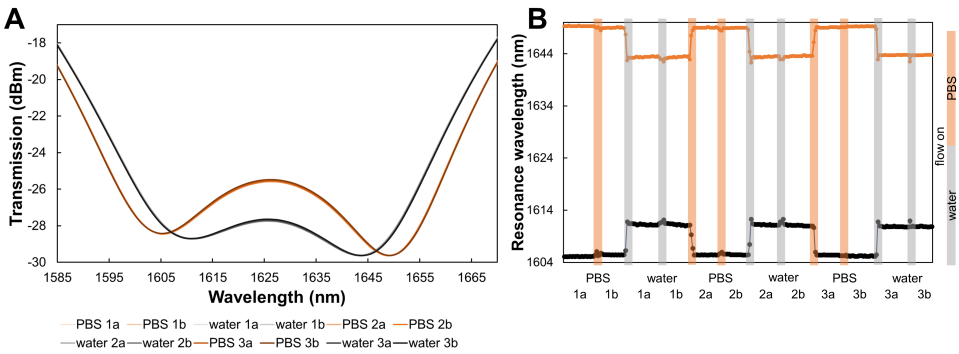

Figure 2.10: LPFG response during measurements in flow cell filled with PBS or water. (A) Transmission spectra recorded in PBS or water during each step. Spectra for each liquid (PBS or water) are overlapping. (B) Resonance wavelength during measurements in PBS and water for both resonances. Disturbs are observed during liquid injection marked in orange and gray for PBS and water, respectively.

the LPFG.

High RI sensitivity (∼2000 nm/RIU) obtained for LPFG that I was using indicated great potential for label-free biosensing. Additionally, very important findings concerning LPFG surface drying were demonstrated in this chapter. The changes in the optical response observed in drying-immersing experiment indicate the possibility of getting misleading conclusions during any experiments in which the liquids are exchanged with the drying of the sensor surface, especially in studies of optical fiber biosensors. Although many optical sensors are studied in flow systems, in which the surface drying is limited, there are still many new works where the surface is subjected to multiple drying steps during detection of an analyte. In those cases, the sensor response may correspond more to changes induced by surface deformations than any molecular binding and this may lead to obtaining false positive results. This should be taken into consideration, especially if only the responses before and after the biological or chemical procedure are compared. Importantly, drying-induced surface alterations can be eliminated by using closed flow cell where changes of liquids take place with no drying of sensor surface. Thanks to those findings, the flow cell was used in my studies for all other measurements with LPFG-based sensors.

2.4 Materials and methods

Chemicals and materials

HF acid, ammonium fluoride, acetone, ethanol, methanol, glycerol, and phosphate buffered saline (PBS) tablets were purchased from Sigma Aldrich. PBS consists of 0.01 M phosphate buffer, 0.0027 M potassium chloride and 0.137 M sodium chloride, pH 7.4 at 25 °C. Polydimethylsiloxane (PDMS) precursor (Sylgard 184 Silicone Elastomer) and curing agent were purchased from Dow Corning GmbH, Germany.

LPFG fabrication and etching

The LPFGs were written in single-mode hydrogen-loaded Corning SMF28 fiber using a Pulse Master 840 high-power KrF excimer laser (λ = 248 nm) from Light Machinery with pulse repetition rate 100 Hz, pulse duration 12 ns, and peak pulse energy 10 mJ. The UV exposure was done through a chromium amplitude mask with period Λ = 226.8 μm on the 5-cm-long fiber section for about 7 minutes and then LPFGs were annealed at 150 °C for 4 h. The LPFGs fabricated this way had a single resonance at the wavelength of λ = 1245 nm due to coupling of the $LP_{0,9}$ cladding mode [13]. As produced LPFGs were obtained from Professor W. J. Bock (Centre de recherche en photonique, Université du Québec en Outaouais, Canada). In order to tune the LPFGs up to DTP and thus enhance their RI sensitivity, the fiber cladding was etched in 40% HF acid for 3 min and then in mixture of 40% HF acid and ammonium fluoride (1:6) for about 1 min. For the optical transmission monitoring a Yokogawa AQ6370B spectrum analyzer and a Leukos SM30 supercontinuum white-light laser source were used. The etching procedure resulted in obtaining a sensing structure operating at the vicinity of the DTP, where the dual resonance regime can be observed. The spectral distance between the resonances measured in water was between 30 and 100 nm depending on the sample (due to little difference in etching time). The RI sensitivity was measured by immersing the sensor structures in glycerol/water solutions with RIs in the range n_{ext} = 1.333–1.439 RIU. The RI of the solutions was determined using a Rudolph J57 automatic refractometer.

Measuring setup and cells

The optical transmission of the LPFG was monitored in the range of λ = 1400–1700 nm or λ = 1500–1700 nm depending on specific needs. Ambient

temperature was set to 25 °C and the tension of the optical fiber was kept constant during all the measurements. Investigations of drying influence were conducted in two different configurations, namely open and closed (flow cell) setups, while RI sensitivity was measured in closed setup. In the open cell the fiber was placed and measured in the liquid-filled aluminum groove supported by a temperature control system (accuracy of 0.1 °C). The length of the cell was 90 mm and the volume of the groove was 700 μL. During liquid exchanges the sensor had time (about 60 s) to dry in air (Figure 2.4A). The closed setup included a specially designed flow cell consisting of aluminum grooves (90 mm long, 700 μL), temperature control system and polydimethylsiloxane cover. A PDMS precursor and a curing agent were mixed at a ratio of 10 to 1, based on weight. The PDMS mixture was poured onto the flat-bottom container, then cured at 65 °C for 1.5 h, and precisely cut to fit the flow cell. The inlet was made in the PDMS cover from one side and the liquid could flow out from the other side of the cell. Liquid exchanges were made with a syringe without drying of the fiber (Figure 2.4B), each time at least 800 μL was injected to the cell to completely replace the previous solution.

Scanning electron microscopy

SEM images of the optical fiber surface were obtained using FEI Nova NanoSEM 450. Images were done both in high vacuum mode and in low vacuum mode. EDS data was obtained using an Octane Elect detector from EDAX in low vacuum mode with 20 kV beam energy. SEM and EDS measurements were done in collaboration with Dr. Martin Jönsson-Niedziółka.

2.5 References

(1) Xuewen Shu; Lin Zhang; Bennion, I. Sensitivity characteristics of long-period fiber gratings. *Journal of Lightwave Technology* **2002**, *20*, 255–266.

(2) Wong, R. Y. N.; Chehura, E.; Staines, S. E.; James, S. W.; Tatam, R. P. Fabrication of fiber optic long period gratings operating at the phase matching turning point using an ultraviolet laser. *Applied Optics* **2014**, *53*, 4669.

(3) Lan, X.; Han, Q.; Wei, T.; Huang, J.; Xiao, H. Turn-Around-Point Long-Period Fiber Gratings Fabricated by CO2 Laser Point-by-Point Irradiations. *IEEE Photonics Technology Letters* **2011**, *23*, 1664–1666.

(4) Shen, F.; Zhou, K.; Zhang, L.; Shu, X.; Shu, X. In *Asia Communications and Photonics Conference*, OSA: Washington, D.C., 2017, Su2A.104.

(5) Colaco, C.; Caldas, P.; Del Villar, I.; Chibante, R.; Rego, G. Arc-Induced Long-Period Fiber Gratings in the Dispersion Turning Points. *Journal of Lightwave Technology* **2016**, *34*, 4584–4590.

(6) Chaubey, S.; Kher, S.; Oak, S. M. In *2011 7th International Workshop on Fibre and Optical Passive Components*, IEEE: 2011, pp 1–4.

(7) Biswas, P.; Basumallick, N.; Bandyopadhyay, S.; Dasgupta, K.; Ghosh, A.; Bandyopadhyay, S. Sensitivity Enhancement of Turn-Around-Point Long Period Gratings By Tuning Initial Coupling Condition. *IEEE Sensors Journal* **2015**, *15*, 1240–1245.

(8) Śmietana, M.; Koba, M.; Mikulic, P.; Bock, W. J. Measurements of reactive ion etching process effect using long-period fiber gratings. *Optics express* **2014**, *22*, 5986–94.

(9) Korposh, S.; James, S.; Tatam, R.; Lee, S.-W. In *Current Trends in Short- and Long-period Fiber Gratings*; InTech: 2013, p 13.

(10) Smietana, M.; Koba, M.; Mikulic, P.; Bock, W. J. Combined Plasma-Based Fiber Etching and Diamond-Like Carbon Nanooverlay Deposition for Enhancing Sensitivity of Long-Period Gratings. *Journal of Lightwave Technology* **2016**, *34*, 4615–4619.

(11) Chen, X.; Zhou, K.; Zhang, L.; Bennion, I. Dual-peak long-period fiber gratings with enhanced refractive index sensitivity by finely tailored mode dispersion that uses the light cladding etching technique. *Applied Optics* **2007**, *46*, 451.

(12) Adams, M. J., *An introduction to optical waveguides*; Wiley: 1981, p 401.

(13) Śmietana, M.; Dominik, M.; Mikulic, P.; Bock, W. J. Temperature and refractive index sensing with Al2O3-nanocoated long-period gratings working at dispersion turning point. *Optics & Laser Technology* **2018**, *107*, 268–273.

(14) Grubsky, V.; Feinberg, J. Long-period fiber gratings with variable coupling for real-time sensing applications. *Optics Letters* **2000**, *25*, 203.

(15) Smietana, M.; Bock, W. J.; Mikulic, P.; Ng, A.; Chinnappan, R.; Zourob, M. Detection of bacteria using bacteriophages as recognition elements immobilized on long-period fiber gratings. *Optics express* **2011**, *19*, 7971–7978.

(16) Chiu, M.-H.; Wang, S.-F.; Chang, R.-S. D-type fiber biosensor based on surface-plasmon resonance technology and heterodyne interferometry. *Optics Letters* **2005**, *30*, 233.

(17) Suzuki, A.; Kondoh, J.; Matsui, Y.; Shiokawa, S.; Suzuki, K. Development of novel optical waveguide surface plasmon resonance (SPR) sensor with dual light emitting diodes. *Sensors and Actuators B: Chemical* **2005**, *106*, 383–387.

(18) Kozma, P.; Hámori, A.; Kurunczi, S.; Cottier, K.; Horvath, R. Grating coupled optical waveguide interferometer for label-free biosensing. *Sensors and Actuators B: Chemical* **2011**, *155*, 446–450.

(19) Patko, D.; Cottier, K.; Hamori, A.; Horvath, R. Single beam grating coupled interferometry: high resolution miniaturized label-free sensor for plate based parallel screening. *Optics Express* **2012**, *20*, 23162.

(20) Bentz, D. P.; Garboczi, E. J.; Quenard, D. A. Modelling drying shrinkage in reconstructed porous materials: application to porous Vycor glass. *Modelling and Simulation in Materials Science and Engineering* **1998**, *6*, 211.

(21) Ebert, W. *The effects of the glass surface area/solution volume ratio on glass corrosion: A critical review*; tech. rep. ANL- 94/34; Los Alamos, NM: Los Alamos National Laboratory (LANL), 1995.

(22) Thurn, J. Water diffusion coefficient measurements in deposited silica coatings by the substrate curvature method. *Journal of Non-Crystalline Solids* **2008**, *354*, 5459–5465.

(23) Wiederhorn, S. M.; Fett, T.; Rizzi, G.; Hoffmann, M. J.; Guin, J. P. The effect of water penetration on crack growth in silica glass. *Engineering Fracture Mechanics* **2013**, *100*, 3–16.

(24) Lindholm, E. A.; Li, J.; Hokansson, A.; Slyman, B.; Burgess, D. In *Proceedings of SPIE*, ed. by Limberger, H. G.; Matthewson, M. J., 2004; Vol. 5, p 25.

(25) Roizin, Y.; Gevelyuk, S.; Prokopovich, L.; Savin, D.; Rysiakiewicz-Pasek, E.; Marczuk, K. Water Absorption and Mechanical Properties of Silica Porous Glasses. *Journal of Porous Materials* **1997**, *4*, 151–155.

(26) Nielsen, K. H.; Kittel, T.; Wondraczek, K.; Wondraczek, L. Optical breathing of nano-porous antireflective coatings through adsorption and desorption of water. *Scientific Reports* **2015**, *4*, 6595.

(27) Zhong, N.; Liao, Q.; Zhu, X.; Wang, Y.; Chen, R. High-quality fiber fabrication in buffered hydrofluoric acid solution with ultrasonic agitation. *Applied optics* **2013**, *52*, 1432–40.

(28) Castaño-Álvarez, M.; Pozo Ayuso, D. F.; García Granda, M.; Fernández-Abedul, M. T.; Rodríguez García, J.; Costa-García, A. Critical points in the fabrication of microfluidic devices on glass substrates. *Sensors and Actuators B: Chemical* **2008**, *130*, 436–448.

Chapter 3

Surface modifications of optical fibers

3.1 Introduction

To obtain a functional biosensor, biological elements have to be immobilized on the sensor surface so they can act as a receptor for desired target. The choice of method depends on the sensor surface material as well as on the bioreceptor type and is crucial in the biosensor production process to obtain proper operation. Many approaches on how to immobilize biological molecules on the surfaces have been reported in the literature. For proteins the most commonly used methods are physical adsorption, covalent bonding, utilization of specific interactions (e.g. biotin-avidin, His-Tag system), and entrapment into polymer matrices [1].

Adsorption provides a straightforward single-step approach to functionalize the surface and it is a spontaneous, reversible dynamic process. Adsorbed proteins are bound to the surface via intermolecular forces, mainly ionic bonds, and hydrophobic or polar interactions. Unfortunately, physisorbed proteins may easily detach from the surface during measurements due to changes in conditions which can lead to false negative results especially in case of label-free biosensors [2]. Physical adsorption is also associated with poor binding of proteins on the surface and loss of protein activity [3]. Therefore, in case of biosensors, proteins are often immobilized on the surface by covalent bonding. Typically, covalent bonds are formed between functional groups of exposed amino acids and properly modified solid substrate resulting in irreversible bond-

ing with high surface coverage. The most commonly used functional groups in proteins are amine from lysine, carboxyl from aspartic or glutamic acid, and thiol from cysteine. Each group requires the solid surface of the sensor to be functionalized with other proper functional groups that can take part in the reaction. Table 3.1 shows examples of functional groups available in proteins and corresponding surface modifications.

Table 3.1: Functional groups available in proteins and required surface modifications [1].

Side groups	**Amino acids**	**Surface functionality**
$-NH_2$	lysine	carboxylic acid active ester (NHS) epoxy aldehyde
–COOH	aspartic acid, glutamic acid	amine
–SH	cysteine	maleimide vinyl sulfone pyridyil disulfide
–OH	serine, tyrosine	epoxy

Amine-carboxyl coupling is the most commonly used method for protein immobilization. Due to the presence of both amine and carboxyl groups on the protein surfaces two approaches are possible: (i) amine group in protein is bound to carboxyl- or active ester-modified surface, or (ii) carboxyl group in protein is used to make a covalent bond to amine-modified surface. To create a stable amide bond between amine and carboxyl groups it is necessary to use carboxyl-reactive crosslinkers that enable direct conjugation to primary amines. Typically, carbodiimide compounds are used, e.g., 1-ethyl-3-(-3-dimethylaminopropyl) carbodiimide hydrochloride (EDC). After carboxyl activation with EDC it can readily react with amines. Because EDC-activated carboxyl is unstable in aqueous solutions N-hydroxysuccinimide (NHS) is often included in EDC coupling protocols to create stable amine-reactive compounds. EDC couples NHS to carboxyls, forming an NHS ester that is considerably more stable and enable reaction with primary amines at physiological pH (around 7.4). EDC-NHS coupling is often used for receptor immobilization in biosensor

development [4]. For example, Pâslaru et al. demonstrated the immobilization of Immunoglubulin G on poly(vinylidene fluoride) surface using EDC-NHS reaction [5]. The surface was pretreated with radiofrequency plasma using CO_2 or N_2 and N_2/H_2 discharge gases to generate carboxyl or amine groups. Application of EDC and NHS for activation of carboxyl groups (on the surface or in protein) enable successful IgG immobilization. Novel approach with the utilization of EDC-NHS was shown by Sun et al. [6]. NHS reactive groups were introduced on the random sites of antibody and then electric field was used to orient the antibody before reaction with amine groups present on the gold surface. Other popular immobilization strategies use thiol groups from cysteine residues to covalently attach protein to maleimide activated, iodoacetyl-modified, or gold surfaces [7–9].

Covalent methods provide robust and usually quite simple protein immobilization. However, due to the presence of many binding sites in one protein molecule, the immobilization is random and protein may not be active after the procedure. Alternative immobilization is based on the biochemical affinity reactions than enable site-directed protein immobilization but often require protein engineering and surface modifications [10]. Affinity immobilization can be done with the use of biotin-avidin/streptavidin interaction that is one of the strongest non-covalent bond ($K_d = 10^{-15}M$) [11, 12]. In this method, proteins biotinylated by protein engineering or by chemical modifications are bound to avidin or straptavidin modified surfaces that are often commercially available. Strong bonding enable using harsh conditions during biochemical assays. Shafiee et al. demonstrated a label-free optical sensor based on nanostructured photonic crystals for detection of HIV in which biotinylated antibodies were bound to neutravidin-modified surface [13]. Other popular affinity immobilization method is based on hexahistidine-tagged (His-Tag) proteins [14]. His-tagged molecules are bound to the nitrilotriacetic acid-modified surface through metal-mediated complexation. One of the main advantage of this technique is the possibility of surface regeneration by using metal chelation agents, such as ethylenediaminetetraacetic acid (EDTA). This approach was used in number of sensing assays, e.g. for electrochemical or optical detection of bacterial lipopolisaccharide by immobilization of His-tagged toll-like receptor-4 or bacteriophage adhesin, respectively [15, 16]. In case of the immobilization of antibodies, utilization of protein A (or protein G) is favorable. Proteins A and G specifically interact with the tail region (F_c) of immunoglubulin G (IgG) en-

abling oriented binding of antibodies on the surface with antigen binding sites (F_{ab}) freely exposed. Protein A is very stable in harsh conditions and is widely used in immunosensors development, e.g. for SPR sensing of human growth hormone [17]. Despite having many advantages, affinity methods typically requires multiple steps of surface modifications and protein engineering.

Taking into account advantages and disadvantages of described methods I focused on covalent immobilization of proteins on an optical fiber surface. In order to make this procedure possible, proper functional groups have to be introduced onto the fiber surface. Optical fiber is the most often made of fused silica which is the glass consisting of silicon dioxide (silica) in amorphous (non-crystalline) form. One of the most commonly used methods for silica surfaces rich in surface-bound hydroxyl groups is modification with organosilanes [18]. This method is not limited to silica, but can be applied to different oxide surfaces (MO_x in which M can be a metal, semiconductor, or a material that forms surface-bound hydroxyl groups upon activation or in air). Typical silanes used for oxide surface modifications are $RSiX_3$ or RY_2SiX, where R is typically alkyl with desirable functional group (e.g. amine or carboxyl), X is a leaving group (e.g. chloride or alkoxy), and Y is alkyl group (usually methyl or isopropyl) [18].

Three-step mechanism of the silane monolayers formation was proposed in the literature(Figure 3.1) [18]. In case of $RSiX_3$ silane, in the first step, water molecules adsorbed on the polar oxide surface hydrolyze the organosilanes to create hydroxysilanes. Then, hydroxysilanes are hydrogen bonded to the oxide surface and are capable of lateral movement across the surface. Attractive forces between neighboring silanes (e.g. van der Waals forces, hydrogen-bonding, dipole-dipole interactions) cause aggregation and reduction of mobility. At the end, Si-O-Si bonds are formed by condensation between Si-OH groups and surface -OH groups or with neighboring silanol groups. Surface modification with silanes is typically done by either reaction in solution, or in vapor phase. For reaction in solution, organic solvents are required, and the crucial factors are solvent polarity, viscosity, and amount of water available to hydrolyze the silane [19, 20]. Unfortunately, in most cases silane films prepared from solution are not uniform and hard to reproduce, which limit their application potential [21]. Therefore, the vapor phase reactions, described first by Haller [22], are often used instead. They offer limited formation of siloxane oligomers and surface contamination, and thus are more reproducible and effective [23,

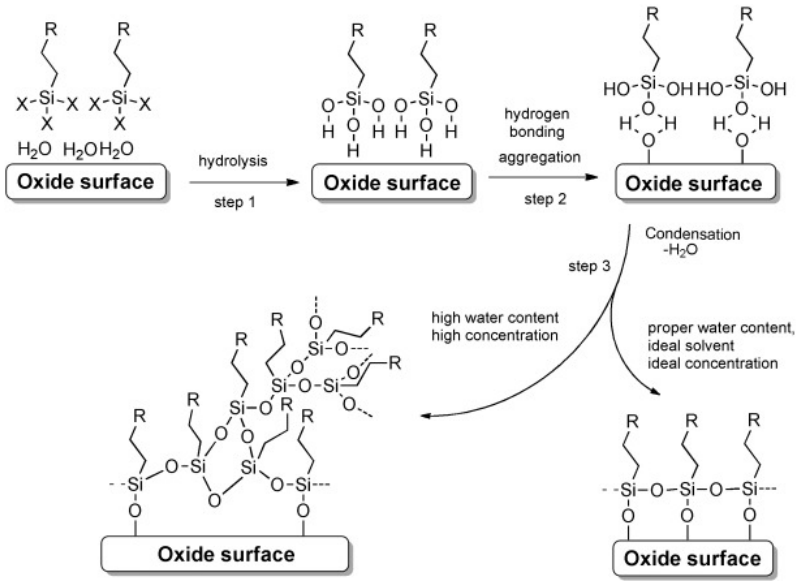

Figure 3.1: Three-step mechanism of the formation of silane monolayer on oxide surface. Depending on the reaction conditions step 3 may result in ordered laterally cross-linked monolayer or disordered inhomogeneous multilayer. Reproduced with permission from [18]. Copyright 2014 Wiley-VCH Verlag GmbH & Co. KGaA, Weinheim.

24]. Both reaction schemes are widely used in industrial and research applications. Modifications with silanes are often applied for preparation of water- and oil-repellent surfaces, to increase material durability, and to introduce proper functional groups onto the oxide surfaces [25–27].

3.2 Results and discussion

3.2.1 Silanization of silicon wafers

For the development of LPFG biosensors I decided to use covalent bonding of proteins onto sensing surface. Therefore, first step was the surface treatment to introduce appropriate functional groups which enable covalent bonding with proteins. In this work I was using two silanes, (3-aminopropyl)triethoxysilane (APTES) and 3-(triethoxysilyl)propylsuccinic anhydride (TESPSA), to introduce amine or succinic anhydride functional groups, respectively (Figure 3.2) [28, 29]. Vapor methods were selected for APTES and TESPSA modifications to avoid morphological irregularities that may occur during silane layer for-

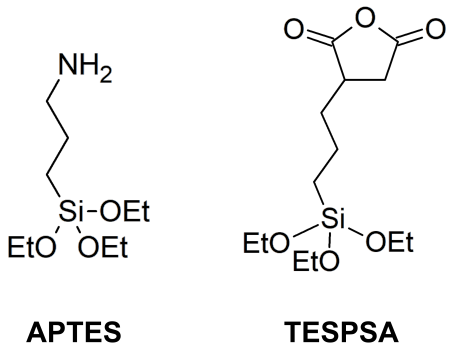

Figure 3.2: Chemical structure of (3-Aminopropyl)triethoxysilane (APTES) and 3-(triethoxysilyl)propylsuccinic anhydride (TESPSA).

mation from solution [21]. I adapted literature methods for both silanes and modify the procedures in order to use them for flat and non-flat (e.g. optical fiber) surfaces. To chose the best reaction conditions I first investigated the modification of oxidized silicon wafers with APTES and TESPSA performed with different parameters by X-ray photoelectron spectroscopy (XPS).

Modification with APTES was done according to modified procedure that is typically used for functionalization of atomic force microscopy probes [28] (technical details available in section 3.4). I tested different reaction times and also applied additional external heating (IR lamp) to facilitate APTES evaporation. Surface composition (in at%) from XPS spectra before and after modification with APTES are shown in table 3.2 (typical procedure with different times) and table 3.3 (procedure with additional heating). Detailed information about chemical states of particular atoms are available in appendix 1.

Reference sample (without modification) of oxidized silicon wafer had high amount of silicon and oxygen, but also typical carbon and nitrogen contamination. XPS results revealed also that a significant part of oxygen is present on the surface as adsorbed water molecules that is very beneficial for the reaction with silanes [30]. For evaluation of APTES modification efficiency I compared amount of nitrogen (that is a part of amine group) for different procedures. The more the total nitrogen on the surface, the more APTES molecules were bound to the surface. Also, increase of carbon amount was an indicator of effective modification. For all samples modified without external heating (see table 3.2) the increase of total nitrogen and carbon concentration was observed indicating successful surface functionalization. Interestingly, the highest amount of nitro-

gen was observed for the sample modified for 1 h. However, such a high nitrogen content (∼10 at%) may suggest the formation of disordered multilayer instead of a monolayer. The most satisfactory results were therefore obtained for 2- and 5-hour long reactions. The application of additional heating by IR lamp resulted in much lower amount of APTES bound to the surface as shown by total nitrogen concentration in table 3.3. Therefore, for all further modifications with APTES I chose 2-hour procedure without additional heat source.

Table 3.2: Total concentration of elements (in at%) from XPS spectrum before and after surface modification with APTES.

	Reference	APTES 1 h	APTES 2 h	APTES 5 h	APTES 8 h
Si	12.7	2.1	2.4	23.0	20.4
O	72.6	34.6	57.4	34.4	40.0
C	13.1	53.5	34.4	40.0	43.9
N	**1.6**	**9.9**	**5.8**	**5.8**	**7.0**

Table 3.3: Total concentration of elements (in at%) from XPS spectrum before and after surface modification with APTES using additional heating.

	Reference	APTES 1 h/IR	APTES 2 h/IR	APTES 5 h/IR
Si	12.7	28.5	29.5	27.9
O	72.6	47.2	47.1	38.2
C	13.1	21.2	20.3	31.6
N	**1.6**	**2.9**	**3.1**	**2.2**

Formation of TESPSA monolayer was done according to the literature procedure originally used for the modification of flat glass slides [29]. I compared the XPS results for 2- and 4-hour reaction time (table 3.4, detailed information available in appendix 1).

The higher amount of carbon was observed for both modified samples, which was the indication od successful surface functionalization with TESPSA. Better results were obtained for longer procedure and therefore for all further measurements I chose four-hour modification procedure with TESPSA.

Table 3.4: Total concentration of elements (in at%) from XPS spectrum before and after surface modification with TESPSA.

	Reference	TESPSA 2 h	TESPSA 4 h
Si	12.7	27.4	35.3
O	72.6	50.3	38.5
C	**13.1**	**20.5**	**24.9**
N	1.6	0.8	0.7

3.2.2 Modifications of glass slides

For protein immobilization on the sensor surface covalent non-oriented bonding was chosen due to versatility and strong binding, but also due to quite straightforward procedures that do not require many steps or complicated protein engineering. Moreover, in case of optical fiber sensors, in which working principle is evanescent wavefield, the distance of detected molecules from sensor surface should be minimized. Therefore, I decided not to use oriented immobilization of antibodies, e.g. on protein A/G, as it would cause the detection step to occur further from the surface and may decrease sensitivity of LPFG biosensors. I functionalized the surface with APTES or TESPSA as described above to introduce functional groups that are useful for covalent immobilization of proteins. Additionally, as a comparison I tested also physical adsorption on bare and modified surface. Green fluorescent protein (GFP) was immobilized on the surfaces to check the efficiency of protein immobilization by fluorescent confocal microscopy. All the methods were described in the Materials and methods section 3.4. Briefly, five methods were tested (summarized on Figure 3.3):

1. Physisorption on bare surface.
2. Physisorption on APTES-modified surface.
3. Covalent bonding of EDC-activated protein to APTES-modified surface.
4. Covalent bonding to TESPSA-modified surface.
5. Covalent bonding to TESPSA-modified surface with the utilization of EDC.

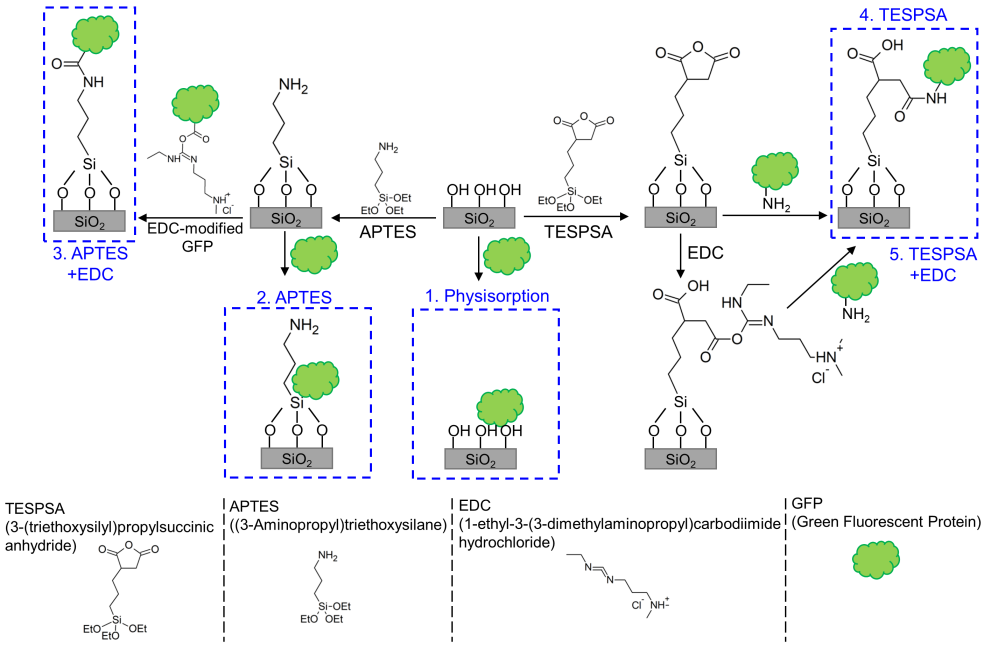

Figure 3.3: Summary of surface functionalization methods.

To test the usefulness of APTES- and TESPSA-modified surfaces in biosensor development I first investigate immobilization efficiency of green fluorescent protein on glass coverslips. Glass substrates were modified with APTES or TESPSA as described in section 3.4. As mentioned above I tested five methods, two of them with physical adsorption of the protein on bare or modified surface and three involving covalent bonding (Figure 3.3). Results from confocal microscope are shown in Figure 3.4.

As can be seen, physisorption methods, both on bare and APTES-modified surface, were not very efficient. In both cases the amount and quality of immobilized protein film (manifested as the intensity and distribution of fluorescence) was poor. In both methods only single protein aggregates were visible as green spots and the majority of glass surface remained free from proteins (no fluorescence coming from GFP). Much better results were obtained with covalent bonding methods. Method with APTES and EDC-activated GFP resulted in good surface coverage. In this method carboxyl-reactive carbodiimide (EDC) was added to the protein sample. EDC reacts with carboxyl groups to form an active O-acylisourea intermediate that can be easily displaced by nucleophilic attack of primary amines. Amine group forms an amide bond with the original

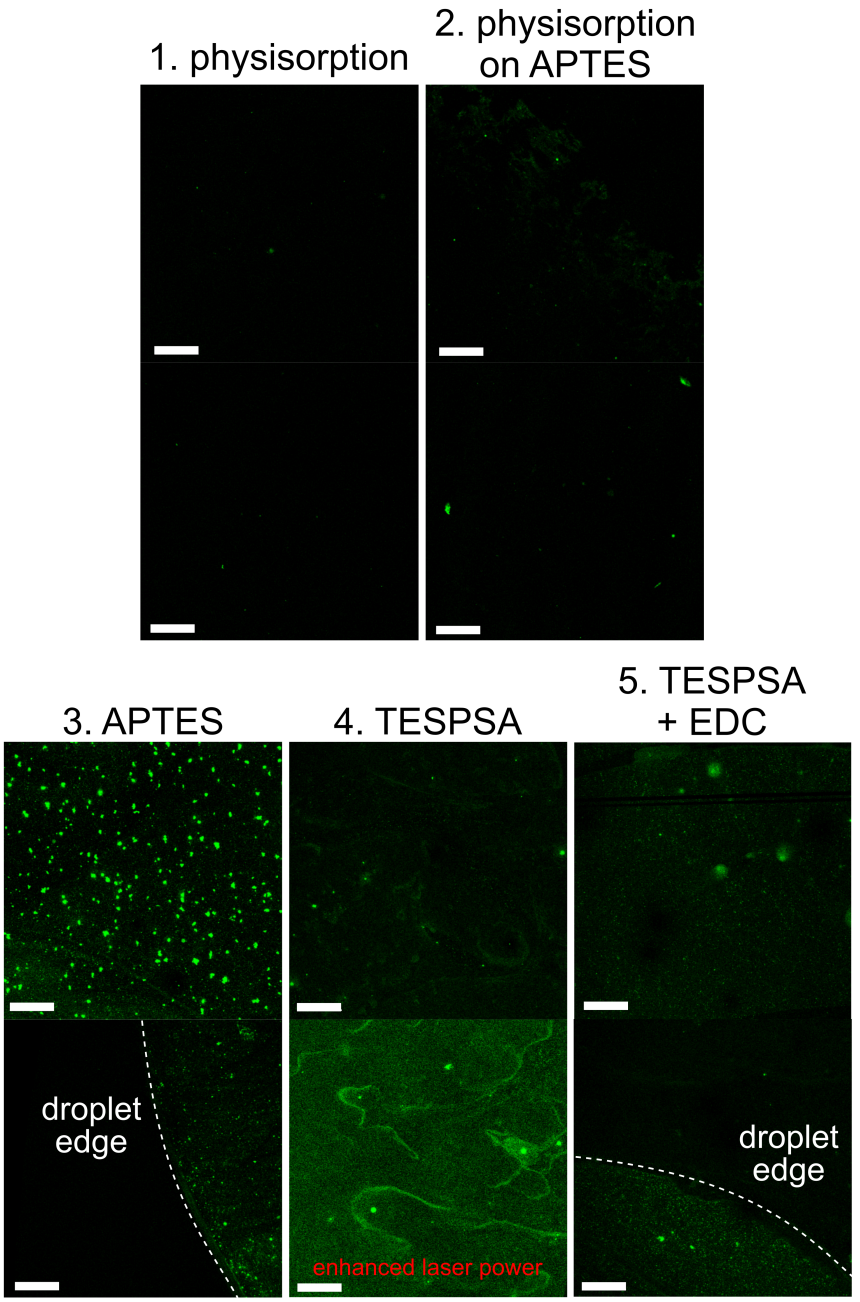

Figure 3.4: Confocal microscopy images of glass slides modified with GFP using different immobilization methods: (1) Physisorption on bare surface; (2) Physisorption on APTES-modified surface; (3) Covalent bonding to APTES-modified surface; (4) Covalent bonding to TESPSA-modified surface; (5) Covalent bonding to TESPSA-modified surface with the utilization of EDC. Scale bar 100 μm. For each method two different spots were shown.

carboxyl group, and soluble EDC by-product is released. The O-acylisourea intermediate is unstable in aqueous solutions and therefore reaction with amine groups have to be done just after activation. EDC coupling protocols often includes N-hydroxysuccinimide (NHS) to stabilize amine-reactive intermediates. However, it was shown that using EDC alone gave better immobilization efficiency than using EDC and NHS [4]. Therefore in my work I was using only EDC. The main disadvantage of this method in case of protein immobilization is the formation of protein aggregates. This is caused by creation of amide bonds between activated carboxyl groups on one protein molecule with amine groups present on another protein molecule. This may lead to the formation of big protein aggregates in the solution that were then immobilized on the surface and in our case were easily visible on the images due to their high fluorescence. In protocols with TESPSA and EDC-activated TESPSA almost uniform surface coverage was obtained and only some aggregates were present. In "TESPSA" method proteins were covalently bound to the surface in the ring-opening reaction between succinic anhydride on the surface and amine groups on the protein surface [29]. Proteins probably formed a monolayer that was manifested as week but uniform fluorescence. For further analysis the laser power was enhanced to observe protein distribution on the surface and it can be seen that the whole glass surface is covered with GFP. "TESPSA + EDC" method included additional step. TESPSA-modified samples were first incubated in EDC solution to open the succinic anhydride rings and activate carboxyl groups, and then incubated in protein sample. The results for last two methods were similar, and therefore the "TESPSA" method is advantageous in case of biosensor development due to the smaller number of steps while maintaining the same performance.

3.2.3 Modifications of optical fibers

To verify if the proposed modification methods may be used not only for flat substrates but also for cylindrical optical fibers I adjusted the reaction setup. In case of silanization of glass coverslips, they were glued on the plastic Petri dish that was placed above regents and therefore only one side of the glass slide was modified with the silane (see Figure 3.6). To modify the optical fibers they were suspended over the reagents so vapor can interact with the surface of the entire optical fiber. Moreover, to make the cladding surface the same as in case of further measurements with LPFG sensors I etched fiber fragments in HF

before cleaning and modifications.

Efficiency of each modification method was analyzed with confocal microscopy. For each analyzed spot two images were recorded, one with focus on the edges and the other with focus on the bottom of the fiber (Figure 3.5). Obtained results were similar as in case of glass coverslips modifications with GFP. Physisorption on bare and APTES-modified surface was not very efficient. In the first method some protein molecules were present on the surface, but the intensity and homogeneity of the fluorescence indicated small amount of immobilized proteins which did not cover the surface completely. In physisorption on APTES-modified surface there was no flourescence indicating that the proteins were not immobilized on the surface. All methods with covalent bond formation resulted in high and uniform surface coverage with GFP. In the method with APTES and EDC some aggregates were present (similarly as in case of glass slides), but the whole fiber surface was modified with proteins. Methods with TESPSA and TESPSA + EDC gave the best results with uniform distribution of GFP on the entire surface of the fiber as indicated by fluorescence intensity and distribution.

3.3 Conclusions

Robust and relatively simple methods are necessary in the case of biosensor development to be able to implement them not only in laboratory, but also in everyday life. Methods that are typically used for modification of LPFG includes physisorption of receptors on bare surface [31], deposition of different additional coatings [32, 33], and silane reaction in the solution [34, 35]. Physical adsorption, although straightforward, is often associated with poor binding and protein detachment from the surface, and therefore should not be used for biosensor preparation. Deposition of additional coatings may be advantageous in case of optical properties of sensors and it may enable immobilization of receptors. On the other hand, this involves additional, often time-consuming, steps. Modification of LPFGs with silanes in solution-based reaction is hard to repeat and gives irregular films as described in section 3.1.

Main goal of this chapter was to test and describe vapor phase silanization methods that would be appropriate for long-period fiber grating biosensors. I demonstrated that silanization of glass with APTES and TESPSA is suitable for functionalization of cylindrical fibers and enable successful covalent immo-

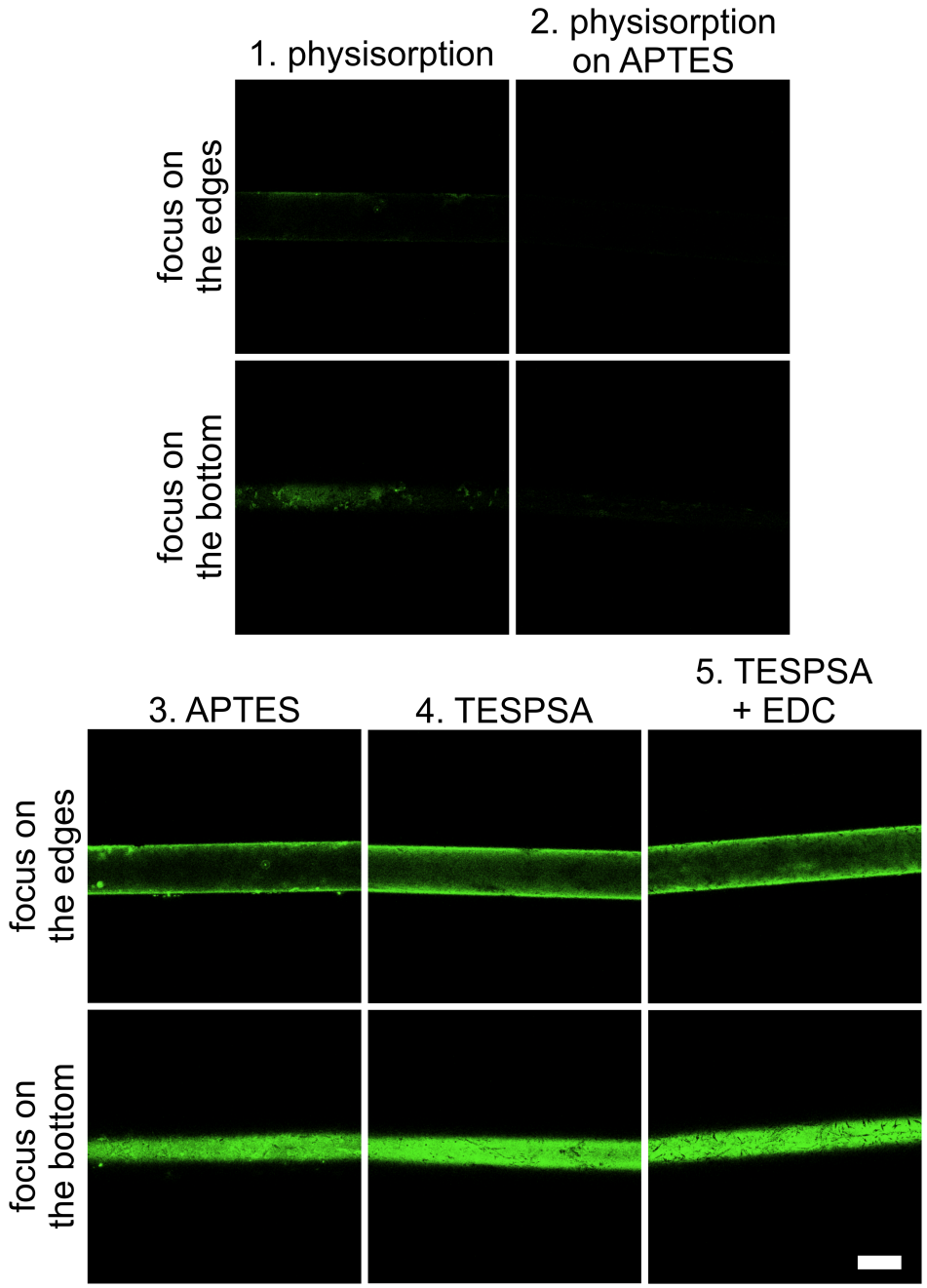

Figure 3.5: Confocal microscopy images of optical fibers modified with GFP using different immobilization methods: (1) Physisorption on bare surface; (2) Physisorption on APTES-modified surface; (3) Covalent bonding to APTES-modified surface; (4) Covalent bonding to TESPSA-modified surface; (5) Covalent bonding to TESPSA-modified surface with the utilization of EDC. Scale bar 100 μm.

bilization of proteins. The best results were obtained for covalent bonding of GFP on TESPSA-modified surfaces. Protein coatings were uniform and clearly visible on the whole surface of both glass slides and optical fibers. The procedure was effective and repeatable, and yet relatively simple. This method was further used for modification of LPFGs with antibodies and other protein receptors as described in chapters 4 and 5.

3.4 Materials and methods

Green fluorescent protein (GFP), sodium hydroxide, hydrofluoric acid, ammonium fluoride, acetone, ethanol, 1-ethyl-3-(3-dimethylaminopropyl)carbodiimide hydrochloride (EDC), and phosphate buffered saline (PBS) tablets were purchased from Sigma Aldrich. PBS consists of 10 mM phosphate buffer, 2.7 mM potassium chloride and 137 mM sodium chloride, pH 7.4 at 25 °C.

3(triethoxysilyl)propylsuccinic anhydride (TESPSA) and (3-aminopropyl)-triethoxysilane (APTES) were purchased from Gelest.

Surface pretreatment

Silicon wafers were used for the investigation of silanization with APTES and TESPSA by XPS. Prior to silanization, the silicon wafers were thermally treated to form silicon oxide layer on top. Surface was consecutively cleaned in acetone, ethanol and water (5 min each) and dried under a stream of argon. Then, wafers were incubated in 0.5 M NaOH for 5 min, washed in water and dried.

Thin glass coverslips were used as a substrate to test different methods of protein immobilization. Prior to silanization, the glass coverslip surface was consecutively cleaned in acetone, ethanol and water (5 min each) and dried under a stream of argon.

Fragments of optical fibers (the same type as used for LPFG fabrication) were used to test different methods of protein immobilization on cylindrical surface. To made the cladding surface the same as in case of LPFG sensors I etched fiber fragments in HF before cleaning and modification. The jacket of optical fiber was removed and the fiber cladding was etched in 40% HF for 3 min and then in mixture of 40% HF and ammonium fluoride (1:6) for 1 min. Then, the surface was cleaned as described above for glass coverslips.

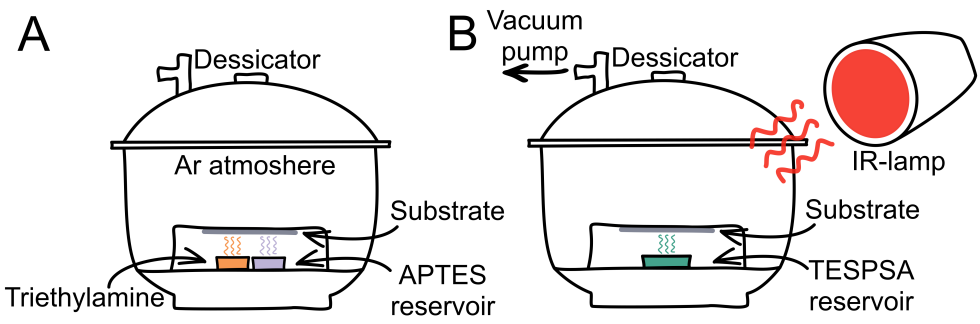

Figure 3.6: The silanization procedures with APTES (A) and TESPSA (B).

Silanization with APTES

The samples were placed in a desiccator over two small containers, one containing a 30 μL of the silane precursor (APTES), and the second 10 μL of catalyst (triethylamine) and left at room temperature under an argon atmosphere for 1, 2, 5, or 8 h (Figure 3.6 A). Similar samples were also prepared with additional heating using externally positioned IR-lamp (1, 2, or 5 h). Next, according to the procedure described in [28], the reagents were removed from the desiccator and the samples were left for 48 h under an argon atmosphere for curing of the silane layer.

Silanization with TESPSA

Silanization was done according to the procedure given in [29] with its further modifications. Briefly, the samples were placed in a desiccator over an open container with TESPSA. To evaporate the silane a vacuum of about 1 mbar and additional heating using externally positioned IR-lamp was applied (Figure 3.6 B). The reaction was continued for 2 or 4 h. Then, the sensor surface was cured and annealed in a furnace at 120 °C for 1.5 h to dehydrate succinic anhydride groups.

Modification with GFP

GFP solution was prepared by diluting of the stock solution in phosphate buffered saline (PBS) to final concentration 0.01 mg/mL. For one method carboxyl groups on the surface of proteins were activated with EDC (final concentration 4 mg/mL, i.e. 21 mM) for 15 minutes. Five different methods for GFP immobilization (Figure 3.3) were verified, i.e.: (1) Physisorption on clean surface, where samples were incubated in GFP solution for 1 h; (2) Physisorption

on APTES-modified surface, where APTES-modified samples were incubated in GFP solution for 1 h; (3) Covalent bonding to APTES-modified surface, where APTES-modified samples were incubated in EDC-activated GFP solution for 1 h; (4) Covalent bonding to TESPSA-modified surface, where TESPSA-modified samples were incubated in GFP solution for 1 h and covalent bonds were formed in ring opening reaction; (5) Covalent bonding to TESPSA-modified surface with the utilization of EDC, where TESPSA-modified samples were first incubated in EDC solution for 15 minutes to open the succinic anhydride rings and activate carboxyl groups and then incubated in GFP solution for 1 h. All the samples were finally washed extensively with water, dried under the stream of argon and kept in darkness before further measurements.

Confocal microscopy

Nikon Ti Eclipse with confocal system A1R was used for evaluation of the efficiency of different immobilization methods. The system included ion laser IMA101040AL5 (Melles Grior, USA) emitting light of wavelength of 488 nm, bandpass filter 550/50, objective CFI Plan Fluor 40×, and NIS Elements AR 4.13 software. A set of fluorescence images was done for each functionalization method. The same parameters were used for all samples. Additionally, for optical fiber samples transmission images were also recorded.

X-ray photoelectron spectroscopy

Surface composition of unmodified silicon wafer and silicon substrates modified with TESPSA and APTES were analyzed by XPS. XPS analysis were done using a spectrometer (Microlab 350 Thermo VG Scientific) equipped with a non-monochromated excitation source of Al Kα (1486.6 eV, 300 W, pressure 1.0×10^{-9} mbar). Survey scans and high resolution XPS spectra for each elements were recorded with the pass energy of 100 and 40 eV with energy resolution of 0.83 eV. The binding energy of the target elements was determined using a reference binding energy of carbon as C1s, 285 eV after a linear or Shirley background subtraction and an asymmetric Gaussian/Lorentzian mixed function for peak deconvolution. XPS measurements were done by Dr. Marcin Pisarek.

3.5 References

(1) Rusmini, F.; Zhong, Z.; Feijen, J. Protein Immobilization Strategies for Protein Biochips. *Biomacromolecules* **2007**, *8*, 1775–1789.

(2) Nakanishi, K.; Sakiyama, T.; Kumada, Y.; Imamura, K.; Imanaka, H. Recent Advances in Controlled Immobilization of Proteins onto the Surface of the Solid Substrate and Its Possible Application to Proteomics. *Current Proteomics* **2008**, *5*, 161–175.

(3) Kusnezow, W.; Hoheisel, J. D. Solid supports for microarray immunoassays. *Journal of Molecular Recognition* **2003**, *16*, 165–176.

(4) Vashist, S. K. Comparison of 1-Ethyl-3-(3-Dimethylaminopropyl) Carbodiimide Based Strategies to Crosslink Antibodies on Amine-Functionalized Platforms for Immunodiagnostic Applications. *Diagnostics* **2012**, *2*, 23–33.

(5) Pâslaru, E.; Baican, M. C.; Hitruc, E. G.; Nistor, M. T.; Poncin-Epaillard, F.; Vasile, C. Immunoglobulin G immobilization on PVDF surface. *Colloids and Surfaces B: Biointerfaces* **2014**, *115*, 139–149.

(6) Sun, Y.; Du, H.; Feng, C.; Lan, Y. Oriented immobilization of antibody through carbodiimide reaction and controlling electric field. *Journal of Solid State Electrochemistry* **2015**, *19*, 3035–3043.

(7) Fowler, J. M.; Stuart, M. C.; Wong, D. K. Y. Self-Assembled Layer of Thiolated Protein G as an Immunosensor Scaffold. *Analytical Chemistry* **2007**, *79*, 350–354.

(8) Mauriz, E.; García-Fernández, M.; Lechuga, L. Towards the design of universal immunosurfaces for SPR-based assays: A review. *TrAC Trends in Analytical Chemistry* **2016**, *79*, 191–198.

(9) Sharma, H.; Mutharasan, R. Half Antibody Fragments Improve Biosensor Sensitivity without Loss of Selectivity. *Analytical Chemistry* **2013**, *85*, 2472–2477.

(10) Turková, J. Oriented immobilization of biologically active proteins as a tool for revealing protein interactions and function. *Journal of chromatography. B, Biomedical sciences and applications* **1999**, *722*, 11–31.

(11) Haugland, R. P.; You, W. W. Coupling of antibodies with biotin. *Methods in molecular biology (Clifton, N.J.)* **2008**, *418*, 13–24.

(12) Chivers, C. E.; Koner, A. L.; Lowe, E. D.; Howarth, M. How the biotin-streptavidin interaction was made even stronger: investigation via crystallography and a chimaeric tetramer. *The Biochemical journal* **2011**, *435*, 55–63.

(13) Shafiee, H.; Lidstone, E. a.; Jahangir, M.; Inci, F.; Hanhauser, E.; Henrich, T. J.; Kuritzkes, D. R.; Cunningham, B. T.; Demirci, U. Nanostructured Optical Photonic Crystal Biosensor for HIV Viral Load Measurement. *Scientific Reports* **2014**, *4*, 4116.

(14) Wegner, G. J.; Lee, H. J.; Marriott, G.; Corn, R. M. Fabrication of Histidine-Tagged Fusion Protein Arrays for Surface Plasmon Resonance Imaging Studies of Protein-Protein and Protein-DNA Interactions. *Analytical Chemistry* **2003**, *75*, 4740–4746.

(15) Mayall, R.; Renaud-Young, M.; Chan, N.; Birss, V. An electrochemical lipopolysaccharide sensor based on an immobilized Toll-Like Receptor-4. *Biosensors and Bioelectronics* **2017**, *87*, 794–801.

(16) Brzozowska, E.; Śmietana, M.; Koba, M.; Górska, S.; Pawlik, K.; Gamian, A.; Bock, W. J. Recognition of bacterial lipopolysaccharide using bacteriophage-adhesin-coated long-period gratings. *Biosensors and Bioelectronics* **2015**, *67*, 93–99.

(17) De Juan-Franco, E.; Caruz, A.; Pedrajas, J. R.; Lechuga, L. M. Site-directed antibody immobilization using a protein A–gold binding domain fusion protein for enhanced SPR immunosensing. *The Analyst* **2013**, *138*, 2023.

(18) Pujari, S. P.; Scheres, L.; Marcelis, A. T. M.; Zuilhof, H. Covalent Surface Modification of Oxide Surfaces. *Angewandte Chemie International Edition* **2014**, *53*, 6322–6356.

(19) McGovern, M. E.; Kallury, K. M. R.; Thompson, M. Role of Solvent on the Silanization of Glass with Octadecyltrichlorosilane. *Langmuir* **1994**, *10*, 3607–3614.

(20) Manifar, T.; Rezaee, A.; Sheikhzadeh, M.; Mittler, S. Formation of uniform self-assembly monolayers by choosing the right solvent: OTS on silicon wafer, a case study. *Applied Surface Science* **2008**, *254*, 4611–4619.

(21) Xiang, S.; Xing, G.; Xue, W.; Lu, C.; Lin, J.-M. Comparison of two different deposition methods of 3-aminopropyltriethoxysilane on glass slides and their application in the ThinPrep cytologic test. *The Analyst* **2012**, *137*, 1669–1673.

(22) Haller, I. Covalently attached organic monolayers on semiconductor surfaces. *Journal of the American Chemical Society* **1978**, *100*, 8050–8055.

(23) Zhang, F.; Sautter, K.; Larsen, A. M.; Findley, D. A.; Davis, R. C.; Samha, H.; Linford, M. R. Chemical Vapor Deposition of Three Aminosilanes on Silicon Dioxide: Surface Characterization, Stability, Effects of Silane Concentration, and Cyanine Dye Adsorption. *Langmuir* **2010**, *26*, 14648–14654.

(24) Lowe, R. D.; Pellow, M. A.; Stack, T. D. P.; Chidsey, C. E. D. Deposition of Dense Siloxane Monolayers from Water and Trimethoxyorganosilane Vapor. *Langmuir* **2011**, *27*, 9928–9935.

(25) Hozumi, A.; Ushiyama, K.; Sugimura, H.; Takai, O. Fluoroalkylsilane Monolayers Formed by Chemical Vapor Surface Modification on Hydroxylated Oxide Surfaces. *Langmuir* **1999**, *15*, 7600–7604.

(26) Shircliff, R. A.; Stradins, P.; Moutinho, H.; Fennell, J.; Ghirardi, M. L.; Cowley, S. W.; Branz, H. M.; Martin, I. T. Angle-Resolved XPS Analysis and Characterization of Monolayer and Multilayer Silane Films for DNA Coupling to Silica. *Langmuir* **2013**, *29*, 4057–4067.

(27) Walker, R. A.; Wilson, K.; Lee, A. F.; Woodford, J.; Grassian, V. H.; Baltrusaitis, J.; Rubasinghege, G.; Cibin, G.; Dent, A. Preservation of York Minster historic limestone by hydrophobic surface coatings. *Scientific Reports* **2012**, *2*, 880.

(28) Ebner, A.; Hinterdorfer, P.; Gruber, H. J. Comparison of different aminofunctionalization strategies for attachment of single antibodies to AFM cantilevers. *Ultramicroscopy* **2007**, *107*, 922–927.

(29) Gang, A.; Gabernet, G.; Renner, L. D.; Baraban, L.; Cuniberti, G. A simple two-step silane-based (bio-) receptor molecule immobilization without additional binding site passivation. *RSC Adv.* **2015**, *5*, 35631–35634.

(30) Helmy, R.; Wenslow, R. W.; Fadeev, A. Y. Reaction of Organosilicon Hydrides with Solid Surfaces: An Example of Surface-Catalyzed Self-Assembly. *Journal of the American Chemical Society* **2004**, *126*, 7595–7600.

(31) Smietana, M.; Bock, W. J.; Mikulic, P.; Ng, A.; Chinnappan, R.; Zourob, M. Detection of bacteria using bacteriophages as recognition elements immobilized on long-period fiber gratings. *Optics express* **2011**, *19*, 7971–7978.

(32) Bandara, A. B.; Zuo, Z.; Ramachandran, S.; Ritter, A.; Heflin, J. R.; Inzana, T. J. Detection of methicillin-resistant staphylococci by biosensor assay consisting of nanoscale films on optical fiber long-period gratings. *Biosensors and Bioelectronics* **2015**, *70*, 433–440.

(33) Esposito, F.; Sansone, L.; Taddei, C.; Campopiano, S.; Giordano, M.; Iadicicco, A. Ultrasensitive biosensor based on long period grating coated with polycarbonate-graphene oxide multilayer. *Sensors and Actuators, B: Chemical* **2018**, *274*, 517–526.

(34) Tripathi, S. M.; Bock, W. J.; Mikulic, P.; Chinnappan, R.; Ng, A.; Tolba, M.; Zourob, M. Long period grating based biosensor for the detection of Escherichia coli bacteria. *Biosensors and Bioelectronics* **2012**, *35*, 308–312.

(35) Baliyan, A.; Sital, S.; Tiwari, U.; Gupta, R.; Sharma, E. K. Long period fiber grating based sensor for the detection of triacylglycerides. *Biosensors and Bioelectronics* **2016**, *79*, 693–700.

Chapter 4

LPFG biosensors[1]

4.1 Introduction

Preparation of highly sensitive LPFGs tuned to their highest refractive index sensitivity as well as development of efficient surface modification techniques were important steps towards preparation of label-free biosensors. One of the main goals of this work was the development of biosensors for the detection of different viruses. Fast and reliable detection of viruses is crucial in clinical and veterinary practice in order to begin proper medical treatment as fast as possible. Moreover, because for every living organism there are many specific viruses, problems with virus infections appears also in basic research and biopharmaceutical and biotechnology industries that are based on variety of organisms ranging from bacteria to mammals. Bacterial cultures and eukaryotic cell lines can be infected with bacteriophages (in short: phages) or eukaryotic viruses, respectively. This creates not only huge financial losses but also conditions hazardous for humans.

Currently, a lot of various methods for virus detection are in use or under investigation. One of the most commonly used approach for determining virus concentration in the sample is plaque assay, that was first developed for enumeration of bacteriophages [1]. In this assay, the layer of host bacteria is infected with the phage at varying dilutions. Infected bacterium cell is forced

[1]Parts of this chapter have been published as:
Janczuk-Richter, M.; Dominik, M.; Roźniecka, E.; Koba, M.; Mikulic, P.; Bock, W.J.; Łoś, M.; Śmietana, M.; Niedziółka-Jönsson, J. *Sensors and Actuators B: Chemical* **2017**, *250*, 32-38

by virus to produce multiple phage copies that are then released from the cell during lysis. The infection is spread to neighboring bacteria where the cycle repeats. The infected area creates a plaque that can be seen with the naked eye. The number of plaques correlates with the number of active phages in the sample. This method was modified by Renato Dulbecco in 1952 for use in animal virology, and since then it has been used for concentration determination of many different virus types [2]. Biological diagnostics methods for viral animal diseases may also involve virus culturing and isolation followed by serological tests. These assays are laborious, require well-trained personnel, are prone to give false negative results, and it can take up to few days to get a result. Other typically used techniques for virus detection are enzyme-linked immunosorbent assay (ELISA) [3, 4] and polymerase chain reaction (PCR) and its variations [5, 6] that are faster and in most cases highly sensitive, but require expensive equipment and reagents, and offer very limited applicability in the field. Due to the drawbacks of aforementioned methods connected mostly with long time of analysis and high cost, a lot of work has been recently focused on biosensor development with particular focus on label-free optical devices [7].

Different types of label-free optical biosensors for virus detection were already demonstrated. In the work of Lee et al. [8] gold nanoparticles (AuNPs) modified with sialic acid were used for colorimetric detection of influenza B virus. Virions formed complexes with the nanoparticles via hemagglutinin–sialic acid binding and caused them to aggregate which could be observed by naked eye or with UV-vis spectrometry as a sample color change from red to purple. A similar approach was demonstrated for T7 bacteriophage detection [9]. Specific antibodies were used as a receptor layer on the AuNPs surface and presence of virus in the sample cause aggregation of nanoparticles. The presented method was rapid with the LOD of 1.1×10^{10} PFU/mL (plaque-forming units per milliliter). By changing the receptor layer from antibodies to carboxymethyl chitosan the LOD was improved and reached 1.2×10^{6} PFU/mL [10]. Label-free detection of viruses can also be done by SPR measurements. For example, gold surface modified with whole cells of *Escherichia coli* bacteria was used for T4 phage detection [11]. The LOD of this short (10 min) method was 1×10^{7} PFU/mL. A similar biosensor was presented for adenovirus detection [12]. In this study the sensor surface was modified with plastic (molecularly imprinted polymers) or natural antibodies and the obtained LODs were 8.1×10^{6} and 1.2×10^{7} PFU/mL, respectively. SPR immunosensor was also shown for se-

lective, multiplexed detection of MS2 phage and Influenza A virus in aerosol [13]. SPR microscopy was used for the imaging, detection, and mass/size measurement of single particles of Influenza A virus [14]. Label-free sensors that utilized interferometry-based techniques, such as Young interferometry for herpes simplex virus type 1 detection [15] and dark-field interferometry for HIV and phage detection [16], were also demonstrated. Novel interferometry-based imaging approach was shown for visualization and counting of recombinant vesicular stomatitis virus Ebola model [17]. Interesting label-free optical device based on photonic crystal was presented by Shafiee et al. [18] Nanostructured photonic crystals modified with specific antibodies were used for capturing and quantifying of HIV viruses. This surface resonantly reflected a narrow wavelength band during illumination with a broadband lightsource. Observed band changed its position after virus capture. Significant shift was observed for concentrations higher than 10^5 copies/mL. Detection of single virions was done for Influenza A by monitoring adsorption of individual particles as a changes in the resonance frequency/wavelength of a whispering-gallery mode excited in a microspherical cavity [19]. Unfortunately, in this study no specificity was provided, because surface was not modified with any receptor layer. Recently, very sensitive method (limit of detection = 95 virus copies/mL) for norovirus detection was demonstrated that involved regeneration of quenched fluorescence of quantum dots/gold nanoparticles upon addition of virus [20]. However, the selectivity of this assay was limited due to the high interferences from other virus particles.

All of the above-described methods share a number of drawbacks that hinder their broad practical implementation. Issues, such as ease of use, small size of the device, and selectivity still need to be addressed. As a step towards improved virus sensor, here I demonstrate LPFG biosensors for the detection of T7 bacteriophage and norovirus virus-like particles (VLPs). Host bacteria of T7 phage is *Escherichia coli* that is one of the most frequently used microorganism in the biotechnology industry. Infections with bacteriophages are one of the most common factors that cause loss of product and in extreme cases closures of bacteria-based factories. More than 70% of biotechnological companies admitted to encounter this problem [21]. Therefore, fast detection of bacteriophages in media and substrates used in such a factory is crucial to avoid infections with phages and therefore financial losses. Second type of biosensor presented in this chapter is prepared for detection of human virus. Norovirus

is a very contagious virus that causes acute gastroenteritis (inflammation of the stomach or intestines) that leads to diarrhea and vomiting. According to Centers for Disease Control and Prevention (CDC) each year norovirus infections end up with more than 600 millions cases of gastroenteritis among which 200 millions are for children under 5. It is estimated that 50,000 children die every year due to norovirus [22]. The laboratory work with this virus is very difficult due to the lack of a robust cell culture system for multiplication of human norovirus. Therefore, in my work I was using norovirus VLPs. VLPs are self-assembled multisubunit protein structures that are build from viral capsid proteins and have identical or highly related structure to their corresponding virus [23]. Lack of genetic material inside such structure as well as similar size and the same capsid proteins as in native virus made VLPs safe and proper model biomolecules for sensor evaluation towards norovirus detection. Norovirus VLPs are also widely used as antigens in diagnostic serological assays and as vaccines against norovirus infections [24]. Therefore, demonstrated biosensor can be advantageous both in the context of norovirus infections and in vaccine research.

4.2 Results and discussion

LPFGs tuned to their highest RI sensitivity (as demonstrated in chapter 2) were used to produce biosensors. Preparation of LPFG-based biosensor requires several steps: (i) introduction of desired functional groups on the transducer surface by chemical modification, (ii) receptor immobilization, (iii) blocking of unspecific binding sites on the sensor surface with neutral protein, (iv) detection of target biomolecule. Steps ii-iv were done in flow cell (described in section 2.4) and the optical transmission of LPFG sensor was monitored. Schematic representation of experimental setup and biosensor preparation steps are shown in Figure 4.1. To check whether all system components and procedures are working well, a sensor for interaction monitoring of model and well defined pair biotin-avidin was prepared first. As a next step, biosensors for detection of T7 bacteriophages and norovirus VLPs were investigated.

4.2.1 Preliminary results - avidin detection

Preliminary work was done with model system biotin-avidin to test usefulness of LPFG-based sensor to study biological interactions. Biotin-avidin/streptavidin

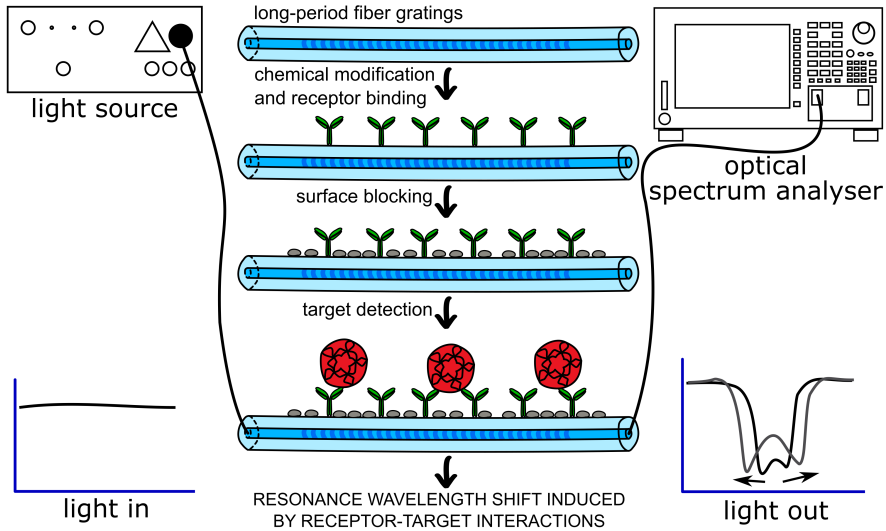

Figure 4.1: Schematic representation of the experimental setup and fiber surface modification steps leading to target biomolecule detection. The modifications take place on whole circular surface of the fiber.

interaction is one of the strongest non-covalent bonds ($K_d = 10^{-15}M$) [25] and its often used to immobilize proteins on the surface or to test new sensing strategies.

In the first step, LPFG surface was modified with APTES to introduce amine groups. Then, carboxyl group present in biotin molecule was activated with EDC. Activated biotin was covalently immobilized and then the surface was thoroughly washed with PBS. As the spectral response of the LPFG significantly depends on the RI of external medium, only results of measurements performed in the same solution can be compared. Therefore, each step was followed by measurements in PBS. Spectra obtained in PBS after biotin immobilization was used as a reference for further measurements. Then, the sensor was used to monitor biotin-avidin interactions. As shown in Figure 4.2A and B, subsequent additions of the solutions of increasing concentration of avidin (from 1 to 100 μg/mL) caused shifts in resonance wavelengths, i.e. blue shift for left and red shift for right resonance. This indicated increase in local refractive index caused by avidin binding to biotin-modified surface. After each step, sensor was washed in PBS twice for 5 min to remove any loosely bound proteins and the results from second washing were taken for further calculations. Spectral shifts from 0.8 nm to 3.9 nm were observed for avidin concentrations from

1 to 100 μg/mL (Figure 4.2C). They were calculated as a difference between average reference left resonance wavelength measured in PBS and average left resonance wavelength measured during second washing after interaction with avidin.

According to Vörös, RI of adsorbed protein layer is around 1.48 RIU [26] and the size of avidin is 5.6 $\times$ 5.0 $\times$ 4.0 nm [27]. Therefore, the attachment of many avidin particles to biotin-modified surface caused local increase of RI on the sensor surface and as consequence resonance wavelength shift. That confirmed the usefulness of LPFG sensor as biosensing device.

4.2.2 Detection of bacteriophages

Immobilization of the receptors on the sensor surface is the critical step in biosensor development. According to previous results (described in detail in chapter 3), for immobilization of antibodies I chose simple and reliable method based on silanization of the sensor surface with TESPSA. This leads to obtain succinic anhydride groups capable of reacting with amine groups, present on the surface of anti-T7 antibody, in a ring opening reaction [28].

First, the LPFG sensor was modified with TESPSA in 4-hour procedure and annealed in a furnace to remove any water from the surface and to dehydrate any hydrolyzed succinic anhydride functionalities. The next modification and detection steps were done with monitoring of optical transmission and each step was followed by extensive washing with PBS. The LPFG sensor was coated with anti-T7 antibody whose concentration was chosen based on previous research [9]. After washing, bovine serum albumin (BSA) solution was injected into the cell in order to block unspecific sites on the sensor surface. Standard concentration of 0.1% was used. As shown in Figure 4.3A both steps resulted in significant wavelength shift of the left resonance towards shorter waves indicating increase of local RI caused by the formation of the bio-overlay on the surface of LPFG sensor. Then, prepared biosensor was used for the detection of T7 bacteriophages. Subsequent injections of the solutions with increasing concentrations of T7 phages caused further changes in the resonance wavelength towards its lower values due to interactions between phages and immobilized antibodies that caused the increase of thickness and density of bio-overlay. Spectra measured in PBS before and after incubation of the LPFG sensor in each phage concentration are shown in Figure 4.3B. Spectral shifts induced by antigen-antibody interactions from 0.7 nm to 2.9 nm were observed

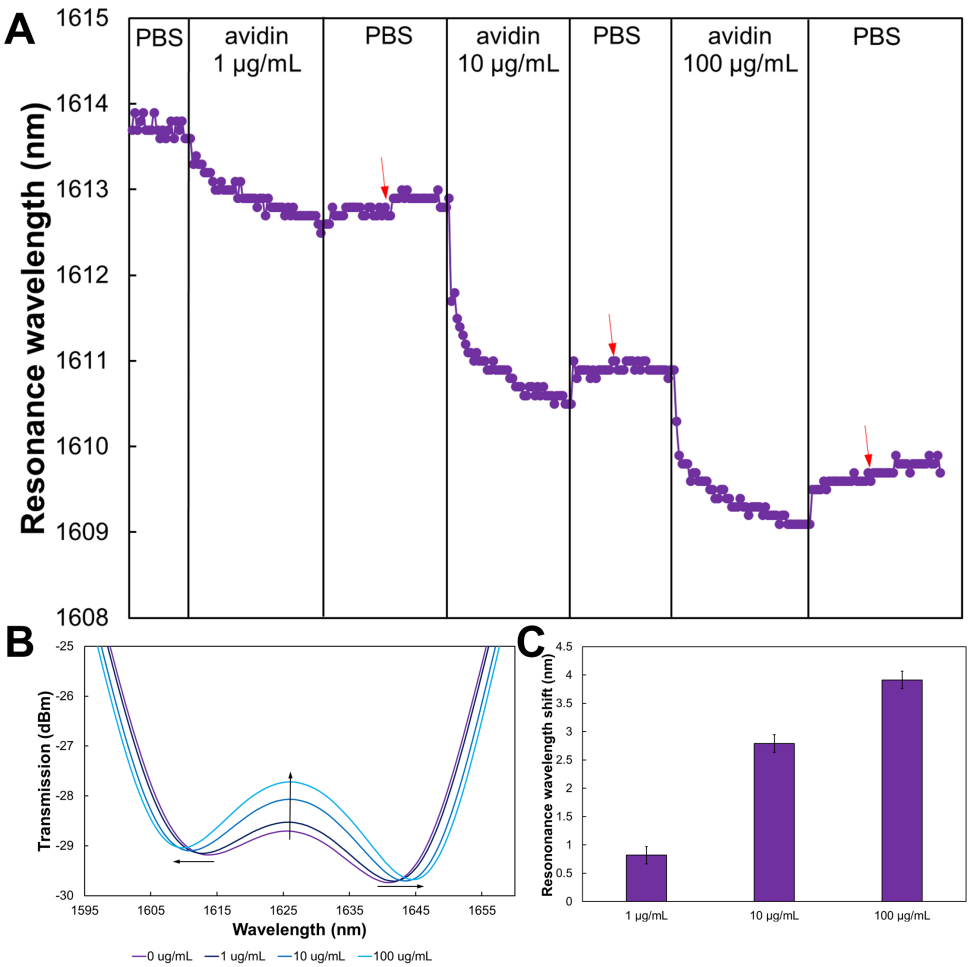

Figure 4.2: Monitoring of biotin-avidin interactions by LPFG sensor. (A) Resonance wavelength at subsequent steps of biotin-avidin interactions monitoring for left resonance. Red arrow indicates injection of second PBS portion (B) Spectra measured in PBS before avidin addition and after incubation in avidin solutions. (C) Resonance wavelength shifts referred to measurement performed in PBS before avidin addition for different avidin concentrations.

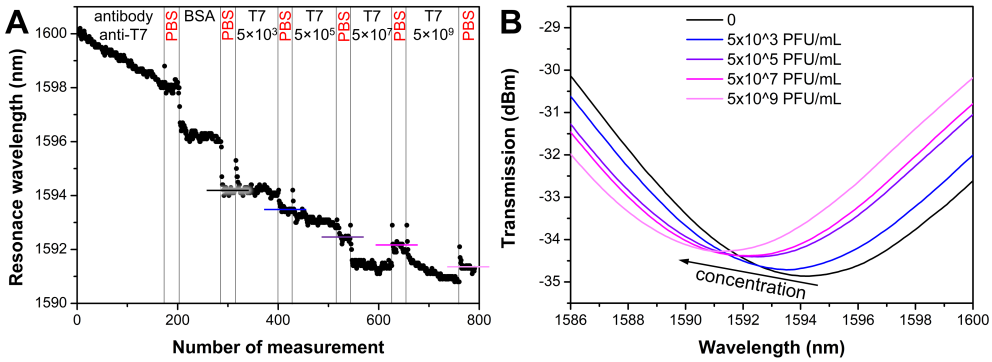

Figure 4.3: T7 phage detection. (A) Resonance wavelength at subsequent steps of bacteriophage detection for left resonance. (B) Spectra measured in PBS before phage addition and after incubation in T7 bacteriophage solutions.

for T7 phage concentration ranging from 5×10^3 to 5×10^9 PFU/mL (Figure 4.4). Observed shifts are in the same range as for biotin-avidin interactions monitoring. The virus is much larger in size than avidin (∼55 nm vs ∼5 nm), but the concentrations used in the experiments were much lower. Therefore, the overall increase in local RI on the surface was similar for avidin and phage T7 detection.

To confirm that the changes in resonance wavelength were induced particularly by the presence of the phages on the sensor surface, I performed additional biological assay. Fragments of optical fibers were prepared and modified in the same way as the LPFG sensor surface and then incubated in samples with different phage concentrations for 30 min. After thorough washing with PBS, the fibers were placed onto the top LB-agar mixed with overnight culture of *E. coli*, similarly as in the typical plaque count method for determination of phage viability (Figure 4.4B). Plates with fiber fragments were incubated for 5 h at 37 °C. As shown in Figure 4.4C, lysis zones on the bacterial lawns were observed for all samples incubated in phage solutions indicating the presence of active phages on the antibody-modified surface. The more phages were attached to the surface, the wider lysis zone was observed.

Selectivity test of prepared sensor was also performed and monitored in real-time. MS2 phage was used as a negative-control (non-specific phage) and T7 phage was used as a target (specific phage), both in concentration of 5×10^7 PFU/mL. The sensor surface was prepared and modified as in previous experiments (i.e. silanization, immobilization of anti-T7 antibody, and blocking with

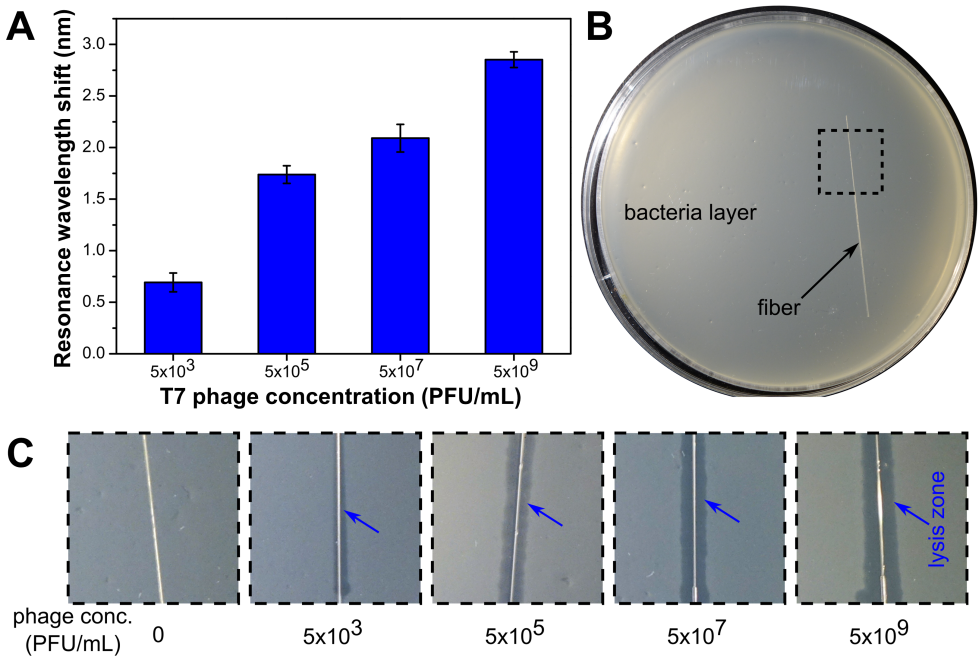

Figure 4.4: Biological confirmation of T7 phage detection. (A) Resonance wavelength shifts referred to measurement performed in PBS before phage addition for different concentration of T7 phage. (B) The photograph of the double layer agar plate with fragment of optical fiber (here without phages) placed onto the top LB-agar mixed with bacteria. (C) Results of phage viability assay for the fragments of fibers modified with different phage concetrations. Lysis zones marked with arrows indicate the presence of viable phages on the fiber surface.

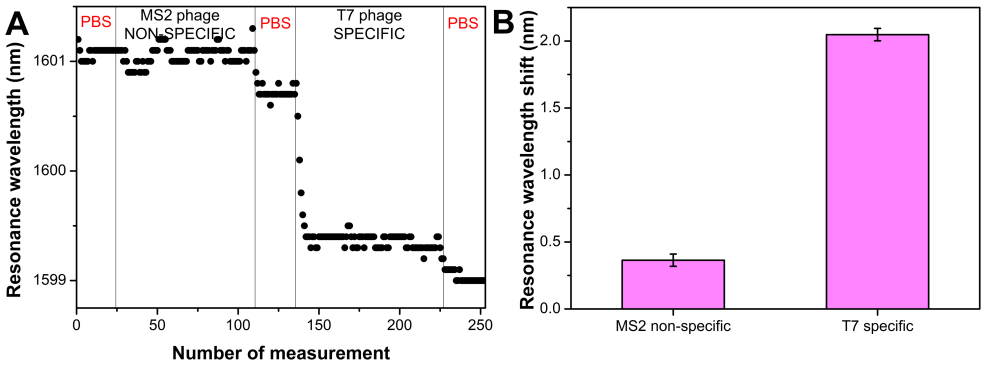

Figure 4.5: Selectivity test of the designed method. (A) Resonance wavelength for left resonance measured during sensor incubation in non-specific MS2 phages and specific T7 phages. (B) Resonance wavelength shifts referred to measurement performed in PBS before phage addition after incubation in non-specific and specific phages.

BSA). Then, it was incubated in non-specific MS2 phage solution and washed in PBS. As shown in Figure 4.5, only a slight difference in resonance wavelength measured in PBS before and after incubation was observed. The sensor was then incubated in T7 phage solution. As expected, this measurements caused a significant wavelength shift (> 2 nm) due to specific antigen-antibody interactions.

Based on the experimental data, a limit of detection lower than 5×10^3 PFU/mL can be achieved with LPFG-based biosensor, which is comparable to the best LOD reported so far in the literature for detection of viruses with optical label-free biosensors. Colorimetric sensors for T7 phage detection based on AuNPs aggregation reached LOD equals to 1.1×10^{10} PFU/mL and 1.2×10^6 PFU/mL for nanoparticles modified with antibodies [9] and carboxymethyl chitosan [10], respectively. The detection of MS2 phages with LOD of 6×10^6 PFU/mL [13] and T4 phages with LOD of 1×10^7 PFU/mL [11] with SPR biosensors was demonstrated. Opto-fluidic ring resonator sensor for the detection of M13 phages was also presented [29] with LOD of 2.3×10^3 PFU/mL. Low detection limit of LPFG-based sensor can be attributed to high RI sensitivity ($\sim$2000 nm/RIU) obtained by careful optimization of the working point of the device. Although lower detection limits can be achieved with biological assays the main advantage of biosensor strategies is the ease of use and the time of analysis. In case of LPFG-based biosensor presented in this work, sample analysis can be done in 40 min including reference measurements in PBS before

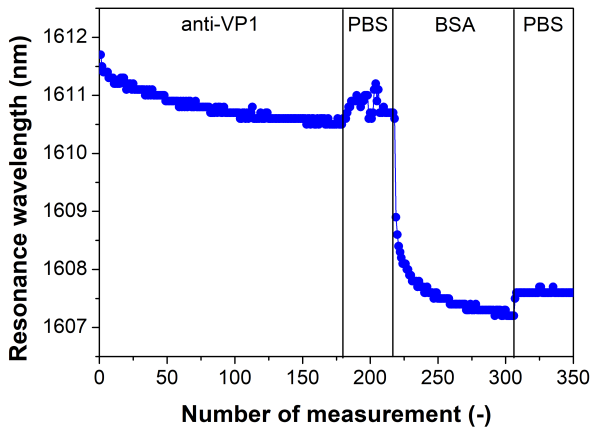

Figure 4.6: Resonance wavelength at subsequent steps of surface biofunctionalization (i.e. antibody immobilization and blocking with BSA) for left resonance.

detection, incubation in the sample, washing and measurements in PBS after detection, and data analysis.

4.2.3 Detection of norovirus virus-like particles

After successful bacteriophage detection with LPFG-based biosensor I decided to prepare the sensor for norovirus. Due to the lack of cell culture system for multiplication of human norovirus, in this studies norovirus virus-like particles were used.

LPFG surface was modified with TESPSA as described earlier. Next experimental steps were done in closed flow cell with monitoring of the LPFG transmission spectra at constant temperature. First, anti-VP1 antibody (targeting norovirus major capsid protein) was immobilized on the surface, and then 0.1% BSA was used to block the surface and avoid non-specific interactions. Both steps resulted in resonance wavelength shift (left resonance shifted towards shorter wavelengths) indicating increase in local RI and successful immobilization of the proteins (Figure 4.6).

Detected norovirus VLPs were produced in Sf9 insect cells infected with the recombinant baculovirus. Obtained norovirus VLPs had about 40 nm in diameter (Figure 4.7A) which corresponds to the size of native norovirus [30]. Antibody-modified LPFG sensor was incubated in VLP samples with different

concentrations ranging from 1 ng/mL to 10 μg/mL and then was washed and measured in PBS. As shown in Figure 4.7B, the higher the concentration of VLP the higher the resonance wavelength shift compared to the measurement done in PBS before detection. The shifts ranged from 0.4 nm to 2.8 nm and were caused by the changes in the thickness and optical density of the biolayer formed as an effect of specific norovirus VLPs binding to antibodies, similarly as in case of bacteriophage detection. Spectral changes observed for norovirus VLPs and bacteriophage detection were comparable. For higher VLPs concentrations, a decrease in sensitivity was observed indicating possible saturation of receptors with VLPs (Figure 4.7C).

Selectivity tests was done with two different negative controls — rabbit hemorrhagic disease virus (RHDV) VLP and influenza hemagglutinin (HA) VLP. The sensor surface was modified as in previous measurements and incubated in negative controls and in positive control (10 ng/mL each) with PBS washing between samples. In case of the negative controls I observed slight shift of resonances in the opposite direction than for specific binding (Figure 4.7D). Negative shift might be caused by detachment of some loosely bound BSA proteins from the surface. Sensor incubation in positive control caused resonance shift that confirmed selective attachment of norovirus VLPs to anti-VP1-modified surface. Due to lower RI sensitivity of LPFG used for selectivity measurements, the shift for 10 ng/mL norovirus VLP was lower than in case of previous measurements, but it was still clearly distinguishable.

By using the LPFG-based biosensor it was possible to detect 1 ng/mL norovirus VLPs in label-free manner. Better detection limits of optical sensors for norovirus and norovirus VLPs were only obtained in label-based methods that are more complicated and require longer procedures. For example, Ashiba et al. [31] proposed sensor in which surface plasmon resonance phenomenon was used to enhance fluorescence of quantum dots used as labels in the assay. This sandwich assay enabled detection of 0.01 ng/mL of norovirus VLPs, but it required multiple incubation and washing steps. Very sensitive method, but with limited specificity, was also recently demonstrated [20]. It involved regeneration of quenched fluorescence of quantum dots/gold nanoparticles upon addition of virus.

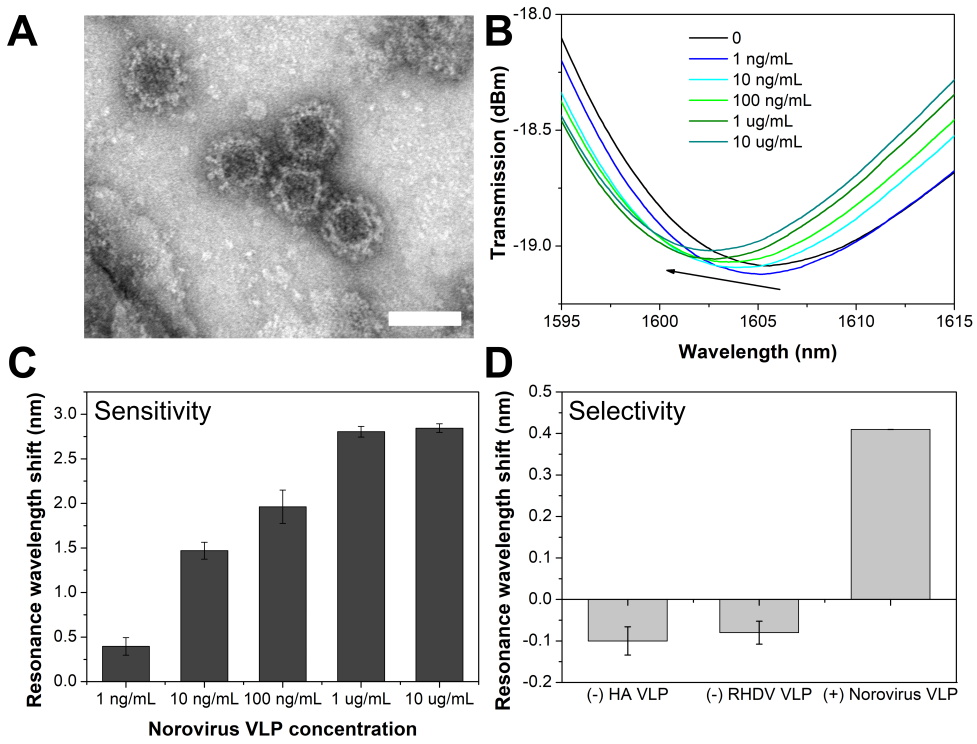

Figure 4.7: (A) Electron micrographs of purified norovirus VLPs (scale bar 50 nm). (B) Spectra measured in PBS before VLPs addition and after incubation in different concentrations of VLPs. (C) Resonance wavelength shift for left resonance referred to measurement performed in PBS before VLP addition for different VLPs concentration. (D) Selectivity analysis - resonance wavelength shifts for left resonance for two negative controls (HA VLP and RHDV VLP) and a positive control (norovirus VLP).

4.2.4 Regeneration of LPFG sensor surface

To decrease the fabrication costs and to enable preparation of different biosensors from the same LPFG structure, the possibility of the LPFG surface regeneration was investigated. After experiment with virus detection, the sensor was immersed in 0.5 M NaOH to remove all organic layers from the sensor surface. Aqueous solution of NaOH enabled the removal of the bottom silane layer together with biomolecules immobilized on top of it. Because NaOH solution could also slowly etch the surface of the silica fiber (< 0.02 nm/min for 0.1 M NaOH and about 0.1 nm for 0.5 M NaOH [32]), it was crucial to carefully control the LPFG transmission signal during whole cleaning procedure. Washing was done in 5-min cycles followed by measurements in PBS and it was continued until the transmission spectrum measured in PBS was similar to the reference one measured before any surface functionalization. As can be seen in Figure 4.8A, each washing step caused an increase in wavelength of left resonance indicating decrease of local RI due to removal of the bio-overlay from the sensor surface. In the demonstrated case, resonance wavelength equals to that measured in PBS before surface modification (1605 nm) was obtained after 4 washing cycles and this number of steps was usually sufficient to regenerate LPFG surface.

After cleaning procedure, the RI sensitivity was measured and results were compared with those obtained before surface modifications. As shown in Figure 4.8B, the results obtained before and after regeneration procedures were very similar, especially for RIs close to that of water. This experiment confirmed successful removal of organic layers from the LPFG surface and further usefulness of the sensor.

4.3 Conclusions

Utilization of antibody-modified LPFGs enabled obtaining simple, rapid, sensitive and versatile biosensors. Due to the application of optical fiber for signal transmission it is possible to introduce separation in location between measurement point, i.e. sensor, and signal processing setup, which may significantly improve safety, especially in case of hazardous samples. In LPFG-based label-free approach, I was able to detect 5×10^3 PFU/mL of T7 phage and 1 ng/mL of norovirus VLPs in 40-min assay. These assays do not require any amplification of genetic material (as in the case of PCR) nor expensive reagents and

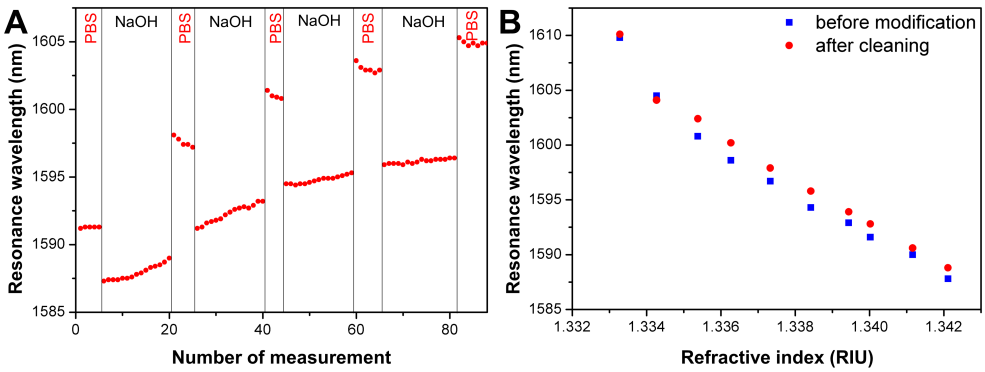

Figure 4.8: (A) Resonance wavelength at subsequent steps of cleaning procedure. (B) Resonance wavelength dependence of the refractive index for left resonance before modification and after regeneration of the sensor surface.

multiple washing and incubation steps (as in ELISA). Such a biosensor for bacteriophage detection can find application in biotechnology industry where the phages are a real threat for bacteria-based processes. Sensor for norovirus VLPs may find application in vaccine testing, because VLPs are widely studied as possible vaccine candidates against norovirus infections. Moreover, due to the morphological and antigen similarity between VLPs and native norovirus, LPFG biosensor can be used for fast norovirus detection. As demonstrated, presented method is versatile and easily applicable for detection of different targets by selecting the appropriate antibodies. Additionally, the method of surface regeneration by removing organic bio-layers was presented. It may decrease production costs and enable conducting different measurements on the same LPFG sensor.

4.4 Materials and methods

Chemicals and materials

Bovine serum albumin (BSA), sodium hydroxide, acetone, ethanol, biotin, avidin, and PBS tablets were purchased from Sigma Aldrich. PBS consists of 0.01 M phosphate buffer, 0.0027 M potassium chloride and 0.137 M sodium chloride, pH 7.4 at 25 °C. LB broth and LB-agar were bought from Carl Roth as instant mixes ready to dissolve in deionized water. LB medium consisted of 10 g/L of tryptone, 5 g/L of yeast extract, and 10 g/L of sodium chloride. LB-agar additionally contained 15 g/L of agar and top LB-agar contained 5 g/L

of agar. APTES and TESPSA were purchased from Gelest. Polyclonal anti-T7 antibody was purchased from MBL International and mouse monoclonal [17E11] to Norovirus GII.4 (VP1 protein) antibody (anti-VP1) was purchased from Abcam. LPFG fabrication is described in section 2.4.

Instrumentation

Yokogawa AQ6370B spectrum analyzer and a Leukos SM30 supercontinuum white light laser source were used. The measurements were done in closed flow cell as described in section 2.4.

Sensor surface functionalization

For immobilization of biotin surface was modified with APTES for 2 h (as described in section 3.4). Then, carboxyl group in biotin was activated by adding EDC (final concentration 0.4 mg/mL) to biotin solution (1 mg/mL in PBS). Activated biotin solution was injected into the measurement cell and sensor was incubated for 1 h. In this step and the following the optical transmission of the LPFG in the range of λ = 1500–1700 nm was monitored. After surface modification with biotin, the sensor was washed and measured in PBS. Avidin detection was done by injecting increasing concentrations of avidin in PBS (from 1 μg/mL to 100 μg/mL) into the system. Incubation was done for 15 min in each concentration and was followed by PBS washing (2 times 5 min).

Immobilization of antibodies was done according to procedure described in section 3.4. First, LPFG was modified with TESPSA in 4-hour procedure. During the next steps the optical transmission of the LPFG in the range of λ = 1500–1700 nm was monitored. Anti-T7 or anti-VP1 antibody solution (0.01 mg/mL in PBS) was injected into the measuring cell for 1 h to covalently bond the antibody to the surface via a succinic anhydride functionality ring opening reaction that leads to the formation of an amide bond. Then, the LPFG sensor surface was washed three times with PBS and kept in fresh portion of PBS for 10 min to obtain reference measurements. Next, BSA solution (0.1% in PBS) was injected into the cell for 30 min to block any remaining unspecific sites and the washing procedure was repeated.

Virus detection

Antibody-modified LPFGs were used for detection of T7 phages or norovirus VLPs. For sensitivity analysis phage solutions in concentrations of 5×10^3,

5×10^5, 5×10^7, and 5×10^9 PFU/mL in PBS were prepared and norovirus VLPs solutions in concentrations of 1 ng/mL, 10 ng/mL, 100 ng/mL, 1 μg/mL and 10 μg/mL in PBS were prepared. For phage selectivity measurements concentration of MS2 and T7 phage solutions was 5×10^7 PFU/mL, while for VLPs two negative controls (HA VLP and RHDV VLP) and positive control (Norovirus VLP) were used in concentration of 10 ng/mL.

During the detection step, solutions with increasing concentrations of target virus were injected into the measuring cell for 30 min each. After the measurements of each concentration, sensor was washed and measured in PBS to obtain reference results. The difference between resonance wavelengths before virus addition and after virus detection was taken as the sensor response.

For selectivity measurements, the sensor was immersed in non-specific samples first and then in positive sample for 30 min in each solution. After the measurements in each solution sensor was washed and measured in PBS.

Bacteriophage preparation

T7 bacteriophages and MS2 bacteriophages were obtained from University of Gdansk (Poland). Phages were prepared and purified according to procedures provided by Sambrook et al. [1] Before experiments the number of active phages in the samples was determined by plaque count method. 20 mL of LB-agar medium was poured onto the plastic petri dish and left to solidify. Then 4 mL of top LB-agar was mixed with 200 μL of overnight culture of *E. coli* MG1655 and poured onto the plate. Tenfold dilutions of phage samples were prepared and 5-μL droplets of each dilution were spotted onto the top agar layer. Plates were incubated overnight at 37 °C and plaques were counted and recalculated to plaque forming units/mL.

Norovirus VLPs preparation

Norovirus VLP, RHDV VLP, and HA VLP (H5N1) were obtained from dr Beata Gromadzka, Intercollegiate Faculty of Biotechnology, University of Gdansk and Medical University of Gdansk (Poland). VLPs were produced in Sf9 insect cells infected with the recombinant baculovirus as described previously [33] and purified using ultracentrifugation and size exclusion chromatography. Transmission electron micrographs were done with Philips CM 100 electron microscope. Norovirus VLPs were adsorbed onto carbon-coated grids, stained with 2% uranyl acetate and examined immediately.

Regeneration of sensor surface

To check the possibility of sensor surface regeneration, all washing steps was monitored by measuring the optical transmission in the range of λ = 1500-1700 nm. The sensor surface after virus detection experiments was immersed in 0.5 M NaOH for 5 min to remove all of the organic layers from the fiber and then measured in PBS. Washing was repeated until the transmission spectrum in PBS was similar to that measured before any surface modifications. RI sensitivity measurements were done in water/glycerol solutions as described in chapter 2, section 2.4.

4.5 References

(1) Sambrook, J.; Fritsch, E. F.; Maniatis, T., *Molecular Cloning, a laboratory manual, vol 1*; Cold Spring Harbor Laboratory Press: 1989.

(2) Dulbecco, R.; Vogt, M. Some problems of animal virology as studied by the plaque technique. *Cold Spring Harbor Symposia on Quantitative Biology* **1953**, *18*, 273–279.

(3) Adams, A. N.; Clark, M. F. Characteristics of the Microplate Method of Enzyme-Linked Immunosorbent Assay for the Detection of Plant Viruses. *Journal of General Virology* **1977**, *34*, 475–483.

(4) De la Rica, R.; Stevens, M. M. Plasmonic ELISA for the ultrasensitive detection of disease biomarkers with the naked eye. *Nature Nanotechnology* **2012**, *7*, 821–824.

(5) Mackay, I. M.; Arden, K. E.; Nitsche, A. Real-time PCR in virology. *Nucleic acids research* **2002**, *30*, 1292–305.

(6) Watzinger, F.; Ebner, K.; Lion, T. Detection and monitoring of virus infections by real-time PCR. *Molecular Aspects of Medicine* **2006**, *27*, 254–298.

(7) Khansili, N.; Rattu, G.; Krishna, P. M. Label-free optical biosensors for food and biological sensor applications. *Sensors and Actuators B: Chemical* **2018**, *265*, 35–49.

(8) Lee, C.; Gaston, M. A.; Weiss, A. A.; Zhang, P. Colorimetric viral detection based on sialic acid stabilized goldnanoparticles. *Biosensors and Bioelectronics* **2013**, *42*, 236–241.

(9) Lesniewski, A.; Los, M.; Jonsson-Niedziółka, M.; Krajewska, A.; Szot, K.; Los, J. M.; Niedziolka-Jonsson, J. Antibody Modified Gold Nanoparticles for Fast and Selective, Colorimetric T7 Bacteriophage Detection. *Bioconjugate Chemistry* **2014**, *25*, 644–648.

(10) Kannan, P.; Los, M.; Los, J. M.; Niedziolka-Jonsson, J. T7 bacteriophage induced changes of gold nanoparticle morphology: biopolymer capped gold nanoparticles as versatile probes for sensitive plasmonic biosensors. *The Analyst* **2014**, *139*, 3563–3571.

(11) Xiao, C.; Jiang, F.; Zhou, B.; Li, R.; Liu, Y. Immobilization of Escherichia coli for detection of phage T4 using surface plasmon resonance. *Science China Chemistry* **2012**, *55*, 1931–1939.

(12) Altintas, Z.; Pocock, J.; Thompson, K. A.; Tothill, I. E. Comparative investigations for adenovirus recognition and quantification: Plastic or natural antibodies? *Biosensors and Bioelectronics* **2015**, *74*, 996–1004.

(13) Usachev, E. V.; Agranovski, E.; Usacheva, O. V.; Agranovski, I. E. Multiplexed Surface Plasmon Resonance based real time viral aerosol detection. *Journal of Aerosol Science* **2015**, *90*, 136–143.

(14) Wang, S.; Shan, X.; Patel, U.; Huang, X.; Lu, J.; Li, J.; Tao, N. Label-free imaging, detection, and mass measurement of single viruses by surface plasmon resonance. *Proceedings of the National Academy of Sciences of the United States of America* **2010**, *107*, 16028–32.

(15) Ymeti, A. et al. Fast, Ultrasensitive Virus Detection Using a Young Interferometer Sensor. *Nano Letters* **2007**, *7*, 394–397.

(16) Mitra, A.; Ignatovich, F.; Novotny, L. Real-time optical detection of single human and bacterial viruses based on dark-field interferometry. *Biosensors and Bioelectronics* **2012**, *31*, 499–504.

(17) Scherr, S. M.; Daaboul, G. G.; Trueb, J.; Sevenler, D.; Fawcett, H.; Goldberg, B.; Connor, J. H.; Ünlü, M. S. Real-Time Capture and Visualization of Individual Viruses in Complex Media. *ACS Nano* **2016**, *10*, 2827–2833.

(18) Shafiee, H.; Lidstone, E. a.; Jahangir, M.; Inci, F.; Hanhauser, E.; Henrich, T. J.; Kuritzkes, D. R.; Cunningham, B. T.; Demirci, U. Nanostructured Optical Photonic Crystal Biosensor for HIV Viral Load Measurement. *Scientific Reports* **2014**, *4*, 4116.

(19) Vollmer, F.; Arnold, S.; Keng, D. Single virus detection from the reactive shift of a whispering-gallery mode. *Proceedings of the National Academy of Sciences of the United States of America* **2008**, *105*, 20701–4.

(20) Nasrin, F.; Chowdhury, A. D.; Takemura, K.; Lee, J.; Adegoke, O.; Deo, V. K.; Abe, F.; Suzuki, T.; Park, E. Y. Single-step detection of norovirus tuning localized surface plasmon resonance-induced optical signal between gold nanoparticles and quantum dots. *Biosensors and Bioelectronics* **2018**, *122*, 16–24.

(21) Calendar, R., *The Bacteriophages*; Oxford University Press: 2006, p 746.

(22) Centers for Disease Control and Prevention (CDC). (2019) Norovirus Worldwide. Available online at: https://www.cdc.gov/norovirus/trends-outbreaks/worldwide.html (Accessed 16 January 2019).

(23) Zeltins, A. Construction and Characterization of Virus-Like Particles: A Review. *Molecular Biotechnology* **2013**, *53*, 92–107.

(24) Aliabadi, N.; Lopman, B. A.; Parashar, U. D.; Hall, A. J. Progress toward norovirus vaccines: considerations for further development and implementation in potential target populations. *Expert Review of Vaccines* **2015**, *14*, 1241–1253.

(25) Haugland, R. P.; You, W. W. Coupling of antibodies with biotin. *Methods in molecular biology (Clifton, N.J.)* **2008**, *418*, 13–24.

(26) Vörös, J. The Density and Refractive Index of Adsorbing Protein Layers. *Biophysical Journal* **2004**, *87*, 553–561.

(27) Pugliese, L.; Coda, A.; Malcovati, M.; Bolognesi, M. Three-dimensional Structure of the Tetragonal Crystal Form of Egg-white Avidin in its functional Complex with Biotin at 2·7 Å Resolution. *Journal of Molecular Biology* **1993**, *231*, 698–710.

(28) Gang, A.; Gabernet, G.; Renner, L. D.; Baraban, L.; Cuniberti, G. A simple two-step silane-based (bio-) receptor molecule immobilization without additional binding site passivation. *RSC Adv.* **2015**, *5*, 35631–35634.

(29) Zhu, H.; White, I. M.; Suter, J. D.; Fan, X. Phage-based label-free biomolecule detection in an opto-fluidic ring resonator. *Biosensors and Bioelectronics* **2008**, *24*, 461–466.

(30) Pogan, R.; Dülfer, J.; Uetrecht, C. Norovirus assembly and stability. *Current Opinion in Virology* **2018**, *31*, 59–65.

(31) Ashiba, H.; Sugiyama, Y.; Wang, X.; Shirato, H.; Higo-Moriguchi, K.; Taniguchi, K.; Ohki, Y.; Fujimaki, M. Detection of norovirus virus-like particles using a surface plasmon resonance-assisted fluoroimmunosensor optimized for quantum dot fluorescent labels. *Biosensors and Bioelectronics* **2017**, *93*, 260–266.

(32) Lin, S. C. H.; Pugacz-Muraszkiewicz, I. Local stress measurement in thin thermal SiO2 films on Si substrates. *Journal of Applied Physics* **1972**, *43*, 119–125.

(33) Huhti, L.; Blazevic, V.; Nurminen, K.; Koho, T.; Hytönen, V. P.; Vesikari, T. A comparison of methods for purification and concentration of norovirus GII-4 capsid virus-like particles. *Archives of Virology* **2010**, *155*, 1855–1858.

Chapter 5

LPFG sensors coated with thin metal oxide overlays[1]

5.1 Introduction

Deposition of thin layers on the LPFG surface can be advantageous in the context of possible application range of LPFG-based sensors and also their sensitivity. As briefly mentioned in chapter 2, one of the possible methods to increase sensitivity of LPFG-based devices is based on the deposition of thin coatings with high RI [1]. It was shown that thin film deposition on the LPFG surface can enhance RI sensitivity by the mode transition effect [2, 3]. For certain thickness and optical parameters of thin film, one of the lowest order cladding modes is gradually transited from the LPFG to overlay. The transition causes modification of the propagation conditions for guided cladding modes and each mode follows the pattern of its adjacent lower order cladding mode. To reach the mode transition (MT) effect it is necessary to precisely chose the properties of thin film. Several different methods for thin film deposition was proposed for LPFG coating, such as Langmuir-Blodgett deposition [2], electrostatic self-assembly [4], physical [5] and chemical [6] vapour-based deposition.

[1] Parts of this chapter have been published as:
Janczuk-Richter, M.; Piestrzyńska, M.; Burnat, D.; Sezemsky, P.; Stranak, V.; Bock, W.J.; Bogdanowicz, R.; Niedziółka-Jönsson, J.; Śmietana, M. *Sensors and Actuators B: Chemical* **2019**, *279*, 223-229
Piestrzyńska, M.; Dominik, M.; Kosiel, K.; Janczuk-Richter, M.; Szot-Karpińska, K.; Brzozowska, E.; Shao, L.; Niedziółka-Jönsson, J.; Bock, W.J.; Śmietana, M. *Biosensors and Bioelectronics*, **2019**, *133*, 8-15

It is also possible to combine the mode transition effect with dispersion turning point. As shown in [7], the optimization of polystyrene coating thickness enable obtaining RI sensitivities approaching 10,000 nm/RIU for RIs around 1.347 RIU.

Applications of thin films on LPFGs are not limited to increasing the sensitivity. By choosing nanomaterial that offers specific response to target chemical species it was possible to obtain sensors for organic vapors, metal ions, humidity, and organic solvents [8–12]. For example, polyethylene glycol/polyvinyl alcohol composite films were used for humidity measurements [11]. Moreover, thin overlays can be used as protective coatings. Several metal oxides deposited by atomic layer deposition technique were tested in alkaline solutions. The Hf_xO_y, Zr_xO_y, and Ta_xO_y proved to be stable for even 20 h in pH 14 on planar substrates [13]. It was also demonstrated theoretically and experimentally, that metal coatings, such as gold or silver, can be used to obtain LPFG-assisted surface plasmon resonance sensors [14–17]. Wei et al. [17] showed a graphene-based LPFG-SPR sensor. A monolayer of graphene was deposited on the Ag film of the LPFG-SPR sensor that increases the intensity of the evanescent field on the surface of the fiber and thereby enhances the interaction between surface plasmons and molecules. Proposed sensor was used for detection of methane vapor.

Deposition of metal coatings and other conductive materials, such as indium tin oxide (ITO) or fluorine-doped tin oxide (FTO), on the optical fiber surface enable to perform electrical/electrochemical and optical measurements simultaneously. This approach was not applied to the LPFG sensors yet, but other optical structures were tested towards the possibility for simultaneous electrochemical and optical sensing. The most developed multi-domain technique is a combination of surface plasmon resonance and electrochemical analysis (EC-SPR). Since the SPR substrates are usually made of thin gold or silver layers deposited on glass, they can be also used as electrodes in electrochemical setups [18, 19]. EC-SPR provides simultaneous information about electrochemical and optical properties of films formed on the sensor surface and makes possible deeper analysis of the studied chemical or biological system. EC-SPR has been already used for characterization of various conductive and electroactive polymer films [20], evaluation of live cancer cells behavior [21], studying enzyme activity [22], and DNA hybridization [23]. Recently, a new solution of this novel multi-domain sensing technique was demonstrated, where EC-SPR

sensor for monitoring of electroactive biofilms was based on optical fiber [24]. Such a sensor showed some advantages resulting from the use of optical fiber instead of planar substrates, i.e., small size, possibility for remote control and capability for measurements in readily available places. Another application of optical fibers in multi-domain sensing was based on lossy-mode resonance (LMR) [25]. This thin-film-based optical effect was obtained by sputtering of ITO on the core of polymer-clad silica fibers. The ITO-LMR sensors were used for real-time monitoring of electrochemical reactions and detection of ketoprofen by its electropolymerization [26]. Application of thin conductive films on LPFG sensors will enable obtaining a new sensitive multi-domain configuration for simultaneous optical and electrochemical measurements.

In this chapter I will show application of tantalum oxide thin film for sensitivity enhancement of LPFG-based device (in both RI sensing and biosensing). Additionally, I will demonstrate utilization of ITO-coated LPFG for simultaneous electrochemical and optical measurements in specially prepared combined setup.

5.2 Results and discussion

5.2.1 Tantalum oxide nano-coated LPFGs

Characterization of TaO_x-coated LPFGs

The improvement in RI sensitivity influences also label-free biosensing capabilities of optical sensors. As explained in previous section, high-RI thin coatings can significantly improve RI sensitivity of LPFG. In my work, I was testing tantalum-oxide-coated LPFG sensors. Prior to deposition of TaO_x on the LPFG surface, numerical analysis was done in order to determine the thickness range of TaO_x film where both dispersion turning point and mode transition effect can be observed. In this working conditions the RI sensitivity should be the highest. According to obtained results (described in details in [27]), the best performance is obtained for TaO_x thickness from 57 to 62.5 nm, assuming that the real part of RI (n) of the film material is from 2 to 2.05 RIU in the investigated for LPFG spectral range. Such conditions enable optimization of the working point of the device to DTP of $LP_{0,10}$ cladding mode. For higher thicknesses the sensitivity drops significantly.

Next, TaO_x films with thickness between 57 and 65 nm were deposited on a set of LPFGs. The most sensitive sensor in the RI range close to that

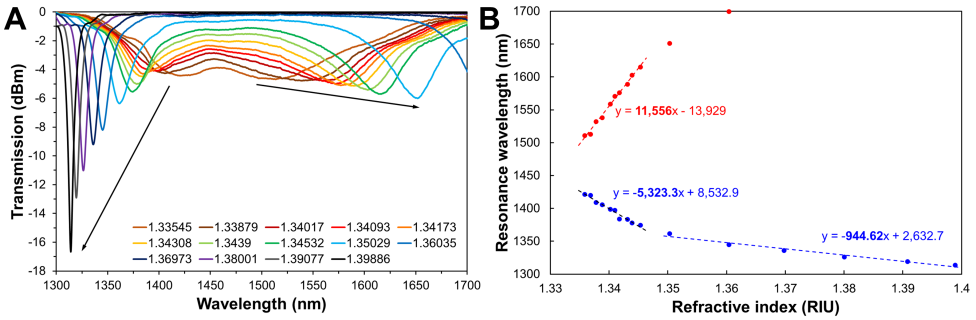

Figure 5.1: Response of TaOx-modified LPFG to external RI. (A) Transmission spectra for selected RIs. (B) Resonance wavelength dependance on RI for left (blue-shifting) and right (red-shifting) resonances.

of water was obtained for the thickness of 63.4 nm which matched well with numerical analysis. Evolution of the transmission spectrum with external RI for this sample is shown in Figure 5.1A. For the right (red-shifting) resonance, the sensitivity exceeded 11,500 nm/RIU in the RI range 1.335–1.345 RIU and for RI greater than 1.36 RIU it was impossible to determine the resonance wavelength due to spectral range limitations of the setup. For the left (blue-shifting) resonance, the RI sensitivity exceeded 5300 nm/RIU in the RI range 1.335–1.345 RIU and dropped below 1000 nm/RIU for RIs greater than 1.35 RIU (Figure 5.1B). Very high sensitivity, especially for right resonance, was possible to obtain due to the precise deposition of a thin TaO_x layer with selected thickness.

Avidin detection

To test the usefulness of TaO_x-coated LPFG for biosensing, the interactions between biotin and avidin was monitored similarly as demonstrated in section 4.2.1. Utilization of TaO_x thin film for sensitivity enhancement enable using the same modification method (silanization) as in case of bare fibers. First, TaO_x-LPFG was modified with APTES and then activated biotin molecules were immobilized on the surface. During biotin immobilization and following steps transmission response of the sensor was monitored. In the next steps, increasing concentrations of avidin (from 100 ng/mL to 1 mg/mL) were injected into the measuring cell and the sensor was incubated for 30 min in each concentration. Washing and reference measurements in PBS were done between those steps. The results of the experiment are shown in Figure 5.2. As can be seen in panel

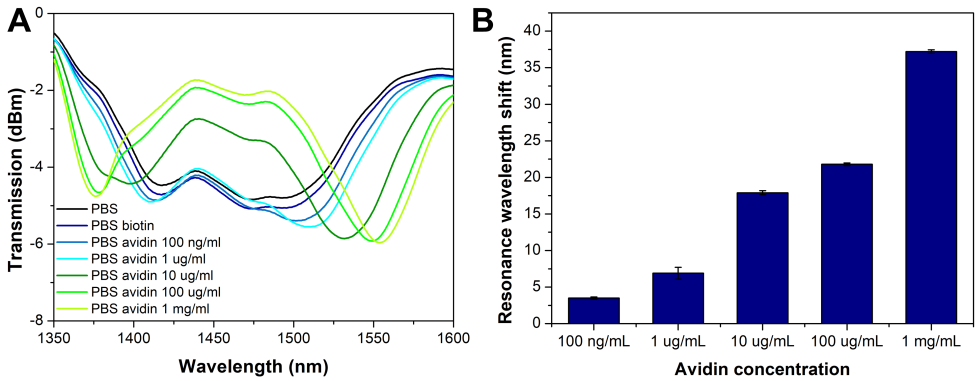

Figure 5.2: Monitoring of biotin-avidin interactions by TaO_x-coated LPFG. (A) Spectra measured in PBS before biotin immobilization, after biotin immobilization, and after incubation in avidin solutions. (B) Resonance wavelength shift referred to measurement performed in PBS before avidin addition for differenr avidin concentrations.

A, the shape of the spectrum made it hard to follow the minimum of right resonance, especially for the initial steps. Therefore, in panel B, the resonance wavelength shifts referred to the measurements done after biotin immobilization for increasing avidin concentrations are shown for left resonance. The shifts ranged from 2.7 to 37 nm for avidin solutions in concentration from 100 ng/mL to 1 mg/mL. Comparing to results obtained on bare LPFG fiber, the spectral shifts observed for TaO_x-LPFG were about one order of magnitude higher. For example, incubation of TaO_x-coated sensor in 1 μg/mL of avidin resulted in resonance shift of 6.9 nm while for bare LPFG shift reached 0.8 nm.

Bacteria detection

Additionally, bacteria detection experiments were also performed with TaOx-LPFGs. The results are described in details in [27]. The sensor was functionalized with layer of bacteriophage adhesin proteins that specifically binds bacteria *E. coli*. In this case, attachment of receptor molecules induced a significant wavelength shift that moves resonances away from DTP and therefore the sensitivity of the grating has already been greatly reduced (Figure 5.3A). Sensor incubation in increasing concentration of bacteria (from 10^3 to 10^7 colony forming units (CFU)/mL) induced a measurable wavelength shifts but the maximum shift of only 3.3 nm was obtained for highest studied bacteria concentration (10^7 CFU/mL) as shown in Figure 5.3B. This experiment demonstrated that the in-

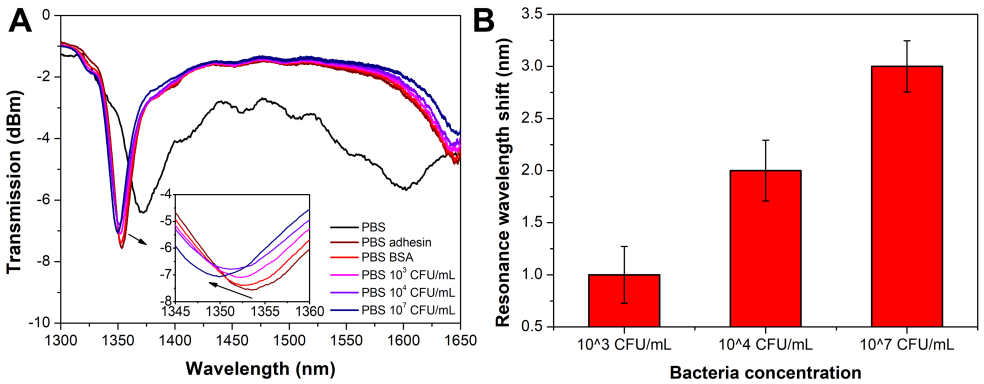

Figure 5.3: Detection of bacteria *E. coli* by TaO_x-coated LPFG. (A) Spectra measured in PBS before and after adhesin immobilization, and after incubation in bacteria solutions. (B) Resonance wavelength shift referred to measurements performed in PBS before bacteria detection for different bacteria concentrations.

fluence of the biofunctionalization process, i.e. receptor immobilization, on the working conditions of ultrasensitive sensor has to be taken into consideration. This is particularly important when large biomolecules are used as receptors, because their immobilization may significantly reduce RI sensitivity that was initially adjusted for non-modified sensor.

5.2.2 Indium tin oxide nano-coated LPFGs

Characterization of ITO-coated LPFGs

Deposition of optically transparent and electrically conductive ITO films on LPFGs enables to use the device not only to monitor local external RI changes but also as working electrode in electrochemical setup. Prepared system that was suitable for such measurements is presented in Figure 5.4. To obtain sensitive structures operated in the vicinity of DTP it was required to over-etch the fiber cladding and then deposit thin ITO film. To check the influence of the ITO overlay on the RI sensitivity, a series of optical measurements was done in water/glycerol solutions, similarly as in the case of bare and TaO_x-coated sensors. In particular, two samples were chosen (denoted as Sample A and Sample B) that differ only in the HF etching time (longer for Sample A). Based on trial processes, the deposition parameters were adjusted to get 40 nm of the ITO coating.

Spectral response of the ITO-LPFG samples to external RI changes is shown

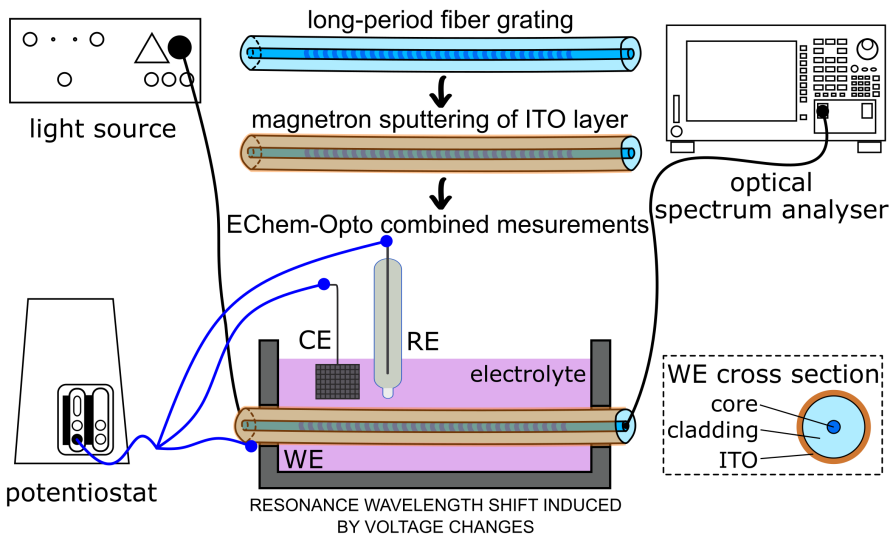

Figure 5.4: Schematic representation of the combined setup used for simultaneous optical and electrochemical measurements, where the electrodes were marked as WE, RE and CE for working, reference and counter electrodes, respectively. Additionally, a cross-section of the working electrode was shown.

in Figure 5.5. Sample A operated in close proximity of the DTP. With the increase of RI, the resonance first got dipper and then splitted into the pair of resonances for RIs higher than 1.36 RIU. The highest RI sensitivity can be obtained here, but the resonance wavelength for lower external RIs cannot be determined. In the RI range from 1.36 to 1.39 RIU the sensitivity exceeded 5,000 nm/RIU. For Sample B resonances were already separated and shifted away from the DTP for all applied external RIs. Left resonance was visible during all the measurements and it shifted towards shorter wavelengths with increasing RI while right resonance was outside the spectral range of the setup. RI sensitivity reached about 2,200 nm/RIU for external RIs $>$ 1.341 RIU. Sensitivities of ITO-LPFGs were comparable with those obtained for fiber-optic SPR devices that typically reached up to a few thousands nm/RIU [28]. For example, fiber-optic SPR sensor coated with thin gold layer (39 nm) reached RI sensitivity of about 4,000 nm/RIU [29].

Further characterization of ITO-LPFGs was done with scanning electron microscopy. SEM images were done to verify the thickness of the ITO layer and its uniformity on the fiber. The cross-sections of the fiber (Sample B) are shown in Figure 5.6A and B. ITO thickness analysis was done on a series of

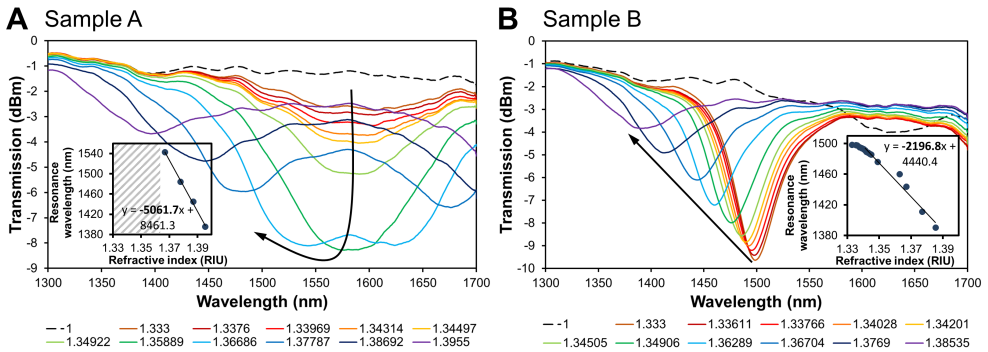

Figure 5.5: Spectral responce of the ITO-LPFGs to changes in external RI for Sample A (A) and Sample B (B). Arrows show the direction of changes for increasing external RI. Insets show resonance wavelength dependance on RI. For Sample A it was impossible to determine resonance wavelength for most external RIs due to vicinity of the DTP.

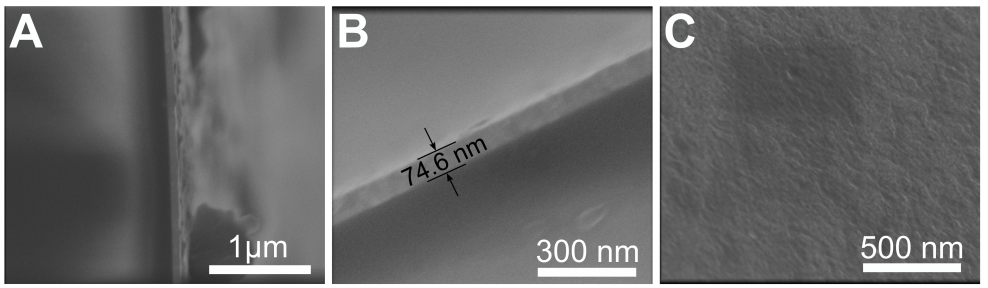

Figure 5.6: SEM images of the cross-section of the ITO-LPFG in lower magnification (A) and higher magnification with indicated ITO thickness (B), and ITO surface (C).

SEM images showing different fragments of the fiber cross-section. Measured thickness was 74.6 ± 2.6 nm as marked in Figure 5.6B. Thickness observed in the SEM images was higher than this measured on reference Si samples used in trial processes (40 nm), the most probably due to different geometrical configuration of these samples. The ITO surface deposited on the fiber was smooth and uniform as shown in Figure 5.6C.

Simultaneous electrochemical and optical measurements

In the experiments with simultaneous electrochemical and optical measurements, ITO-LPFG served as both working electrode in electrochemical setup

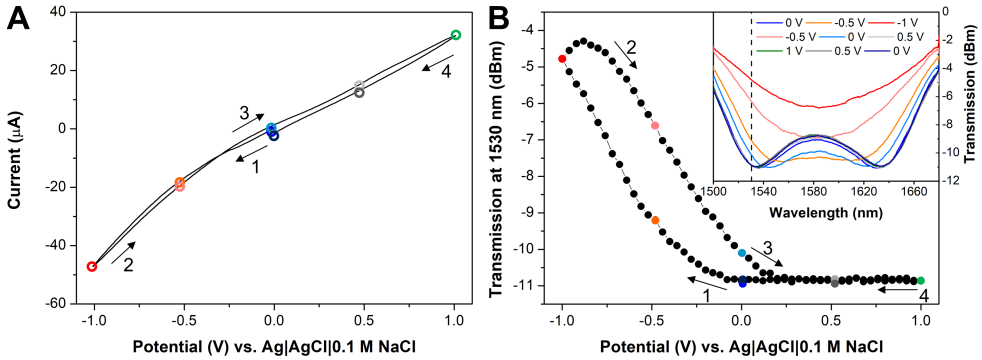

Figure 5.7: Response of Sample A to applied potential during simultaneous electrochemical and optical measurements in 5 mM $K_3[Fe(CN)_6]$ and 5 mM $K_4[Fe(CN)_6]$ in PBS, where (A) is the electrochemical response (cyclic voltammogram) and (B) shows transmission measured at $\lambda = 1530$ nm. Inset: transmission spectra at selected potentials. Points corresponding to certain spectra are marked with the same color in (A) and (B).

and as a structure optically sensitive to the phenomena taking place on the ITO surface or in its vicinity. Cyclic voltammetry (CV) was used to apply potential to the ITO-LPFG. The potential was sweeping from 0 V to -1 V then to 1 V and back to 0 V with the scan rate of 10 mV/s. This rate enable to measure between 60 to 80 transmission spectra per CV cycle depending on the chosen wavelength range. PBS solution containing redox probes (5 mM $K_3[Fe(CN)_6]$ and 5 mM $K_4[Fe(CN)_6]$) was used to check both the electrochemical and optical response. No electrochemical reaction related to oxidation and reduction of redox probe was observed on the voltammogram (Figure 5.7A), probably due to low thickness of ITO film and thus its high resistivity [30]. Interestingly, significant changes were observed in the transmission spectra when the varying potential was applied. Decrease and increase in potential induced shift of the resonances towards and away from DTP, respectively. Because the working point of Sample A was adjusted to DTP, it was impossible for most of the applied potentials to determine resonance wavelength. Therefore, I was tracing the changes in transmission at fixed wavelength ($\lambda = 1530$ nm that was on the left slope of the resonance). The results are summarized in Figure 5.7B. As can be seen, changes reaching up to 9 dBm/V were observed for negative potentials while almost no changes in optical response were monitored for positive potentials. Moreover, there was a hysteresis observed for negative potentials.

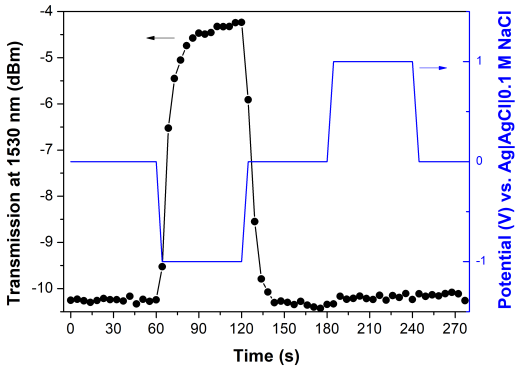

Figure 5.8: Dynamic optical response of Sample A during electrochemical stimulation in 5 mM $K_3[Fe(CN)_6]$ and 5 mM $K_4[Fe(CN)_6]$ in PBS. Each potential was applied for 60 s.

To better understand the process, I also investigated the optical response time to the potential changed stepwise (rather than gradually as applied earlier). The potential was applied in the following order: 0 V, -1 V, 0 V, 1 V, 0 V, and kept 60 s in each step. Results showing transmission measured at $\lambda = 1530$ nm vs. time are demonstrated in Figure 5.8. After rapid potential change from 0 V to -1 V the transmission changed immediately (the resonance shifted towards DTP). Optical signal stabilized after about 30 s. Next potential switch from -1 V to 0 V caused sudden decrease in the transmission, i.e., shift away from DTP, that was followed by its stabilization. Change of potential to 1 V and then back to 0 V resulted in almost no change in the optical signal. Observed behavior, i.e., direction and size of changes, was similar to this obtained for gradual potential changes in cyclic voltammetry.

Changes in optical response observed for both of the above experiments correspond to changes in external RI. They can be attributed to two factors: (i) changes in optical properties of the ITO thin film, and/or (ii) changes in external medium in close vicinity of the ITO surface. (i) In ITO (n-type semiconductor), the electrons are majority carriers. According to the Drude-Lorentz model, real part of RI (n) of a metal or semiconductor depends on the number of free carriers in the material [31]. Therefore, any changes in electron density induced, e.g., by application of potential, affect the optical properties of ITO. In negative potentials, concentrations of electrons is higher near the surface so its n is decreased [32]. It was also demonstrated for thin ITO films, that potential

alterations induce changes of the imaginary part of RI (k) [33]. These changes in optical properties of ITO induce variations of ITO-LPFG optical response. (ii) The optical properties of the external medium near the electrode surface are modified by the formation and rearrangements in the Helmholtz double layer [34]. The layer is formed on the surface of charged electrode immersed in electrolyte by attraction of counterions and repelling of co-ions. It can be modeled as a capacitor in which potential changes are followed by changes in charge, i.e., concentrations and charges of ions. The alterations in double layer composition influences the external RI in vicinity of ITO what is observed in optical response of ITO-LPFG. Changes in the properties of electrical double layer are likely responsible for the presence of hysteresis (Figure 5.7B) and limitations in dynamics of optical response presented in Figure 5.8. Similar modulation of optical response by changes in the applied potential were previously demonstrated for SPR-based measurements on gold surfaces [24, 35, 36] and also ITO-based LMR sensor [25].

In case of SPR measurements combined with electrochemistry it was shown that the changes in optical response upon modulation of potential depend on the compositions of the electrolyte solution [35]. Therefore, optical response to applied potential of Sample B was monitored in PBS and in PBS with redox probes (5 mM $K_3[Fe(CN)_6]$ and 5 mM $K_4[Fe(CN)_6]$), and compared in Figure 5.9. The optical response was analyzed by tracing the shift of the resonance wavelength. Three CV scans were performed in both solution (each scan followed the scheme 0 V $\rightarrow$ -1 V $\rightarrow$ 1 V $\rightarrow$ 0 V). Response in PBS with redox probe was similar as for Sample A, i.e., big changes for negative potential and almost no changes in positive potentials (Figure 5.9A and C). Interestingly, when measurements were done solely in PBS, the shifts were over 3 times higher and observed also for positive potentials (Figure 5.9B and D). The current response for Sample B is shown in Figure 5.10. Similarly as in case of Sample A, no peaks related to oxidation and reduction of redox probe are present in the voltammogram.

Differences observed in optical response measured in PBS and in PBS with redox probes can be attributed to the presence of big negatively charged ions $[Fe(CN)_6]^{3-/4-}$ [37]. Smaller changes in the wavelength shifts in solution containing the redox probe may be caused by the interactions of the $[Fe(CN)_6]^{3-/4-}$ ions with the ITO surface. Their presence near/on the surface causes that the migration of other ions under the influence of applied potential is less visible

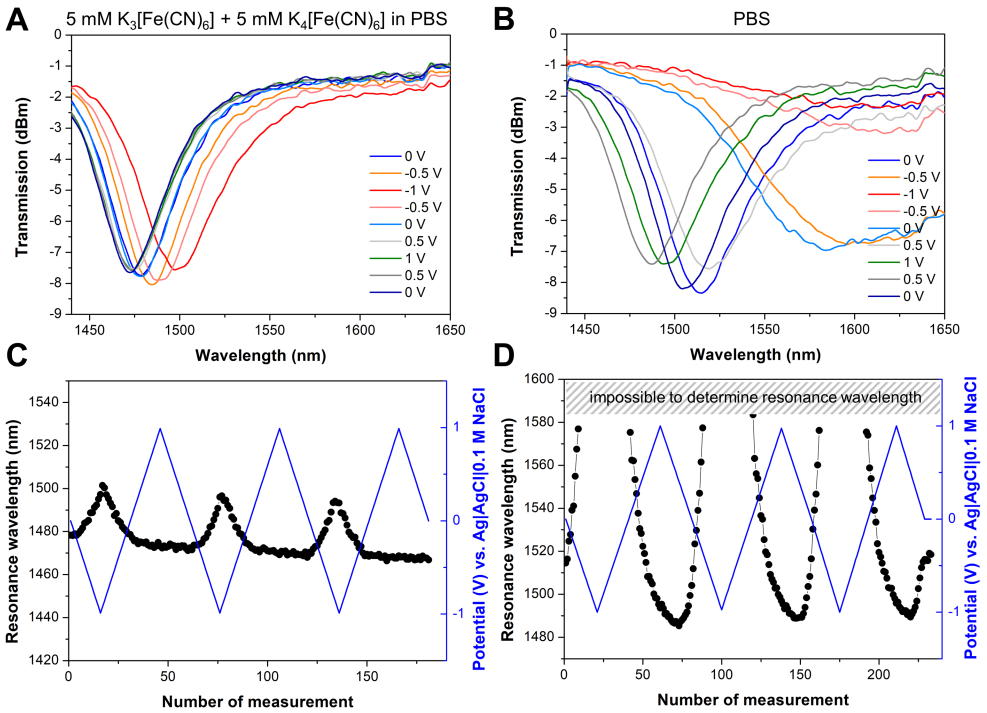

Figure 5.9: Optical response of Sample B during electrochemical measurements (three CV scans). Transmission spectra for selected potentials are shown for first scan in PBS with redox probe (A) and in PBS only (B), and corresponding resonance wavelength is shown in (C) for PBS with redox probe and (D) for PBS. For some measurements performed in PBS it was impossible to determine resonance wavelength, due to vicinity of the DTP.

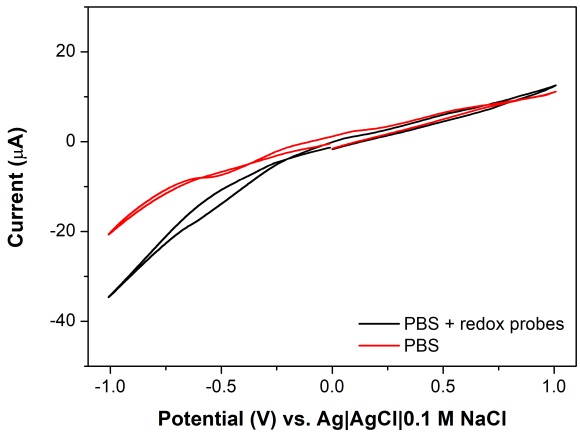

Figure 5.10: Electrochemical response (cyclic voltammogram) of Sample B measured in PBS and in PBS with redox probes.

in the optical response. It must also be noticed that the transmission spectra measured for Sample A in PBS in negative potentials corresponds to external RI between water and air (as shown in Figure 5.5B). In addition to the changes in optical properties of ITO and double layer formation, this response may be influenced by hydrogen evolution that occurs in negative potentials [38] and formation of gas-like external RI on the ITO surface.

5.3 Conclusions

Utilization of thin metal oxide films as LPFG overlays enable not only to increase the sensitivity to external RI, but also to expand possible applications of LPFG-based sensors. To obtain ultrasensitive LPFG-based sensor it is essential to properly tune film thickness. As shown in the example of TaO_x-coated LPFGs, deposition of metal oxide layer with the thickness chosen according to numerical analysis enable obtaining RI sensitivity higher than 11,500 nm/RI in 1.335–1.345 RIU range. Comparing to bare LPFGs used in my work, the improvement of RI sensitivity is almost sixfold. Better RI sensitivity also translated into better label-free sensitivity of prepared biosensors. The spectral shifts observed in the experiment with avidin detection were one order of magnitude better for TaO_x-LPFG than for bare fiber. The experiments regarding avidin and bacteria detection also showed that the influence of the receptor immobilization on optical response of the sensor has to be taken into consideration.

This is particularly important when the LPFGs is optimized to ultra-high sensitivity and when relatively large biomolecules are used as recognition elements, because their immobilization on the surface may significantly reduce initially optimized RI sensitivity.

Additional advantage of thin metal oxide films is the possibility to expand application range of LPFG-based sensors. As demonstrated, ITO-coated LPFG can serve as both working electrode in electrochemical setup and as sensor highly sensitive to refractive index in simultaneous electrochemical and optical measurements. The optical response of the device was strongly dependent on the applied potential, especially in negative potentials range. Changes observed in optical spectra during gradual and sudden changes of the potential may be attributed to the alterations in optical properties of both ITO overlay and the electrolyte in the vicinity of electrode surface (double layer formation and rearrangements). Combined optical and electrochemical measurements enable gathering significantly more information on the investigated processes than the methods applied separately. Proposed approach gives also a possibility to initiate a specific process in one domain and monitor its progress in other domain (e.g. measurements of nanometer changes in the layer thickness deposited by electropolymerization [26]). The developed ITO-LPFG structures can be further used as fiber-based sensors and biosensors with integrated opto-electrochemical readout.

5.4 Materials and methods

Chemicals and materials

Acetone, ethanol, methanol, glycerol, chloroform, biotin, avidin, and PBS tablets were purchased from Sigma Aldrich. PBS (pH 7.4 at 25 °C) consists of 0.01 M phosphate buffer, 0.0027 M potassium chloride and 0.137 M sodium chloride. Potassium hexacyanoferrate(III) and potassium hexacyanoferrate(II) trihydrate were purchased from Sigma Aldrich and POCh (Poland), respectively.

Instrumentation

For optical measurements Yokogawa AQ6370B spectrum analyzer and a Leukos SM30 supercontinuum white light laser source were used. The measurements were done in closed flow cell as described in section 2.4. For electrochemical

measurements Autolab 302N potentiostat was used.

Deposition of ITO and TaO_x on LPFG

LPFGs were fabricated as described in section 2.4.

Before ITO deposition gratings were etched in HF acid. To obtain sensitive structures after thin layer deposition, it was necessary to over-etch LPFGs beyond DTP observed for LPFG immersed in deionized water. Thin, optically transparent, high-RI, and electrically conductive ITO films were deposited directly on the surface of the LPFGs using magnetron sputtering method. The sputtering was done in collaboration with Institute of Physics and Biophysics, Faculty of Science, University of South Bohemia, Czech Republic. Two samples were prepared. The only difference between them was slightly different working conditions due to the difference in etching time. The deposition process was conducted in a UHV chamber with the sputtering gun equipped with 3-inch ITO target (the composition of In_2O_3:SnO_2 was 9:1 by weight). The COMET Cito1310 RF source was applied, with power of 150 W at frequency 13.56 MHz, under a pressure of 1 Pa and 100 sccm Ar flow. The LPFGs were exposed to sputtering guns for 11 min. The samples placed in the holder were rotated during the deposition to provide homogeneity of the thin film. SEM images of the ITO films were obtained using FEI Nova NanoSEM 450. Sample B was cut in the middle after all other measurements and analyzed by SEM. SEM measurements were done in collaboration with Dr. Martin Jönsson-Niedziółka.

TaO_x films were deposited on non-etched LPFGs by atomic layer deposition (ALD) method in collaboration with Institute of Electron Technology, Poland [13]. The process was performed in Beneq TFS-200-190 system at temperature of 100 °C. All the films have been deposited on LPFGs and simultaneously on approximately 1 cm^2 p-type $< 100 >$ silicon reference wafers. Deionized water and tantalum pentachloride ($TaCl_5$) were used as oxygen and tantalum precursors, respectively. Between gas pulses the chamber was purged with argon (1000 mL/min). The thickness of the nano-films was controlled by the number of cycles of the ALD process.

TaO_x surface functionalization and measurements

The RI sensitivity was measured in flow cell by immersing the sensor structures in glycerol/water solutions with RIs in the range n_{ext} = 1.333–1.401 RIU. The RI of the solutions was determined using a Rudolph J57 automatic refractome-

ter.

For biotin-avidin interactions measurements the TaO_x-coated LPFG was washed in chloroform and dried in nitrogen stream and then cleaned in acetone, ethanol and water (5 min each) and dried under a stream of argon. Then, 2-hour modification with APTES was done as described in section 3.4. Then, carboxyl group in biotin was activated by adding EDC (final concentration 0.4 mg/mL) to biotin solution (1 mg/mL in PBS). Activated biotin solution was injected into the measurement cell and sensor was incubated for 30 min. In this step and the following the optical transmission of the LPFG in the range of λ = 1300–1700 nm was monitored. After surface modification with biotin, the sensor was washed and measured in PBS. Avidin detection was done by injecting increasing concentrations of avidin in PBS (from 100 ng/mL to 1 mg/mL) into the system. Incubation was done for 30 min in each concentration and was followed by PBS washing.

For bacteria detection the TaO_x-LPFG was washed as described for biotin-avidin interactions measurements. Because the receptor (recombinant protein gp37 - adhesin) contained His-Tag, the method with metal-mediated complexation was chosen for LPFG modification. First, 4-hour modification with TESPSA was done as described in section 3.4. Next steps were done in closed flow cell. The TaO_x-LPFG was incubated in 5 mM Ni-NTA (nickel complex with nitrilotriacetic acid derivative - N,N-Bis(carboxymethyl)-L-lysine) in a 5 mM $NaHCO_3$ for 1 h. Next, the sample was incubated for 1 h in a solution of the adhesin (2.5 μg/mL) and then in 0.1% BSA solution for 20 min. After each incubation the sample was washed three times in PBS for 5 min. Target bacteria (*Escherichia coli* BL21) were obtained from the Polish Collection of Microorganisms of the Institute of Immunology and Experimental Therapy, Polish Academy of Sciences (Wroclaw, Poland). In the first step, a single colony of bacteria from agar plate was inoculated into a lysogeny broth (LB) (10 g/L Bacto Tryptone (Difco), 5 g/L yeast extract, 10 g/L sodium chloride) for overnight culturing in 37 °C (200 rpm). Next, overnight culture was diluted in LB to obtain $OD_{600} = 0.1$, centrifuged (5000 rpm, 5 min), and bacteria were resuspended in PBS. A number of bacteria in solution was determined by colony count method. To analyze binding capability of bacteria by adhesin-modified TaOx-LPFG sensor, several concentrations of bacteria solutions were prepared: 10^3, 10^4, and 10^7 CFU/ml (as calculated from colony count method). The incubation time for each concentration was 30 min. After each step, the sensor

underwent three 5-min washing steps in PBS to remove any unbound bacteria, and optical transmission of the LPFG was measured in PBS for 15 min.

ITO-LPFG optical and electrochemical measurements

The RI sensitivity was measured in flow cell by immersing the sensor structures in glycerol/water solutions with RIs in the range n_{ext} = 1.333–1.423 RIU. The RI of the solutions was determined using a Rudolph J57 automatic refractometer.

All the measurements were done in a dedicated setup containing specially designed cell, optical spectrum analyzer, light source, and potentiostat. ITO-LPFG, platinum net, and Ag|AgCl|0.1 M NaCl were used as working (WE), counter (CE), and reference (RE) electrodes, respectively (Figure 5.4). Electrical contact with WE was done by attaching copper tape directly to the ITO-coated cladding away from LPFG section and outside measuring cell. Cyclic voltammetry measurements were done in aqueous solutions consisting of 5 mM $K_3[Fe(CN)_6]$ and 5 mM $K_4[Fe(CN)_6]$ in PBS or solely in PBS at a scan rate 10 mV/s. Potential from 0 V to -1 V to 1 V and back to 0 V was applied and 3 cycles were measured. Chronoamperometry was also done in 5 mM $K_3[Fe(CN)_6]$ and 5 mM $K_4[Fe(CN)_6]$ in PBS. Each potential (0 V, -1 V, 0 V, 1 V, and 0 V) was applied for 60 s. Simultaneously with electrochemical measurements, optical transmission of ITO-LPFG was monitored. Wavelength range was chosen according to dynamics of changes observed each time in the transmission spectra.

5.5 References

(1) Korposh, S.; James, S.; Tatam, R.; Lee, S.-W. In *Current Trends in Short- and Long-period Fiber Gratings*; InTech: 2013, p 13.

(2) Rees, N. D.; James, S. W.; Tatam, R. P.; Ashwell, G. J. Optical fiber long-period gratings with Langmuir–Blodgett thin-film overlays. *Optics Letters* **2002**, *27*, 686.

(3) Del Villar, I.; Matías, I. R.; Arregui, F. J.; Lalanne, P. Optimization of sensitivity in Long Period Fiber Gratings with overlay deposition. *Opt. Express* **2005**, *13*, 56–69.

(4) Wang, Z.; Heflin, J. R.; Stolen, R. H.; Ramachandran, S. Analysis of optical response of long period fiber gratings to nm-thick thin-film coating. *Optics Express* **2005**, *13*, 2808.

(5) Lee, J.; Chen, Q.; Zhang, Q.; Reichard, K.; Ditto, D.; Mazurowski, J.; Hackert, M.; Yin, S. Enhancing the tuning range of a single resonant band long period grating while maintaining the resonant peak depth by using an optimized high index indium tin oxide overlay. *Applied optics* **2007**, *46*, 6984–6989.

(6) Smietana, M.; Szmidt, J.; Korwin-Pawlowski, M. L.; Bock, W. J.; Grabarczyk, J. Application of diamond-like carbon films in optical fibre sensors based on long-period gratings. *Diamond Related Materials* **2007**, *16*, 1374–1377.

(7) Pilla, P.; Trono, C.; Baldini, F.; Chiavaioli, F.; Giordano, M.; Cusano, A. Giant sensitivity of long period gratings in transition mode near the dispersion turning point: an integrated design approach. *Optics Letters* **2012**, *37*, 4152.

(8) Keith, J.; Hess, L.; Spendel, W.; Cox, J.; Pacey, G. The investigation of the behavior of a long period grating sensor with a copper sensitive coating fabricated by layer-by-layer electrostatic adsorption. *Talanta* **2006**, *70*, 818–822.

(9) Korposh, S.; Selyanchyn, R.; Yasukochi, W.; Lee, S.-W.; James, S. W.; Tatam, R. P. Optical fibre long period grating with a nanoporous coating formed from silica nanoparticles for ammonia sensing in water. *Materials Chemistry and Physics* **2012**, *133*, 784–792.

(10) Corres, J.; del Villar, I.; Matias, I.; Arregui, F. In *2006 5th IEEE Conference on Sensors*, IEEE: 2006, pp 193–196.

(11) Wang, Y.; Liu, Y.; Zou, F.; Jiang, C.; Mou, C.; Wang, T. Humidity Sensor Based on a Long-Period Fiber Grating Coated with Polymer Composite Film. *Sensors (Basel, Switzerland)* **2019**, *19*, DOI: 10.3390/s19102263.

(12) Corres, J. M.; Matias, I. R.; del Villar, I.; Arregui, F. J. Design of pH Sensors in Long-Period Fiber Gratings Using Polymeric Nanocoatings. *IEEE Sensors Journal* **2007**, *7*, 455–463.

(13) Kosiel, K.; Dominik, M.; Ściślewska, I.; Kalisz, M.; Guziewicz, M.; Gołaszewska, K.; Niedziółka-Jonsson, J.; Bock, W. J.; Śmietana, M. Alkali-resistant low-temperature atomic-layer-deposited oxides for optical fiber sensor overlays. *Nanotechnology* **2018**, *29*, 135602.

(14) He, Y. J. Investigation of LPG-SPR sensors using the finite element method and eigenmode expansion method. *Optics Express* **2013**, *21*, 13875.

(15) Gu, Z.; Lan, J.; Gao, K. Characteristics of plasmon coupling mode in SPR based LPFG. *Optical and Quantum Electronics* **2016**, *48*, 171.

(16) Li, Z.; Chen, T.; Zhang, Z.; Zhou, Y.; Li, D.; Xie, Z. Highly sensitive surface plasmon resonance sensor utilizing a long period grating with photosensitive cladding. *Applied Optics* **2016**, *55*, 1470.

(17) Wei, W.; Nong, J.; Zhang, G.; Tang, L.; Jiang, X.; Chen, N.; Luo, S.; Lan, G.; Zhu, Y. Graphene-Based Long-Period Fiber Grating Surface Plasmon Resonance Sensor for High-Sensitivity Gas Sensing. *Sensors* **2016**, *17*, 2.

(18) Szunerits, S.; Boukherroub, R. Electrochemical investigation of gold/silica thin film interfaces for electrochemical surface plasmon resonance studies. *Electrochemistry Communications* **2006**, *8*, 439–444.

(19) Szunerits, S.; Castel, X.; Boukherroub, R. Preparation of Electrochemical and Surface Plasmon Resonance Active Interfaces: Deposition of Indium Tin Oxide on Silver Thin Films. *The Journal of Physical Chemistry C* **2008**, *112*, 10883–10888.

(20) Sriwichai, S.; Baba, A.; Deng, S.; Huang, C.; Phanichphant, S.; Advincula, R. C. Nanostructured Ultrathin Films of Alternating Sexithiophenes and Electropolymerizable Polycarbazole Precursor Layers Investigated by Electrochemical Surface Plasmon Resonance (EC-SPR) Spectroscopy. *Langmuir* **2008**, *24*, 9017–9023.

(21) Wu, C.; ur Rehman, F.; Li, J.; Ye, J.; Zhang, Y.; Su, M.; Jiang, H.; Wang, X. Real-Time Evaluation of Live Cancer Cells by an in Situ Surface Plasmon Resonance and Electrochemical Study. *ACS Applied Materials & Interfaces* **2015**, *7*, 24848–24854.

(22) Baba, A.; Taranekar, P.; Ponnapati, R. R.; Knoll, W.; Advincula, R. C. Electrochemical surface plasmon resonance and waveguide-enhanced glucose biosensing with N-alkylaminated polypyrrole/glucose oxidase multilayers. *ACS Applied Materials and Interfaces* **2010**, *2*, 2347–2354.

(23) Salamifar, S. E.; Lai, R. Y. Application of electrochemical surface plasmon resonance spectroscopy for characterization of electrochemical DNA sensors. *Colloids and Surfaces B: Biointerfaces* **2014**, *122*, 835–839.

(24) Yuan, Y.; Guo, T.; Qiu, X.; Tang, J.; Huang, Y.; Zhuang, L.; Zhou, S.; Li, Z.; Guan, B. O.; Zhang, X.; Albert, J. Electrochemical Surface Plasmon Resonance Fiber-Optic Sensor: In Situ Detection of Electroactive Biofilms. *Analytical Chemistry* **2016**, *88*, 7609–7616.

(25) Smietana, M.; Sobaszek, M.; Michalak, B.; Niedzialkowski, P.; Bialobrzeska, W.; Koba, M.; Sezemsky, P.; Stranak, V.; Karczewski, J.; Ossowski, T.; Bogdanowicz, R. Optical Monitoring of Electrochemical Processes With ITO-Based Lossy-Mode Resonance Optical Fiber Sensor Applied as an Electrode. *Journal of Lightwave Technology* **2018**, *36*, 954–960.

(26) Bogdanowicz, R. et al. Optical Detection of Ketoprofen by Its Electropolymerization on an Indium Tin Oxide-Coated Optical Fiber Probe. *Sensors* **2018**, *18*, 1361.

(27) Piestrzyńska, M.; Dominik, M.; Kosiel, K.; Janczuk-Richter, M.; Szot-Karpińska, K.; Brzozowska, E.; Shao, L.; Niedziółka-Jonsson, J.; Bock, W. J.; Śmietana, M. Ultrasensitive tantalum oxide nano-coated long-period gratings for detection of various biological targets. *Biosensors and Bioelectronics* **2019**, *133*, 8–15.

(28) Roh, S.; Chung, T.; Lee, B. Overview of the characteristics of micro- and nano-structured surface plasmon resonance sensors. *Sensors (Basel, Switzerland)* **2011**, *11*, 1565–88.

(29) Lee, B.; Roh, S.; Kim, H.; Jung, J. Waveguide-based surface plasmon resonance sensor design. *Proceedings of SPIE* **2009**, *7420*, 74200C–74200C–12.

(30) Eshaghi, A.; Graeli, A. Optical and electrical properties of indium tin oxide (ITO) nanostructured thin films deposited on polycarbonate substrates "thickness effect". *Optik - International Journal for Light and Electron Optics* **2014**, *125*, 1478–1481.

(31) Reed, G. T.; Jason Png, C. Silicon optical modulators. *Materials Today* **2005**, *8*, 40–50.

(32) Mendoza-Alvarez, J. G.; Nunes, F. D.; Patel, N. B. Refractive index dependence on free carriers for GaAs. *Journal of Applied Physics* **1980**, *51*, 4365–4367.

(33) Han, X.; Mendes, S. B. Spectroelectrochemical properties of ultra-thin indium tin oxide films under electric potential modulation. *Thin Solid Films* **2016**, *603*, 230–237.

(34) Grimnes, S.; Martinsen, Ø. G.; Grimnes, S.; Martinsen, Ø. G. In *Bioimpedance and Bioelectricity Basics*; Elsevier: 2015, pp 179–254.

(35) Lioubimov, V.; Kolomenskii, A.; Mershin, A.; Nanopoulos, D. V.; Schuessler, H. a. Effect of varying electric potential on surface-plasmon resonance sensing. *Applied optics* **2004**, *43*, 3426–3432.

(36) Abayzeed, S. A.; Smith, R. J.; Webb, K. F.; Somekh, M. G.; See, C. W. Sensitive detection of voltage transients using differential intensity surface plasmon resonance system. *Optics Express* **2017**, *25*, 31552.

(37) Prampolini, G.; Yu, P.; Pizzanelli, S.; Cacelli, I.; Yang, F.; Zhao, J.; Wang, J. Structure and Dynamics of Ferrocyanide and Ferricyanide Anions in Water and Heavy Water: An Insight by MD Simulations and 2D IR Spectroscopy. *The Journal of Physical Chemistry B* **2014**, *118*, 14899–14912.

(38) Hwang, B.-J.; Chen, H.-C.; Mai, F.-D.; Tsai, H.-Y.; Yang, C.-P.; Rick, J.; Liu, Y.-C. Innovative Strategy on Hydrogen Evolution Reaction Utilizing Activated Liquid Water. *Scientific Reports* **2015**, *5*, 16263.

Chapter 6

Outlook

6.1 Summary

Biosensors technology has been developing rapidly during the last decade and great advances were made in the field of optical biosensing. The main achievements described in this thesis include the development of surface modification methods for cylindrical surfaces, preparation of label-free long-period fiber grating biosensors for detection of bacteriophage and norovirus with the use of the developed modification methods, and preparation of new LPFG-based sensors for simultaneous optical and electrochemical measurements.

To develop a functional label-free biosensor it is necessary to prepare a transducer that is highly sensitive to changes in external refractive index. Therefore, I optimized the working point of the device to dispersion turning point by chemical etching in hydrofluoric acid [1]. By careful etching it was possible to obtain RI sensitivity reaching almost 2000 nm/RIU in the RI range close to that of water. During preliminary measurements I observed significant changes in transmission spectra of the LPFG before and after surface drying. Therefore, this effect was carefully studied by cyclic surface drying and immersing in water. The significant changes in the transmission spectra measured in water after each drying indicated some alterations on the surface that occurred during drying and had an impact on local refractive index. Observed changes may lead to misleading conclusions during experiments in which the surface is dried between modification or detection steps. Thanks to those findings, the flow cell, in which the drying is avoided, was prepared and used for other measurements with LPFG-based sensors.

Next step was to develop methods for surface modifications that enable quick and reliable immobilization of receptors on the LPFG surface. I tested methods of vapor phase silanization to introduce different functional groups onto the surface of cylindrical fibers. These methods have so far been used for modification of flat glass substrates [2, 3], but results presented in my thesis demonstrated that they are useful also for modification of cylindrical optical fibers. Covalent bonding of proteins was done on the surface with amine groups or succinic anhydride functionalities that comes from different silanes. Both methods resulted in successful immobilization of receptors as shown by using green fluorescent protein and confocal microscope. Obtained protein coatings were uniform and clearly visible on the whole surface of optical fibers. The methods were further used for immobilization of receptors during preparation of LPFG-based biosensors.

Then, I prepared and described LPFG-based biosensors for detection of different viruses. Thanks to the utilization of highly sensitive LPFGs and developed surface modification methods it was possible to obtain simple, rapid, sensitive, and versatile biosensors working in label-free configuration. I was testing LPFG sensors modified with specific antibodies for the detection of bacterial and eukaryotic viruses. I was able to detect 5×10^3 PFU/mL of T7 bacteriophage and 1 ng/mL of norovirus virus-like particles in analysis time shorter than 40 minutes. Moreover, such a sensor do not require any amplification of genetic material (as in the case of PCR) nor expensive reagents and multiple washing and incubation steps (as in ELISA). Demonstrated biosensors are easily applicable for detection of different viral targets by selecting appropriate antibodies as receptors.

Further achievements were related to the use of thin high-RI films as LPFGs overlays. It was shown in the literature that utilization of such films may be advantageous from the point of view of sensitivity [4, 5], durability [6], and possible applications [7, 8]. In my thesis, I demonstrated that metal oxide coatings can be used for sensitivity improvement (both RI sensitivity and label-free sensitivity of biosensors) and also for preparation of sensor working in electrochemical and optical domains simultaneously. For sensitivity enhancement, tantalum oxide layers with precisely chosen thickness were used. They enabled to reach RI sensitivity higher than 11,500 nm/RIU in 1.335–1.345 RIU range and thus improved label-free biosensing capabilities comparing to bare LPFG biosensor. Based on those LPFGs, biosensors for detection of avidin and bacteria *E. coli*

were demonstrated. Preparation of multi-domain sensor was possible due to the application of thin, optically transparent, electrically conductive indium tin oxide layer on LPFG. It was the first optical-electrochemical sensor based on this configuration. ITO served both as working electrode in electrochemical setup and as a coating that enhances RI sensitivity of LPFG device. I demonstrated that the optical response of ITO-LPFG was strongly dependent on potential applied to the surface. Described device can be further used as sensor or biosensor with integrated optical and electrochemical readout.

6.2 Future perspectives

Solutions presented in this thesis make a significant contribution into fiber-based sensors and biosensors field. Several findings described in this work, such as surface modifications methods, biosensors for virus detection, or sensor for simultaneous electrochemical and optical measurements, can be further utilized in broader application range. Silanization methods demonstated in this work as a method for modification of non-flat surfaces can be further used for functionalization of other optical fiber devices and also different transducers made from glass or other oxides with flat and non-flat geometry. Presented LPFG-based biosensors can be implemented into practical detection. Biosensor for bacteriophage detection would be particularly useful in biotechnology industry where bacterial viruses are a real threat for bacteria-based production technologies [9]. Fast detection of bacteriophages in media and substrates used, e.g., in biopharmaceutical factory is crucial to avoid infections with phages and resulting financial losses. Detection of norovirus VLPs can be implemented in the field of vaccine research in which the VLPs are widely studied as vaccine candidates, but methods for their enumeration are not very efficient [10]. Additionally, due to the morphological and antigen similarity between VLPs and native norovirus, LPFG biosensor can be used in diagnosis process for fast norovirus detection. Utilization of thin oxide overlays, such as tantalum oxide, that enhance the sensor sensitivity, can be useful for the detection of small concentrations of target analytes. On the other hand, it increases the cost and introduces additional technologically complicated step into the biosensors production scheme. More interesting is, in my opinion, the utilization of conductive overlays, such as indium tin oxide, to prepare the sensors that can work in two domains: electrochemical and optical. Thanks to that, ITO-LPFG devices can be used for

simultaneous optical and electrochemical measurements that enable gathering more information on the investigated process than the methods applied separately. Additionally, this approach gives the possibilities to measure in one domain the process that was initiated in other one. For example, the method can be useful for measurements of changes in the layer thickness deposited on the surface by electropolymerization (as shown for different fiber structures in [11]). Additionally, very important findings concerning influence of surface drying on the optical response of the LPFG sensor was described. Results indicate the possibility of getting misleading conclusions in any experiment in which the sensor surface is dried between measurements made in liquids. This should be taken into consideration in any optical fiber sensor and, if possible, flow cells should be used to avoid surface drying.

To implement presented solutions in practical applications further work is needed. Despite the huge interest and progress in sensing and biosensing field, commercialization of optical biosensors and biosensors in general does not develop as fast as the number of publications would indicate.

Use of the optical fiber sensors working in label-free configuration enable developing portable devices that are sensitive, relatively low-cost, and reliable. Therefore, in the case of LPFGs, further work should be done on miniaturization of optical devices, such as optical spectrum analyzer, because the sensing structure itself is small and light. Additionally, to introduce into the market biosensing solutions based on LPFGs, proper packaging is necessary. It should protect the sensor from breakage and impurities and provide easy way for sample injection. Preparation of integrated microfluidics can be a solution for both packaging and reduction of the sample volume.

Further work with LPFG-based biosensors should also focus more on the measurements in real samples. As it was shown in the thesis, antibody-modified LPFG-based biosensors provide sensitive and rapid solution for virus detection. However, next step is to repeat developed assays in real samples, such as liquid substrates used in biotechnology industry (for bacteriophage detection) or in serum (for norovirus detection) to take into consideration the influence of real sample matrix.

Solutions discussed in the thesis can be useful tools in different analytical fields and they should be developed to meet the requirements of practical applications. I am looking forward to see further advancements that will bridge the gap between laboratory work and real-life expectations.

6.3 References

(1) Biswas, P.; Basumallick, N.; Bandyopadhyay, S.; Dasgupta, K.; Ghosh, A.; Bandyopadhyay, S. Sensitivity Enhancement of Turn-Around-Point Long Period Gratings By Tuning Initial Coupling Condition. *IEEE Sensors Journal* **2015**, *15*, 1240–1245.

(2) Vashist, S. K. Comparison of 1-Ethyl-3-(3-Dimethylaminopropyl) Carbodiimide Based Strategies to Crosslink Antibodies on Amine-Functionalized Platforms for Immunodiagnostic Applications. *Diagnostics* **2012**, *2*, 23–33.

(3) Gang, A.; Gabernet, G.; Renner, L. D.; Baraban, L.; Cuniberti, G. A simple two-step silane-based (bio-) receptor molecule immobilization without additional binding site passivation. *RSC Adv.* **2015**, *5*, 35631–35634.

(4) Rees, N. D.; James, S. W.; Tatam, R. P.; Ashwell, G. J. Optical fiber long-period gratings with Langmuir–Blodgett thin-film overlays. *Optics Letters* **2002**, *27*, 686.

(5) Del Villar, I.; Matías, I. R.; Arregui, F. J.; Lalanne, P. Optimization of sensitivity in Long Period Fiber Gratings with overlay deposition. *Opt. Express* **2005**, *13*, 56–69.

(6) Kosiel, K.; Dominik, M.; Ściślewska, I.; Kalisz, M.; Guziewicz, M.; Gołaszewska, K.; Niedziółka-Jonsson, J.; Bock, W. J.; Śmietana, M. Alkali-resistant low-temperature atomic-layer-deposited oxides for optical fiber sensor overlays. *Nanotechnology* **2018**, *29*, 135602.

(7) Keith, J.; Hess, L.; Spendel, W.; Cox, J.; Pacey, G. The investigation of the behavior of a long period grating sensor with a copper sensitive coating fabricated by layer-by-layer electrostatic adsorption. *Talanta* **2006**, *70*, 818–822.

(8) Wei, W.; Nong, J.; Zhang, G.; Tang, L.; Jiang, X.; Chen, N.; Luo, S.; Lan, G.; Zhu, Y. Graphene-Based Long-Period Fiber Grating Surface Plasmon Resonance Sensor for High-Sensitivity Gas Sensing. *Sensors* **2016**, *17*, 2.

(9) Calendar, R., *The Bacteriophages*; Oxford University Press: 2006, p 746.

(10) Zeltins, A. Construction and Characterization of Virus-Like Particles: A Review. *Molecular Biotechnology* **2013**, *53*, 92–107.

(11) Bogdanowicz, R. et al. Optical Detection of Ketoprofen by Its Electropolymerization on an Indium Tin Oxide-Coated Optical Fiber Probe. *Sensors* **2018**, *18*, 1361.

Appendix 1

Table 6.1: Surface composition (in at%) from XPS spectrum before and after surface modification with APTES.

Sample	**Chemical state**	**Concentration [at.%]**
Si/SiO_2 substrate	C1s – 286.6 eV (C-C)	11.8
	C1s – 288.6 eV (C-O-C)	1.3
	O1s – 534.9 eV (Si-O, C-O)	67.0
	O1s – 536.2 eV (H_2O)	5.6
	Si2p – 105.1 eV (Si-O)	12.7
	N1s – 400.8 eV (C-N, N-H, -NH_2)	1.2
	N1s – 405.3 eV (N-O)	0.2
	N1s – 402.7 eV (N-H, -NH_3^+)	0.1

Si/SiO_2/APTES 1 h	C1s – 286.7 eV (C-C)	34.8
	C1s – 288.1 eV (C-OH, C-N)	14.1
	C1s – 289.8 eV (O=C-O)	4.5
	O1s – 534.3 eV (Si-O, C-O)	30.2
	O1s – 532.5 eV (OH-)	2.3
	O1s – 535.8 eV (H_2O)	2.1
	Si2p – 104.4 eV (Si-O)	2.1
	N1s – 401.1 eV (C-N, N-H, -NH_2)	6.9
	N1s – 402.6 eV (N-H, -NH_3^+)	2.7
	N1s – 404.3 eV (N_3-)	0.3
Si/SiO_2/APTES 2 h	C1s – 286.8 eV (C-C)	24.1
	C1s – 288.1 eV (C-OH, C-N)	8.0
	C1s – 289.9 eV (O=C-O)	2.3
	O1s – 534.5 eV (Si-O, C-O)	51.0
	O1s – 536.0 eV (H_2O)	4.0
	O1s – 532.6 eV (OH-)	2.4
	Si2p – 104.8 eV (Si-O)	2.4
	N1s – 401.1 eV (C-N, N-H, -NH_2)	3.8
	N1s – 402.6 eV (N-H, -NH_3^+)	1.6
	N1s – 404.3 eV (N_3-)	0.4

Si/SiO_2/APTES 5 h	C1s – 286.5 eV (C-C)	30.7
	C1s – 287.8 eV (C-OH, C-N)	7.0
	C1s – 289.6 eV (O=C-O)	2.3
	O1s – 534.2 eV (Si-O, C-O)	25.2
	O1s – 535.3 eV (C=O)	4.2
	O1s – 532.6 eV (C-O, OH-)	1.6
	Si2p – 104.4 eV (Si-O)	20.0
	Si2p – 103.6 eV (Si-H, Si-O)	3.0
	N1s – 401.0 eV (C-N, N-H, -NH_2)	4.2
	N1s – 402.3 eV (N-H, -NH_3^+)	1.4
	N1s – 403.9 eV (N_3-)	0.3
Si/SiO_2/APTES 8 h	C1s – 286.5 eV (C-C)	32.4
	C1s – 287.9 eV (C-OH, C-N)	9.0
	C1s – 289.8 eV (O=C-O)	2.5
	O1s – 534.2 eV (Si-O, C-O)	24.4
	O1s – 535.4 eV (C=O)	2.6
	O1s – 532.4 eV (C-O, OH-)	1.4
	Si2p – 104.5 eV (Si-O)	15.7
	Si2p – 103.8 eV (Si-H, Si-O)	4.7
	N1s – 401.0 eV (C-N, N-H, -NH_2)	5.3
	N1s – 402.3 eV (N-H, -NH_3^+)	1.5
	N1s – 403.8 eV (N_3-)	0.3

Table 6.2: Surface composition (in at%) from XPS spectrum before and after surface modification with APTES using additional heating.

Sample	**Chemical state**	**Concentration [at.%]**
Si/SiO_2 substrate	C1s – 286.6 eV (C-C)	11.8
	C1s – 288.6 eV (C-O-C)	1.3
	O1s – 534.9 eV (Si-O, C-O)	67.0
	O1s – 536.2 eV (H_2O)	5.6
	Si2p – 105.1 eV (Si-O)	12.7
	N1s – 400.8 eV (C-N, N-H, -NH_2)	1.2
	N1s – 405.3 eV (N-O)	0.2
	N1s – 402.7 eV (N-H, -NH_3^+)	0.1
Si/SiO_2/APTES 1 h/IR	C1s – 286.9 eV (C-C)	15.9
	C1s – 288.4 eV (C-OH, C-N)	4.2
	C1s – 290.2 eV (O=C-O)	1.1
	O1s – 534.7 eV (Si-O, C-O)	42.6
	O1s – 536.3 eV (H_2O)	2.8
	O1s – 532.7 eV (OH-)	1.8
	Si2p – 104.9 eV (Si-O)	28.5
	N1s – 401.1 eV (C-N, N-H, -NH_2)	1.8
	N1s – 402.6 eV (N-H, -NH_3^+)	0.8
	N1s – 404.3 eV (N_3-)	0.3

Si/SiO_2/APTES 2 h/IR	C1s – 286.9 eV (C-C) C1s – 288.4 eV (C-OH, C-N) C1s – 290.2 eV (O=C-O) O1s – 534.8 eV (Si-O, C-O) O1s – 536.0 eV (H_2O) Si2p – 105.0 eV (Si-O) N1s – 401.1 eV (C-N, N-H, -NH_2) N1s – 402.6 eV (N-H, -NH_3^+) N1s – 404.9 eV (N_3-)	14.8 4.0 1.5 45.6 1.5 29.5 1.8 1.1 0.3
Si/SiO_2/APTES 5 h/IR	C1s – 286.5 eV (C-C) C1s – 288.0 eV (C-OH, C-N) C1s – 289.8 eV (O=C-O) O1s – 534.5 eV (Si-O, C-O) O1s – 536.2 eV (H_2O) Si2p – 104.7 eV (Si-O) N1s – 400.8 eV (C-N, N-H, -NH_2) N1s – 402.5 eV (N-H, -NH_3^+) N1s – 404.9 eV (N_3-)	26.1 4.4 1.0 36.9 1.3 27.9 1.5 0.5 0.2

Table 6.3: Surface composition (in at%) from XPS spectrum before and after surface modification with TESPSA.

Sample	**Chemical state**	**Concentration [at.%]**
Si/SiO_2 substrate	C1s – 286.6 eV (C-C)	11.8
	C1s – 288.6 eV (C-O-C)	1.3
	O1s – 534.9 eV (Si-O, C-O)	67.0
	O1s – 536.2 eV (H_2O)	5.6
	Si2p – 105.1 eV (Si-O)	12.7
Si/SiO_2/TESPSA 2 h	C1s – 286.9 eV (C-C)	15.7
	C1s – 288.8 eV (C-OH, C-O-C)	2.6
	C1s – 290.9 eV (O=C-O)	2.2
	O1s – 534.9 eV (Si-O, C-O)	47.2
	O1s – 537.8 eV (H_2O)	1.6
	O1s – 532.7 eV (OH-)	1.5
	Si2p – 105.1 eV (Si-O)	27.4
Si/SiO_2/TESPSA 4 h	C1s – 286.9 eV (C-C)	19.4
	C1s – 288.9 eV (C-OH, C-O-C)	3.0
	C1s – 290.9 eV (O=C-O)	2.8
	O1s – 534.9 eV (Si-O, C-O)	46.0
	O1s – 537.9 eV (H_2O)	1.5
	Si2p – 105.1 eV (Si-O)	25.6